64

STUDY OF Pt-Ge INTERACTION USING THIN FILM AND LATERAL DIFFUSION COUPLES

Rudzani Nemutudi

University of Cape Town

Thesis submitted to the Faculty of Science
of the University of Cape Town in fulfilment of the requirements
for the M.Sc. degree in Physics

Department of Physics, University of Cape Town

21 February 1997

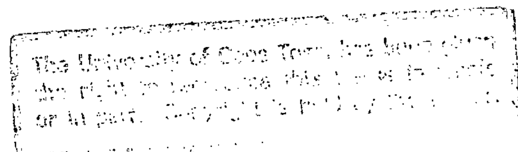

The copyright of this thesis vests in the author. No quotation from it or information derived from it is to be published without full acknowledgement of the source. The thesis is to be used for private study or non-commercial research purposes only.

Published by the University of Cape Town (UCT) in terms of the non-exclusive license granted to UCT by the author.

University of Cape Town

My father, Vho-Raudzingana Nemutudi, had his life tragically terminated on the $27^{th}/03/95$ at the very beginning of this thesis. I never got a chance to do anything material for him when his body and soul were still intact. This thesis is dedicated to him and his memory

Abstract

The formation of germanides of platinum has been investigated using both conventional thin films and lateral diffusion couples. The investigation was carried out using such established techniques as XRD, RBS and SEM. Using results from both thin film and lateral diffusion couples, a comparison has been made of the behaviour of Pt-Ge system in parameters such as phase formation sequence, growth kinetics and dominant diffusing species.

In their sequential order of formation, three distinct phases, Pt_2Ge, PtGe and $PtGe_2$, have been identified in thin films in the temperature range 200 - 300°C. The first phase, Pt_2Ge, was found not to follow a layered mode of formation. Both PtGe and $PtGe_2$ phases were found to obey a $(t)^{\frac{1}{2}}$ law, indicating a diffusion limited growth process. By employing Ti as an inert marker, platinum was observed as the dominant diffusing species during Pt_2Ge formation. On the dominant diffusing species during PtGe and $PtGe_2$ formation, the thin film results were but tentative.

Upon annealing at 500°C/30,90,180min, lateral diffusion couples of Pt rich source (on Ge thin film) resulted in only a limited lateral growth, and multiple phases were not observed. However, when samples of Ge rich source (on Pt thin film) were annealed at the same temperature and times, lateral interaction was observed proceeding on a relatively large scale. Germanium atoms were found to have encroached into the surrounding Pt thin film as far as $\pm 30\mu m$ away from the Ge source region, with multiple phases growing simultaneously, viz $PtGe_2$, PtGe and Pt_2Ge_3. Inside the source region, the composition of the innermost compound corresponded to $PtGe_2$ phase. Pt_2Ge_3 was located between $PtGe_2$ and the initial island/thin film interface line. The compound outside the source region was characterised as PtGe. Pt_2Ge_3 phase was observed to have resulted from $PtGe_2$ disintegration through the mechanism $2PtGe_2 \rightarrow Pt_2Ge_3 + Ge$. Plots obtained from μRBS and SEM lateral measurements indicate that the growth of observed phases ($PtGe_2$, Pt_2Ge_3 and PtGe) all follow a square-root-of-time law, a characteristic of diffusion limited growth process.

Acknowledgements

The success of this project is attributable to a number of people whose immense contribution I can never fully express in words. Their help, guidance, assistance and support has not passed without note on my part. I would like to express to them my deepest gratitudes and heartfelt appreciation. Only sheer shortage of space restricts me to mentioning just a few.

- My supervisor, Assoc Prof Comrie, who worked tirelessly in guiding me throughout this project. At all times when the project seemed to frustrate me, my supervisor was always there to assist me in steering it back to the envisaged route. Had it not been for his determination and excellent supervising skills, this task would have been much more dense.
- Dr Pretorious, the head of Van der Graaf division of NAC, and his entire team, for providing a well equiped laboratory with high quality alpha particle beam.
- UCT scholarship for providing financial assistance
- Douw Steyn for his ever preparedness to impart his expertise in matters pertaining to LaTeX Texnicalities
- The *μRBS* data acquisition part of the project would have been a nightmare without the vast experience of Dr Churms. His computer expertise and meticulous attention to details deepened my interest in Physics. Those late night μRBS runs were made much more enjoyable with the charming character of Dr Churms.
- Chris Theron was of great assistance in the handling of "*dynamic RBS*" data. His advice and thought provoking discussions will remain forever commendable.
- My special thanks go out to Dr C.P. De Leeuw(and company). I am still to comprehend fully the magnanimity of his generousity. He consistently assisted me ever-since my undergraduate days. I can never thank him enough.

- To my tall pastor "Tham-Tham" Samuele Phupheli whose help, guidance and vision provided reason for me to always strive on. His pastoral inspiration and encouragement could never have been more pivotal in my life. In my standards, Sam Phupheli passes for a perfect pastor who was never passive.

- To uncle Mathatha: Mathatha Tsedu, my loving uncle who stands out amongst all my nuclear relatives as the one from whom I learnt more in my life. Words alone do not begin to express the depth of my respect for him. Uncle Mathatha, you remain forever great to your nephew.

- To all my friends, especially those I attended with under the trees at Sendedza Primary School back in the mid-70's. I will remain forever unforgiving to those who tailored and perpetuated the education system skewed in favour of white children, for I saw it frustrating and ultimately suffocating the distinguished talent and potential of many of my friends who could have done it much better than myself. They were denied the opportunity to study through to the level that I have reached. That I survived the system is still miraculous to me. Guys, you remain my friends, for it was your friendship that modelled me to a person that I am today.

- Finally, and most importantly, to my family, especialy my mother, Mulambilu, without whom none of this would have been possible. As I grew up, I saw her struggling through thick and thin, supporting me with enthusiasm and nourishing me with parental love and tender care. Mom, thanks for doing all you could to bring me up under those circumstances. And here also lies the opportunity to mention my profound and deep seated adoration for my grandmother, Kuku Vho-Nyamukamadi Nemutudi. I always surpassed others as her favourate at home, in that I was the only one who could interprete financial figures in a way she understood. "Ndi mbili na disheleni kuku", I would say to her as my brother Semu spoke to her in terms of five rands. My wonderfull granny, as I watch her growing older by day now, my admiration for her seems to multiply by a factor of Pi (Π). She remains my towering pillar of strength.

Contents

1 Introduction **2**

1.1 Background 2

1.2 Reactions in Bulk and Thin Films 4

1.3 Lateral Diffusion Reactions 5

1.4 Phase Formation Sequence 8

1.4.1 Walser-Bene and other Rules 9

1.4.2 Effective Heat of Formation (EHF) Model 12

1.5 Growth Kinetics 14

1.6 Growth Kinetic Analysis by Temperature Ramping 15

1.7 Diffusion 16

1.8 Scope of this investigation 19

2 Experimental Techniques and Procedure **23**

2.1 Rutherford Backscattering 23

2.1.1 Kinematic Factor(k) 25

2.1.2 Energy Loss (dE/dx) 26

2.1.3 Differential Scattering cross section ($\frac{d\sigma}{d\Omega}$) 28

2.1.4 Interpretation of the spectrum. 29

2.2 Marker Technique 30

2.3 Procedure 32

2.3.1 Sample Preparation 32

2.3.2 Vacuum Evaporation 33
2.3.3 Annealing 33
2.3.4 X-Ray Diffraction 34
2.3.5 *Dynamic* RBS 35

3 Thin film study of Pt-Ge system **37**

3.1 Phase Formation 37
3.1.1 Experimental conditions 37
3.1.2 Results 37
3.1.3 Discussion 45
3.2 Growth Kinetics 46
3.2.1 Experimental conditions 46
3.2.2 Results 47
3.2.3 Discussion 53
3.3 Dominant Moving Species 54
3.3.1 Introduction 54
3.3.2 Dominant Moving Species during Pt_2Ge Formation 55
3.3.3 Dominant Moving Species during PtGe Formation. 58
3.3.4 Dominant Moving Species during $PtGe_2$ Formation. 61
3.3.5 Discussion 63

4 Lateral Diffusion in Pt-Ge system **66**

4.1 Introduction 66
4.2 SEM Results 67
4.2.1 Pt islands on Ge thin Film 68
4.2.2 Ge islands on Pt thin film 70
4.3 Microprobe Results 75
4.3.1 Ge islands on Pt thin film. 75
4.4 Discussion 88

4.4.1 Dominant Moving Species and Phase Formation Sequence 88
4.4.2 Growth Kinetics 90

5 Summary, Conclusion and proposal for possible future work 91

A RBS simulations 97

B Calculations of Diffusion ratios to estimate dominant diffusing species 100

C Calculations of the total number of Ge atoms present in reacted zones. 102

List of Figures

1.1 *Schematic illustration of lateral diffusion sample showing platinum island on germanium thin film. Vertical arrows indicate the direction of atomic mobilty during initial stages of the reaction. Once the underlying atoms are consumed, the island starts to supply atoms in the lateral direction. It is assumed in this sketch that the metal(M) is the dominant diffusing species during first metal-germanide formation.* 6

1.2 *Schematic diagram showing lateral diffusion couple for Pt-Ge system both before and after annealing. Different compounds are indicated with* $z > y > x > w > u$. 7

1.3 *Phase diagram for Pt-Ge system* 13

1.4 *Schematic illustration of three main diffusion mechanisms. (a). Rotational/Interchange mechanism (b). Interstitial mechanism (c). Vacancy/Substitutional mechanism* 18

2.1 *Schematic diagram illustrating the experimental setup of Rutherford Backscattering. A 2 MeV alpha beam is incident on a sample. The sample normal is tilted by* ϕ*=10° from the incident beam and* θ*=165° is the scattering angle. The incident beam and the detector are on the same plane with the sample normal. All quantities refer to a laboratory frame of reference.* 24

2.2 *Schematic representation of elastic collision between a projectile of mass* m_1*, velocity* v_0 *and a target of mass* M_2 *initially at rest.* 25

2.3 *Diagram illustrating scattering of incident particles on the surface and at depth* x *below the surface.* 27

2.4 *A typical Backscattering spectrum simulated to show signal heights and compound thickness.* 30

2.5 *Schematic representation of relative shift in the position of the marker.(a) Germanium diffusion. (b) Metal diffusion.* 32

2.6 *Schematic illustration of high vacuum system used for the electron beam evaporation of thin films. Upper section contains sample holder, thickness monitor and electron gun. The baffle valve is closed to ensure that the lower section of the system is maintained under vacuum when the system is not in use or during sample changing.* 34

2.7 *Schematic diagram showing the scattering chamber containing the cylinder used as a heating stage during insitu RBS measurements of solid state reactions.* 35

3.1 *RBS spectra(top) obtained from samples before and after annealing at 250 and 300°C for annealing periods of 10 and 20 minutes. RBS results are summarised in a schematic diagram below.* 38

3.2 *RBS spectra obtained after annealing at 250 and 300°C for 10 and 20 minutes at each temperature. On each spectra, the solid line is a simulation obtained from RUMP showing good agreement with actual data.* 39

3.3 *X-ray diffraction spectra displayed side by side with their corresponding backscattering spectra. The spectra were obtained from samples annealed at 250°C/1hour to form Pt_3Ge_2 (a) and 300°C/30min to form PtGe(b). The lines of highest intensities on XRD spectra are indicated by their Miller indices.* 41

3.4 *X-ray diffraction spectra displayed side by side with their corresponding backscattering spectra. The spectra were obtained from two samples(with different thicknesses) annealed at the same temperature 350°C/30min to form Pt_2Ge_3(a) and $PtGe_2$(b). The lines of highest intensities on XRD spectra are indicated by their Miller indices.* 42

3.5 *X-ray diffraction spectra displayed side by side with their corresponding backscattering spectra. The spectra were obtained from samples annealed at 250 and 300°C for 10 and 20 minutes at each temperature. The lines of highest intensities on XRD spectra are indicated by their Miller indices. There is no convincing evidence of either Pt_3Ge_2 or Pt_2Ge_3 from both XRD and RBS data.* 43

3.6 *RBS spectra obtained from an as deposited sample and from samples annealed at 200, 220, 250 and 275°C for higher annealing periods of 80 minutes.* . . . 44

3.7 *RBS spectra collected from one sample annealed in situ at two different constant temperatures, 260 and 320°C. PtGe was first grown at 260°C (top). After complete formation of PtGe, the sample temperature was increased to 320°C to grow $PtGe_2$ (bottom). Thus the spectrum at 140 min from the top figure is essentially the same as the one at 0 min from the bottom. The $t^{\frac{1}{2}}$ nature of the growth is more evidently clear during $PtGe_2$ growth.* 49

3.8 *The kinetics of formation of PtGe at 260°C. The thickness is expressed in total atoms(Pt+Ge) per unit area. The two plots display the same data. The best fit is more in agreement with the x^2 vs t data, suggesting that PtGe formation process is diffusion limited.* 50

3.9 *Plots of x^2 vs t showing parabolic growth of $PtGe_2$ at 310, 320, 327 and 335°C. The thickness is expressed in total atoms(Pt+Ge) per unit area. The straight lines are indicative of a diffusion limited process.* 51

3.10 *Arrhenius plot, $ln(x^2/t)$ vs 1000/T, showing temperature dependence of $PtGe_2$ diffusion rate, yielding an average activation energy of 1.9 ± 0.1 eV. The interdiffusion coefficients are slopes obtained from plots in Figure 3.8* 51

3.11 *Kissinger plot for PtGe(a) and $PtGe_2$(b) formation obtained from temperature ramping in the range 240-350°C at a ramp rate ρ = 1°C/min. The activation energies for PtGe and $PtGe_2$ are 1.52 ± 0.02 eV and 2.5 ± 0.2 eV respectively.* 52

3.12 *Backscattering spectra from Ti-Ge samples annealed in the temperature range 300-500°C. The results clearly show no interaction between Ti and Ge at temperatures as high as 400°C. It is also evident that Ti-Ge interaction only starts at temperatures around 500°C.* 55
3.13 *RBS spectrum from an as deposited sample(~1500Å Ge on ~500Å with a thin layer of Ti(~12Å) between Ge and Pt) and from a sample annealed at 250°C/10 min showing atomic mobility during Pt_2Ge formation. The relative shift of the Ti marker signal to the lower energy is clearly visible.* 56
3.14 *RBS spectrum from a sample annealed at 250°/10 min. Simulation suggests platinum as the dominant diffusing species during Pt_2Ge formation. Thicknesses are given in units of $10^{15}at/cm^2$. The region with Ti signal has been blown up on to show the agreement on marker position between actual data and RUMP simulation.* 57
3.15 *Schematic representation illustrating relative marker movement during Pt_2Ge formation. Dominant diffusing species is determined from amounts of Pt_2Ge and PtGe above and below the marker. Pt is found to be the dominant diffusing species during Pt_2Ge formation. Thicknesses are in units of $10^{15}atm/cm^2$.* . . 58
3.16 *Schematic representation of a sample prepared and annealed to form Pt_2Ge without atoms diffusing past the Ti marker. Upon further annealing, Ti marker will start to monitor the direction of atomic mobility during the formation of PtGe. The nominal thicknesses are given in units of $10^{15}atm/cm^2$.* 59
3.17 *RBS spectra from a sample annealed at 250°C/80 min. The total number of germanium atoms(~370) above the marker suggest that platinum is the sole diffusing species during PtGe formation. Thicknesses are given in units of $10^{15}at/cm^2$. The region with Ti signal has been blown up to show the agreement on marker position between actual data and RUMP simulation.* . . 60

3.18 *RBS spectra from a sample annealed at 280°C/40 min. The total number of germanium atoms(~370) above the marker suggest that platinum is the sole diffusing species during PtGe formation. Thicknesses are given in units of 10^{15}at/cm^2. The region with Ti signal has been blown up on the bottom spectrum to show the agreement on marker position between actual data and RUMP simulation.* 61

3.19 *Schematic representation of a sample prepared and annealed to form PtGe without atoms diffusing past the Ti marker. Upon further annealing, Ti marker will monitor the direction of atomic mobility during the formation of $PtGe_2$. The nominal thicknesses are given in units of 10^{15}at/cm^2.* 62

3.20 *RBS spectrum from an as deposited sample. A thin layer of Ti(12Å) between two germanium layers serves as an inert marker to monitor atomic mobility during $PtGe_2$ formation. The region with Ti signal has been blown up to show the agreement on marker position between actual data and RUMP simulation.* 63

3.21 *RBS spectra from a sample annealed at 260°C/40 min. The simulation shows that PtGe phase had formed completely behind the marker. The marker position is still the same as that of the an as deposited sample, and so is surface germanium thickness. The marker would then start to monitor atomic mobility during $PtGe_a$ formation.* 64

3.22 *RBS spectra from a sample annealed at 300°C/50 min. The simulation shows that $PtGe_2$ phase had formed below and above the marker. Thicknesses are given in units of 10^{15}at/cm^2. The total number of germanium atoms above the marker suggest that germanium is the dominant diffusing species.* 65

4.1 *Schematic diagram showing the side view of the specimens prepared and examined in this study. (a) Germanium island on platinum thin film, (b) Platinum Island on germanium thin film.* 67

4.2 *Scanning Electron Micrograph from an as deposited sample with Pt island(1500Å) on Ge(400Å) thin film. The image was recorded using backscattered electrons* 68

4.3 *Scanning Electron Micrographs obtained from samples of Pt island(1500Å) on Ge(400Å) thin film annealed at 500° C/30min(top) and 500° C/180min(bottom). Both images were recorded using backscattered electrons.* 69

4.4 *Scanning Electron Micrograph obtained from an as prepared sample with Ge island(1350Å) on Pt(330Å) thin film. The bright region represents the Ge island and the dark the Pt thin film. The image was recorded using backscattered electrons.* 70

4.5 *Scanning Electron Micrographs obtained from a sample of Ge island(∼1350Å) on Pt(330Å) thin film annealed at 500° C/90min. The bottom image is the enlarged end of the top one. Region E is the Pt thin film and A is the Ge source. Regions B, C and D are mixtures of Pt and Ge. Both images were recorded from backscattered electrons.* 71

4.6 *Scanning Electron Micrographs obtained from a sample of Ge island(∼1350Å) on Pt(330Å) thin film annealed at 500° C/30min. Region E is the Pt thin film and A is the Ge source. The bottom image is the magnified end of the top one. Both images were recorded from backscattered electrons.* 73

4.7 *Scanning Electron Micrographs obtained from a sample of Ge island(∼1350Å) on Pt(330Å) thin film annealed at 500° C/180min. Region E is the Pt thin film and A is the Ge source. The bottom image is the magnified end of the top one. Both images were recorded from backscattered electrons.* 74

4.8 *Two RBS spectra(top), (a) and (b), obtained from an as prepared lateral diffusion couple of Ge island(∼1360Å) on Pt thin film(∼330Å). The spectra are displayed with their RUMP simulation to show good agreement with collected data. At the bottom is a plot of Pt and Ge integrated counts from RBS peaks across Ge island and Pt thin film regions.* 77

4.9 *RBS spectra, (a) and (b), obtained from lateral diffusion couple of Ge island(~1360Å) on Pt thin film(~330Å) annealed at 500°C/90min. The spectra are displayed in the sequence ranging from the innermost region(A) to the outermost one(E). The numbering of regions corresponds to that used in the SEM micrographs. Both Pt and Ge peaks were integrated and their counts plotted against beam position in (c). Four different regions are clearly in their decreasing order of germanium content. The vertical line corresponds to the original interface between Ge island and the surrounding Pt thin film.* 78

4.10 *(a) A plot of compound composition ($PtGe_x$) versus beam position for a lateral diffusion couple of Ge island (~1350Å) on Pt (~330Å) thin film annealed at 500°C/90min. The vertical line at ~76μm indicates the initial position of island/thin film boundary (or interface line). (b) A plot of compound thickness versus beam position across the reacted zones. Thicknesses were obtained from RUMP simulations. Vertical dotted lines were drawn to partition different Pt-Ge compounds identified in (a). The horizontal dotted lines indicate the expected total thickness for a particular germanide, assuming that the deposited platinum film was uniform and that only germanium atoms were the moving species.* 80

4.11 *A plot of Pt and Ge counts versus beam position for a diffusion couple of Ge island(~1360Å) on Pt thin film(~330Å) annealed at 500°C/30min. The number of counts were obtained from RUMP using integration command. The vertical line corresponds to the position of the initial interface between Ge island and the surrounding Pt thin film. A well pronounced platinum dip at ~85μm is clear indication that platinum atoms have migrated to the left of the dip and are congregating in the region between the interface line and the dip. On both platinum and germanium data, a "spur" is notable on the interface line.* 82

4.12 *(a) A plot of compound composition($PtGe_x$) versus position for a lateral diffusion couple(Ge island(~1350Å)) on Pt (~330Å) thin film annealed at 500°C/30min. The vertical line at ~62μm indicates the initial interface between island and surrounding thin film. (b) A plot of compound thickness versus beam position across the reacted zones. Thicknesses were obtained from RUMP simulations. Vertical dotted lines were drawn to partition different Pt-Ge compounds identified in (a). The horizontal dotted lines indicate the expected total thickness for a particular germanide, assuming that the deposited platinum film was uniform and that only germanium atoms were the moving species.* 83

4.13 *A plot of Pt and Ge counts versus beam position for a diffusion couple of Ge island(~1360Å) on Pt thin film(~330Å) annealed at 500°C/180min. The number of counts were obtained from RUMP using integration command. The vertical line corresponds to the position of the initial interface between Ge island and the surrounding Pt thin film. A more prominent platinum dip at ~129μm is clear indication that platinum atoms have migrated to the left of the dip and are congregating in the region between the interface line and the dip. On both platinum and germanium data, a "spur" is notable on the interface line.* 84

4.14 *(a) A plot of compound composition($PtGe_x$) versus position for a lateral diffusion couple(Ge island(~1350Å)) on Pt (~330Å) thin film annealed at 500°C/180min. The vertical line at ~89μm indicates the initial interface between island and surrounding thin film. (b) A plot of compound thickness versus beam position across the reacted zones. Thicknesses were obtained from RUMP simulations. Vertical dotted lines were drawn to partition different Pt-Ge compounds identified in (a). The horizontal dotted lines indicate the expected total thickness for a particular germanide, assuming that the deposited platinum film was uniform and that only germanium atoms were the moving species.* 85

4.15 *(a) Annealing time vs length(L_D) of individual germanide phases at 500°C showing phase formation sequence and parabolic dependence of compound growth on annealing time in Pt-Ge lateral diffusion couples. Lateral measurements used are those from SEM micrographs. Alphabetical letters indicate different regions as labelled on SEM micrographs. The plots in (b) are only displayed to reflect a more conventional version of the ones in (a).* 87

A.1 *RBS spectra obtained from an as deposited sample displayed with RUMP simulation to confirm composition and thickness agreement with actual data.* . . 97

A.2 *RBS spectra(top) obtained from samples annealed at 200(top) and 220°C(bot) for annealing periods of 80 minutes. Both spectra are displayed with their RUMP simulations to confirm agreement with actual data.* 98

A.3 *RBS spectra(top) obtained from samples annealed at 250(top) and 275°C(bot) for annealing periods of 80 minutes. Both spectra are displayed with their RUMP simulations to confirm agreement with actual data.* 99

B.1 *RBS spectrum from a sample annealed at 250°/10 min. Simulation suggests platinum as the dominant diffusing species during Pt_2Ge formation. Thicknesses are given in units of 10^{15} at/cm^2.* 100

List of Tables

1.1 *Comparison between predicted and observed first phase formation in metal-germanium systems. Corresponding metal-silicides are also listed in the last column for comparison Wittmer et al* 11

1.2 *Summary of results for phase formation in Pt/Ge system obtained by Hsie and Chen [1], Marshal et al [2] and Grimaldi et al [40].* 22

3.1 *Table showing sample to sample variation in* $PtGe_2$ *activation energy.* 53

4.1 *Table summarising lateral dimensions(widths) of growing platinum germanide compounds observed using SEM and micro-Probe measurements. Alphabetical letters* **B**, **C** *and* **D** *indicate different regions as labelled on SEM micrographs.* 86

Chapter 1

Introduction

1.1 Background

Material science research has long been on the forefront of technological advancement. Research output in material science has not only achieved tremendous progress in our knowledge of materials and their interaction processes, but also contributed considerably to both realized and prospective betterment of human condition. Unlike in other exotic fields, whenever a positive research output is announced in material science, the benefit does not only satisfy academic enquirey, it has profound impact in such areas as the fabrication of microelectronic devices which drive today's modern technology.

Wherever two dissimilar materials were put into intimate contact and thermally treated at elevated temperatures to effect a solid state reaction, the information exposed about the behaviour of specific materials had generated even more research interest. Metal silicides, in particular, have so far received a relatively large share of research effort. A wide range of transition metal silicide systems has been intensively investigated, viz Ni-Si, Co-Si, Pt-Si, Pd-Si etc. The intensive investigation in metal silicides has been provoked by their wide application in microelectronics industry.

Most silicides have low electrical resistivity and can sustain their stability at high temperatures, making them suitable candidates for application in integrated circuits devices, either

as contacts or inter-connects. Low resistivity is crucial in intergrated circuits in that it improves the speed of electronic devices and reduces ohmic heating. In metal oxide silicon field effect transistors (MOSFET), silicide layers are introduced at junction depth specifically to lower the resistance of source and drain areas. Another advantage of silicides is that they readily lend themselves in passivation processes, i.e. they oxidise in air producing a self protective SiO_2 surface barrier. For these and many other advantages in microelectronic technology, the family of M_xSi_y remains the subject of intensive investigation in material science.

In contrast to the case of metal silicides, the study of metal germanides has been relatively dormant [1, 2]. The only prominent research attention paid to metal germanides was in the late 50s, and since then, metal germanides research had largely remained dormant. It was only recently, in the late 80's, that germanides received renewed research interest [3]. With the possible introduction of SiGe in the microelectronic industry, a more thorough investigation in metal germanides becomes even more crucial. Silicon and germanium are very similar in structure and atomic properties. Their atoms are tetravalent, they both have four electrons in their outermost shell, they are both elemental semiconductors, and can be subjected to a large scale of processing steps without problems of decomposition, which suggests that the substitution of one element by the other should be possible [4].

From literature review of recent publications, it would appear that current research trends involving germanium have shifted the focus more to Ge_x-Si_{1-x} alloys [5-8] The shift to GeSi research had come as a result of the emergence of bandgap engineering of semiconductor heterostructures, a relatively new technique in which arbitrary band structures of new semiconductor materials and devices are produced by doping and spatially varying the composition of a semiconductor over distances ranging from a few angstroms ($\sim 2.5\mathring{A}$) to a few microns. Si and Ge have 4% difference in the lattice constants [9], and if critical thickness is exceeded during growth of one on the other, it results in strains, which may be used to vary bandgap energy and band discontinuities. A more detailed account of bandgap engineering can be found in ref [10].

The wide range of techniques established in the study of metal silicides are equally applicable in metal germanides. It was reported in previous studies that in parameters such as first phase nucleation, phase formation sequence, dominant diffusing species and growth kinetics, the behaviour of metal germanides is largely similar to their corresponding silicides [1, 2]. Germanium is of particular importance for the following reasons: it has high mobility for both electrons and holes, which opens the possibilities of high speed complementary transistor, it has very low carrier freeze-out temperatures, it can be used as ohmic contact material to n-type in GaAs devices [2, 11, 12], and it is commonly used in solid state radiation detectors. Moreover, strained layer (Ge,Si)/Si heterostructures were reportedly shown to exhibit a variety of interesting properties attributed to band structure modifications [13].
An understanding of Metal/GeSi contacts and metal-GeSi compounds is essential for developing novel GeSi devices and large scale integrated circuits [14]. The compound PtSi is currently one of the widely used silicides in Si devices due to its highest barrier Schottky contact ($\sim$ 0.68 eV) for bipolar devices [15]. This and the possibility of a new 8-12 μm Pt(Ge_xSi_{1-x}/GeSi Schottky barrier infrared photodetector, had resulted in thermal reaction between platinum and GeSi alloy receiving particular research attention.
For succesfull implementation of SiGe alloy technology, knowledge of Metal-Germanium interaction is as important as that of the corresponding Metal-Silicon. It is therefore of interest to investigate platinum-germanium interaction in depth.

1.2 Reactions in Bulk and Thin Films

Bulk and thin film diffusion couples are two extreme regimes in which solid state interactions are usually investigated. Analytical tools used to monitor phase formation in bulk diffusion couples include microprobe tracing of a reacted section to obtain compositional information, and light microscopy of etched cross sections of a sample for phase identification [16]. X-Ray diffraction is also used to accomplish phase identification. The thickness of coupling phases in bulk couples may vary from several hundreds of micrometers to a few millimeters, and

all intermediate phases predicted in phase diagrams can co-exist and grow simultaneously during solid state reaction [17]. High temperatures and long annealing times are required due to the large interdiffusion zones [18].

Unlike in the bulk, one phase is usually found to grow at a time in thin film diffusion couples. The sequence of phase formation follows a well defined pattern in which one compound forms untill the metal film is consumed and the next phase starts to grow. The failure to observe "multi-phases" in thin film reactions has been attributed to the presence of "critical thickness" of a single compound layer, which is defined as the thickness beyond which the second compound layer can coexist with the first [19, 20]. In thin film studies, the deposited metal layer which serves as a source of supply during first phase formation is usually so thin that it gets exhausted before the first compound grows to its "critical thickness". Reaction kinetics in thin films are largely monitored with a non-destructive RBS technique [21]. As in the bulk diffusion couples, phase identification in thin films is also accomplished by X-Ray diffraction methods. Other usefull techniques include Resistivity measurements [22], Transmission and Scanning Electron Microscopy (TEM and SEM respectively). If thin film and bulk diffusion couples are seen as two extremely opposite regimes, then the link between the two is to be found in lateral diffusion couples.

1.3 Lateral Diffusion Reactions

First developed by Zheng [23], the novel technique of lateral diffusion was to bridge the gap between conventional thin films and bulk diffusion couples. An excellent treatment on the transition between thin film and bulk diffusion couples can be found in Ref. [24] where Zheng et al investigate the behaviour of Ni/Si system in one of the most detailed lateral diffusion experiments. Sample preparation techniques used in conventional thin films are equally applicable in lateral diffusion couples. In brief, lateral diffusion couples are prepared by vacuum deposition of a thin layer of semiconductor on substrates of NaCl, Al_2O_2 or SiO_2. Metal layer is then subsequently deposited through the aperture windows of a patterned

silicon mask made by photolithographic techniques and selective etching on Si wafer. The result is a thin film of semiconductor, with metal islands on top, see Fig 1.1 where a schematic illustration of this state of affairs is shown for the case of metal islands on germanium thin film. The same procedure is followed when preparing samples of semiconductor islands

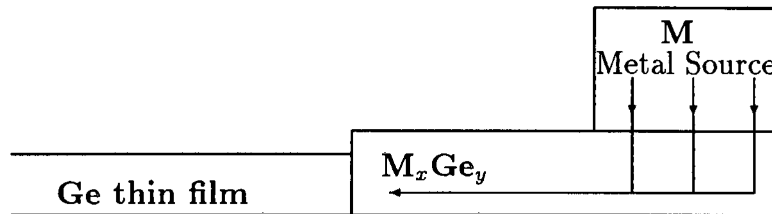

Figure 1.1: *Schematic illustration of lateral diffusion sample showing platinum island on germanium thin film. Vertical arrows indicate the direction of atomic mobilty during initial stages of the reaction. Once the underlying atoms are consumed, the island starts to supply atoms in the lateral direction. It is assumed in this sketch that the metal(M) is the dominant diffusing species during first metal-germanide formation.*

on metal thin film, see Figure 1.2. Prior to lateral diffusion sample preparation, it is of importance to establish the dominant diffusing species during the first compound formation, for this provides a pointer to sample configuration.

It is important to prepare islands of dominant diffusing material on a thin film of choice, as the inward flux of atoms from the surrounding thin film (to the source region) can result in thin diffusion zone and ultimately a crack between thin film and source region. Differences on the diffusing species are are however not uncommon between conventional thin films and lateral diffusion couples. Chu et al [25] investigated Ni-Si interaction in thin films and found Ni as the "dominant diffusing species at a temperature of 325°C". Zheng et al [24] investigated the same system(Ni-Si) using lateral diffusion technique, and observed that "both Ni and Si are the dominant diffusing species at temperatures above 400°C".

The initial stage in lateral diffusion couples is similar to that of conventional thin film couples, i.e. initial reaction takes place between atoms from the island and those from the

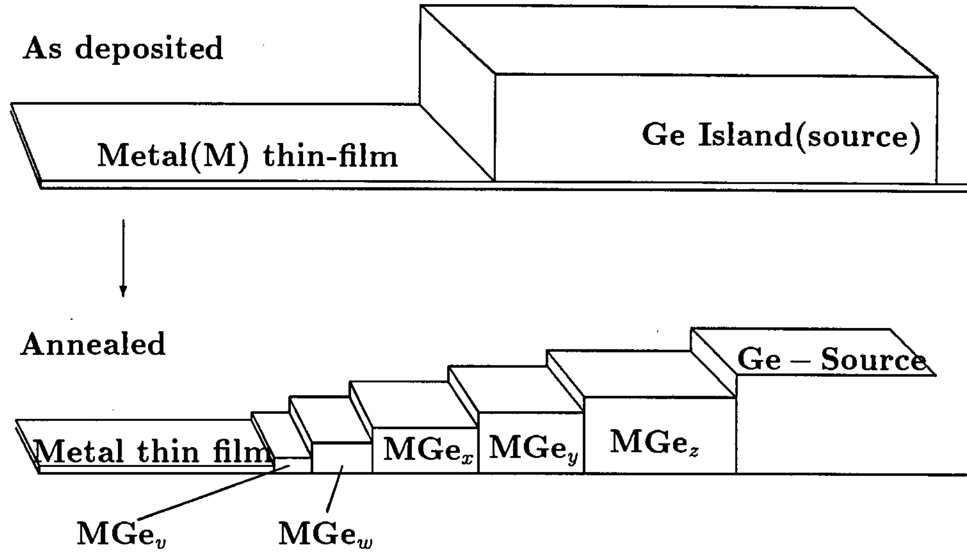

Figure 1.2: *Schematic diagram showing lateral diffusion couple for Pt-Ge system both before and after annealing. Different compounds are indicated with $z > y > x > w > u$.*

underlying thin film. This continues untill total consumption of atoms directly below the island region. Excess atoms in the islands will then start to diffuse laterally to react with atoms in the thin film surrounding the island. In order to have sufficient atomic diffusion from the source of supply, it is crucial that during deposition, the thickness ratio of island to thin film be far greater than that of the phase most rich in island element [17].

Once atomic depletion starts in the source region, the growing phase starts to extend laterally, and nothing stops it but its critical length. As the resulting phase grows laterally out, the supplying source shrinks in, lengthening the diffusion zone to a point where the supply of atoms gets too weak at the compound/thin film interface, resulting in a change in phase. Change in the supply of atoms determines when the growth of the next phase is initiated, however, prediction of the growing compounds depends on empirical rules [26]. With enough atoms in the supplying source, long time anneals at high temperatures result in the formation of several phases predicted in the phase diagram. In Figure 1.2 displays a schematic diagram simulating lateral diffusion experiment results for Metal-Ge system.

Qualitative analysis of diffusion length is readily accomplished with Scanning Electron Microscopy(SEM) and TEM(Transmission Electron Microscopy). Microprobe tracing provides a strong complementary technique to both SEM and TEM. By scanning across reacted zones with a micro-beam of α particles, RBS can be done on a micro-scale. Compound thicknesses can therefore be resolved at different reacted zones.

With the knowledge of deposited thin film and island thicknesses, resolving compound thicknesses at different reacted regions will therefore provide a pointer to dominant diffusing material. Both SEM and TEM are limited in their resolution of dominant diffusing species at specific reacted regions. Microprobe tracing thus suggests itself as an evident supplement to SEM and TEM in the study of lateral diffusion reactions. It is therefore suprising that only one article, Ding et al [27], had so far reported the use of nuclear microprobe in the study of lateral diffusion reactions.

To unravel reaction kinetics, the width of individual phases are plotted against annealing time. Information about composition in the reacted zones can be obtained from either Energy Dispersive Spectroscopy(EDS) or Rutherford Backscattering Spectrometry(RBS). Long diffusion distances, and the ease to perform compositional and structural measurements, are amongst the advantages of using lateral diffusion couples to study solid state reactions [19]. The simplicity in determining the moving species without interposing extra material between coupling layers adds to advantage.

1.4 Phase Formation Sequence

Binary systems usually have several equilibrium phases, though not all equilibrium phases might exist as dominant growing phases during solid state reactions. It is of crucial importance in thin films studies to know which of the stable phases forms first during solid state reactions. In any given system, phase transformation occurs when the initial state of the system becomes unstable relative to the final state. Under thermal treatment, binary systems always strive for the most stable state.

The reason why phase transformation takes place at all is that the previous phase had become unstable, and must therefore give way for a more stable phase. In cases where phase formation/transformation) is effected through isothermal treatment of binary alloys at constant pressure, (as is a long standing tradition in thin film studies), a good measure of phase stability is Gibbs Free energy of the system. Gibbs Free energy of the system is given by:

$$G = H - TS \tag{1.1}$$

where H is the Enthalpy S the Entropy and T the absolute temperature. In thermodynamic terms, a system is said to be at its equilibrium state when its Gibbs free energy is most negative. Phases which exist when the system is at stable equilibrium are called stable phases. Phases which exist when the system is not at its equilibrium state (i.e. when G is not minimum), are called metastable phases. Phase formation/transformation results as the system strives for its lowest possible free energy state. The consequence of Gibbs free energy rule is that for any transformation between two phases, the change in Gibbs free energy (ΔG) must be negative.

Various rules (and models) were proposed to predict the sequence of phase formation during solid state reactions. One of the earliest rules was the so called WB rule in which Walser and Bene [26] used the huge data available on metal-silicon systems to device an empirical rule to predict the first phase to form during solid state reactions.

1.4.1 Walser-Bene and other Rules

The first phase prediction rule proposed by Walser and Bene states: "*The first compound nucleated in planar binary reaction couples is the most stable congruently melting compound adjacent to the lowest temperature eutectic on the bulk equilibrium phase diagram*" [26]. Several experiments were done to check against the validity of WB rule when extended to germanides systems. A thorough investigation in metal-germanides was carried out by Wittmer et al [28]. In their experiments, the formation of germanides were investigated for Co, Hf, Mn, Ni, Pd and Rh at temperatures ranging between 100 and 600°C. It was reported

in their results that the WB rule was succesfull in predicting the first phase to form in Co, Hf, Ni, Pd and Rh germanide systems. It was however only in the case of Pd on Ge that their results showed inconsitency with the WB rule. The results of Wittmer experiment are summarised in Table 1.1. In another experiment, an equally thorough investigation was done by Marshal et al [2] on a number of "representative metals on Ge", viz Al, Ag, Au, Er, Ni, Pd, Ta and Ti. They reported in their results that germanides formation characteristics were found to be similar to those of their corresponding silicides. As in the case of Wittmer et al, Marshal et al also noted that there exceptional cases existed where some germanides systems violate the WB first phase prediction rule.

Since WB rule [26] was based on M-Si systems, its relative success in germanides systems seems to suggest that the phase formation sequence in some metal germanides systems can be predicted by direct inference from the corresponding metal-Si systems [2]. There is however no rule which succesfully applies to all either metal-germanide or metal-silicon system.

The WB rule is largely succesfull in predicting first phase formation in M-Si systems, but that is how far it goes. Tsaur et al extended the WB rule to predict the phase following the first in metal silicon systems. After the first silicide phase formation, the rule by Tsaur et al [29] states: "*The next phase formed at interface between the first phase and the remaining element (Si or metal) is the nearest congruently melting compound richer in ureacted element. If the compound between the first phase and the remaining element are all non-congruently melting compounds (such as peritectic and peritectoid phases), the next phase formed is that with the smallest temperature difference between the liquidus curve and the peritectic (or peritectoid) point*".

Earlier phase sequence prediction rules ignored thermodynamic data such as heats of formation (ΔH) and entropy (ΔS) of the systems under consideration. It was not untill Pretorius et al [30, 32] proposed the effective heat of formation (EHF) model that thermodynamic data came to be considered usefull in phase sequence prediction.

PREDICTED AND OBSERVED GERMANIDE COMPOUNDS		
Metal germanide System	Predicted first compound formed	Observed First Compound Formed X-Ray diffraction analysis
Co-Ge	Co_2Ge	Co_2Ge
Hf-Ge	Hf_5Ge_3	Hf_5Ge_3
Mn-Ge	Mn_5Ge_3	Mn_5Ge_3
Ni-Ge	Ni_2Ge	Ni_2Ge
Pd-Ge	PdGe	Pd_2Ge
Rh-Ge	RhGe	RhGe

Table 1.1: *Comparison between predicted and observed first phase formation in metal-germanium systems. Corresponding metal-silicides are also listed in the last column for comparison Wittmer et al*

1.4.2 Effective Heat of Formation (EHF) Model

Recently, Pretorius et al [30] made use of thermodynamic data and proposed the effective heat of formation (EHF) model. Pretorius' EHF model predicts both first phase and subsequent phase formation sequence by considering the effective concentration of two reacting atomic species at growth interface. The effective concentration was chosen to be that of the lowest eutectic (or liquidus minimum) [30, 31].

The model emphasizes that during solid state reaction, phase formation at an interface is a dynamic non-equilibrium process, and one compound phase usually forms at interface, so that the lowest energy state for the system is not a result of a mixture of phases. When phase transformation takes place, the system prefers to lower Gibbs free energy change (ΔG) to a minimum. Following equation 1.1, change in Gibbs free energy is given by:

$$\Delta G^o = \Delta H^o - T\Delta S^o \tag{1.2}$$

where ΔH^o and ΔS^o are, respectively, changes in Enthalpy and Entropy of the system during solid state reaction at absolute temperature T. A good measure of ΔG^o is ΔH^o since ΔS^o is normally too small ($\sim$0.001 kJ.deg^{-1}). The heat released by the system during phase formation/transformation depends on the effective conentration of the limiting element in the compound to be formed. The EHF model defines the effective heat of formation (ΔH') as follows [32, 33]:

$$\Delta H' = \Delta H^o \left(\frac{Effective.concentration.limiting.element}{Compound.concentration.limiting.element} \right) \tag{1.3}$$

Using effective concentration of limiting element at interface and effective concentration of limiting element in the compound to form, the EHF' first phase formation rule states: *"The first compound to form during metal-metal interaction is the phase with most negative effective heat of formation (ΔH') at the concentration of the lowest temperature eutectic(liquidus) of the bimary system".* After first phase formation, the model predicts the subsequent phase formation sequence as follows: *"After first phase formation in metal-metal binary systems, the next phase to form at interface between the compound phase and the remaining element*

is the next phase richer in unreacted element, which has the most negative effective heat of formation ". The EHF model had been tested with measurable success in the prediction of first phase and subsequent phase formation in germanides, silicides, aluminides, Au-metal systems, Cu-metal systems etc.

A phase diagram for the Pt-Ge system is displayed in Figure 1.3. From the (Pt-Ge) phase diagram , the congruent phase with the most negative effective heat of formation is Pt_2Ge, and therefore the one predicted by EHF model as the first phase to form. The 2nd predicted

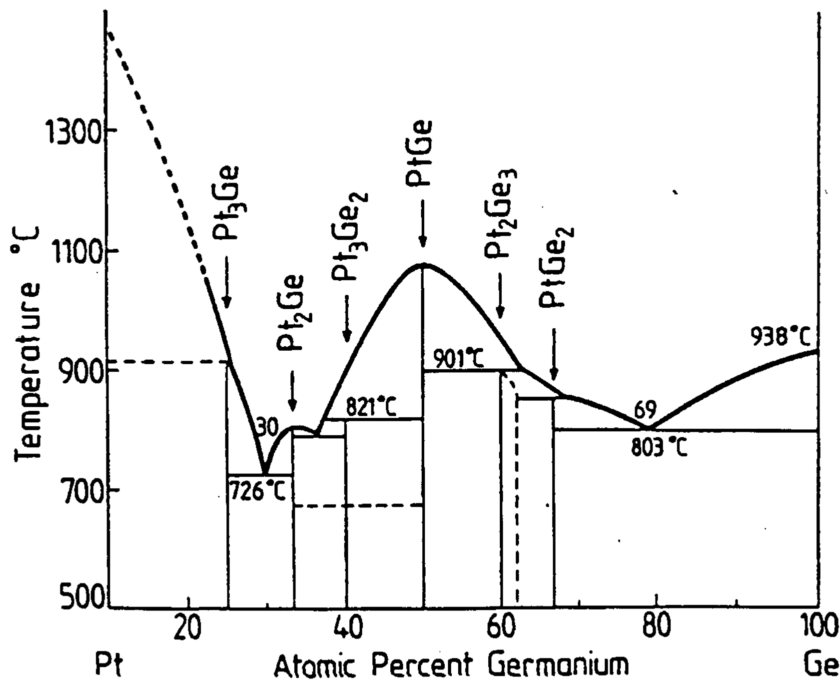

Figure 1.3: *Phase diagram for Pt-Ge system*

phase would be PtGe, followed by $PtGe_2$.

Table 1.4.2 summarises previous experimental observation for Pt-Ge system. The first and second phase results obtained by Hsieh and Chen [1], and Marshal et al [2] are in agreement with the EHF model, see Table 1.4.2 (at the end of Chapter 1). However, the results obtained by Grimaldi et al [40] do not present Pt_2Ge as the first phase to form, and are therefore in disagreement with the EHF model.

In this work the Pt-Ge system will be investigated and the findings will be compared with previous experimental results and those predicted by the EHF model. Specific parameters to be investigated are outlined in the Scope of investigation.

1.5 Growth Kinetics

The rate at which the compound grows at the interface is one aspect of major interest in thin film analysis. To evaluate the growth kinetics of a system, compound growth thickness is measured as a function of annealing time or temperature. There are generally two distinct kinetic patterns followed by solid state reactions that lead to silicide or germanide formation. They are (i) layer-by -layer growth kinetics with well defined temperature dependence, and (ii) rapid non-uniform growth with critical temperature dependence. The latter pattern usually takes place in a narrow temperature range, making it difficult to identify clearly the diffusion kinetics involved. Under this pattern, compound formation is thought to be a result of nucleation process [34] which involves sudden transformation without measurable composition gradient through the thin film thickness. $NiSi_2$ is well known to form via nucleation process [35].

The layer-by-layer kinetic pattern exhibits lateral growth uniformity and takes place over a relatively wide temperature range. The compound growth process in this case may be proportional either to the time or to the $(\text{time})^{1/2}$. The dependence in time follows from limiting mechanisms responsible for compound growth [36].

The parabolic relationship with time indicate a diffusion limited growth process, where the process of growth is limited by transport of the material through the growing compound. The growth rate slows down as the compound grows thicker. The reaction follows the following equation:

$$x_f^2 - x_0^2 = D(t_f - t_0) \tag{1.4}$$

where x_0 and x_f are compound thicknesses at time t_0 and t_f respectively, and D is the diffusion rate constant. The diffusion constant is defined as:

$$D = D_0 exp(-E_a/k_b T) \tag{1.5}$$

where T is the absolute temperature, k_b=Boltzman constant, E_a=activation energy and D_0=pre-exponential factor. Equation 1.5 is commonly reffered to as Arrhenius equation. E_a can be obtained from a plot of ln$D$ *vs* $1/k_b T$.

The linear relationship of growth with time is indicative of an interfacial reaction limited process. The reaction in this mode of growth follows the equation:

$$x_f - x_0 = K(t_f - t_0) \tag{1.6}$$

where K is the interfacial reaction constant, and all other parameters have the same meaning as in equation 1.4.

1.6 Growth Kinetic Analysis by Temperature Ramping

The quickest and most convenient way to monitor closely the growth kinetics of a system is by temperature ramping. By programing the heater over a temperature range of interest, it is possible to observe all phases of a system from one sample, in one experimental run. This is a drastic departure from traditional, conventional isorthermal annealing, where many samples are used to obtain similar parameters. In conjunction with "*dynamic*" RBS, the ramping technique is time effective.

The technique, however, presupposes knowledge of whether the compound formation reaction follows diffusion controlled or interfacial reaction controlled mode [19]. For a diffusion limited reaction, ramped at a rate dt/dT, the compound growth is governed by the following equation.

$$x^2 = \int_0^t 4\tilde{D} dt = \int_{T_0}^{T} 4\tilde{D} \frac{dt}{dT} dT \tag{1.7}$$

Where x is the thickness of the compound formed, $\tilde{D}$ the interdiffusion coefficient in the compound, t the reaction time and $\frac{dT}{dt}$ the constant ramping rate. The interdiffusion coefficient can be written as $\tilde{D} = \tilde{D_0}$ exp(-ΔH/kT), where ΔH is the activation enthalpy of interdiffusion, and $\tilde{D_0}$ the pre-exponetial factor, k and T have usual meaning. By substitution and intergration, equation 1.7 takes the form:

$$x^2 = 4\tilde{D}_0 \frac{dt}{dT}\frac{kT^2}{\Delta H} exp\left(-\frac{\Delta H}{kT}\right) - 4\tilde{D}_0 \frac{dt}{dT}\frac{kT_0^2}{\Delta H} exp\left(-\frac{\Delta H}{kT_0}\right) \tag{1.8}$$

At t = *0*, temperature is typically low, and no reaction occurs, so we can take $T_0 = 0$ K, and the right term of equation 1.8 disappears. Thus, ignoring the right term from equation 1.8, a plot of $\ln(x^2/T^2)$ versus $1/kT$ yields a straight line with slope ΔH. When the compound growth is interfacial reaction controlled, the following equation governs the process:

$$x = \int_0^t K dt = \int_{T_0}^{T} K \frac{dt}{dT} dT \tag{1.9}$$

Where $K = K_0$ exp(-$\Delta H/kT$) is the interfacial reaction constant. By substitution and intergration, equation 1.9 takes the form:

$$x = K_0 \frac{dt}{dT}\frac{kT^2}{\Delta H} exp\left(-\frac{\Delta H}{kT}\right) - K_0 \frac{dt}{dT}\frac{kT_0^2}{\Delta H} exp\left(-\frac{\Delta H}{kT_0}\right) \tag{1.10}$$

Applying the same argument as in diffusion limited equation, see equation 1.8, activation enthalpy, ΔH, is now calculated from slope of $\ln(x/T^2)$ versus $1/kT$.

It must be pointed out that in cases where the compound under consideration has already grown to a measurable thickness at initial temperature T_0, then the right terms of equations 1.8 and 1.10 cannot be ignored.

1.7 Diffusion

Diffusion in solids is important for two cardinal reasons. First, knowledge of diffusion is fundamental to the understanding of changes that occur in solids at higher temperatures. Second, the study of diffusion gives exposure of how atoms move in solids, which is intimately connected to the study of atomic mobility in thin films, where dominant diffusing species

are determined using a marker technique.

In contrast to gases, diffusion in solids is not straight forward. "*As in a gas, diffusion in solid proceeds by transport of mass, thermal conduction by transport of energy, and electrical conduction by transport of charge. But there the similarity ends*" [37]. A gas atom spends most of its time travelling freely through distances that are large in atomic regime, while an atom in solid is strictly confined by attractive forces exerted by its neighbours.

From a macroscopic point of view, diffusion process is relatively straight forward, atoms will diffuse from their region of higher concentration to their region of lower concentration until equilibrium is reached. This general rule does not apply blindly in thin films, it has to respect other factors besides concentration, e.g. energy barrier which the diffusant has to overcome, path followed etc. In thin film studies, main focus is on determining dominant diffusing species and the mechanisms by which they diffuse. Precise determination of dominant diffusing species is difficult to establish, and identification of actual diffusion mechanism is even more complex. Early theories suggested four main possible mechanisms by which atoms diffuse, viz interstitial diffusion, rotational or interchange mechanism, substitutional and grain boundary mechanism. Figure 1.4 shows schematic representation of the first three diffusion mechanisms. In mechanism (a), the diffusion process requires much energy as the surrounding atoms have to be pushed apart. The required energy is even more for closed packed solids, rendering the mechanism highly unlikely. Mechanisms (b) and (c) are commonly encountered in thin films study. The plausible explanation for vacancy mechanism (c) is that in almost all crystals, some of the lattice sites are unoccupied. These sites are called vacancies. If one atom, preferably an impurity, jumps into the vacancy, the atom is said to have diffused through a vacancy mechanism. Vacancy diffusion mechanism has been proposed as the one responsible for the formation of Pd_2Si [38].

An atom is said to have diffused by an interstitial mechanism when it passes from one interstitial site to one of its nearest neighbour interstitial site without permanently displacing any of its host atoms. The interstitial atom faces a constriction due to the host atoms as shown in Figure 1.4(c). Thus an atom has to jump a certain energy barrier for this mechanism to

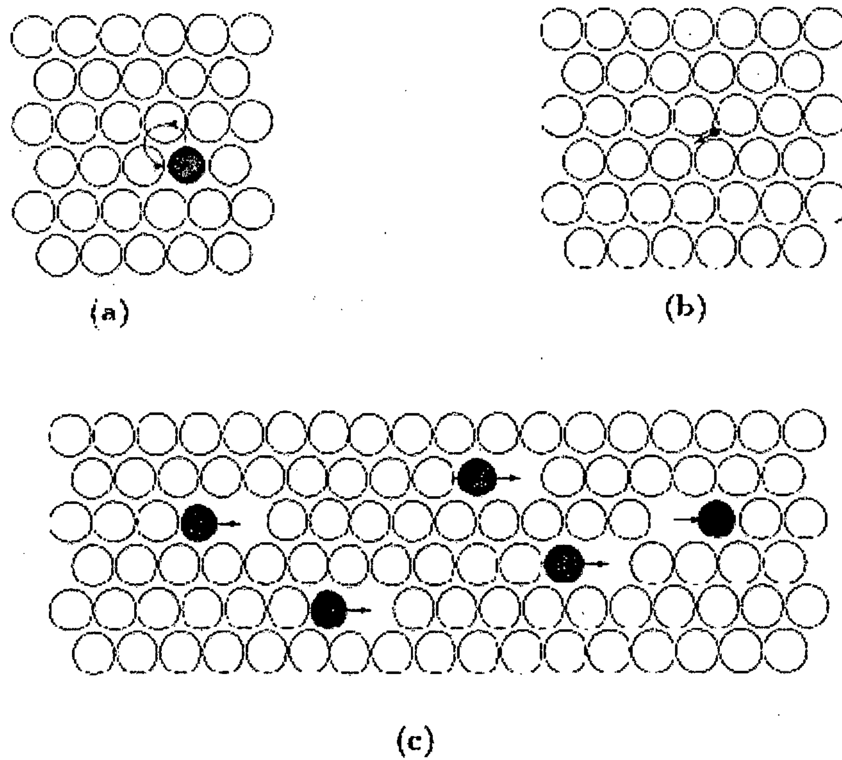

Figure 1.4: *Schematic illustration of three main diffusion mechanisms. (a). Rotational/Interchange mechanism (b). Interstitial mechanism (c). Vacancy/Substitutional mechanism*

occur. One of the commonly encountered mechanisms in thin film studies is grain boundary mechanism. A grain boundary may be viewed as an array of dislocations seperating two single grains of a crystalline material with a misorientation between them.

Experiments have shown that the mean jump frequency of an atom in free surfaces and grain boundaries is higher than that of an atom in the lattice. The diffusivity is therefore higher in this regions. The grain boundary mechanism is perhaps the most important as it is the most probable in thin films. Peterson et al [39] reported grain boudary diffusion as the formation mechanism for $IrSi_3$. Diffusion of solids at macroscopic level is best summarised by Fick's laws of diffusion. The first law states that "*if an inhomogeneous single phase alloy is annealed, there will be a net flux of atoms in a manner which will decrease the concentration gradient.*" The second one states: "*the rate of change of concentration of the species across a plane is proportional to the flux gradient of the species across the plane.*"

1.8 Scope of this investigation

The aim of this study is to obtain a basic understanding of interaction between platinum and germanium thin films. As pointed out earlier, the family of M_xGe_y has not been as well researched as their corresponding metal-silicon systems. If Si-Ge alloy technology is to be implemented successfully in both VLSI and ULSI devices, interaction between metal and germanium must be fully understood.

The understanding of any system is incomplete without knowledge of such basic parameters as various existing phases and their formation temperature ranges, the sequence of phase formation, phase growth kinetics, dominant diffusing species, diffusion mechanisms and activation energies of growing phases. Save for diffusion mechanisms, this study attempts to focus on all parameters above for the Pt-Ge system. While the Pt-Ge system has been investigated before, reported results, however, reveal the existing confusion and uncertainty regarding phases observed at particular temperatures [1, 2, 40].

The Pt-Ge system contains as many as 6 phases in its phase diagram, viz Pt_3Ge, Pt_2Ge,

Pt_3Ge_2, PtGe, Pt_2Ge_3 and $PtGe_2$, see Pt-Ge phase diagram in Figure 1.3. To appreciate the existing confusion and uncertainty regarding these phases and their formation temperatures, we need only review some of the published experimental results on Pt-Ge system. Hsie and Chen [1] reported detecting Pt_2Ge, PtGe, Pt_2Ge_3 and $PtGe_2$ at temperatures of 160, 250, 350 and 400°C respectively. Marshal et al [2] reported observing Pt_2Ge at 250°C, followed by PtGe in the temperature range 260-300°C, Pt_2Ge_3 was observed as the third phase at 400°C and the last phase, $PtGe_2$ was reportedly detected in the range 500-600°C. It can be noted that while the results of Hsie and Chen [1] agree with those of Marshal et al [2] on the sequence of phase formation, they however differ by considerable margins on the formation temperatures. In another experiment Grimaldi et al [40] reported observing (in sequential order) Pt_3Ge_2, PtGe, Pt_2Ge_3 and $PtGe_2$ at 250, 300, 350 and 450°C respectively, See Table 1.4.2 for a summary of these previous experiments.

An attempt is made in this study to clear the confusion surrounding the phase sequence and temperatures of formation in Pt-Ge system. The growth kinetics of the phases shall also be investigated. In their experiment, Marshal et al [2] also investigated the dominant diffusing species for a particular observed phase, Pt_2Ge. In this study, we attempt to extend the investigation of dominant diffusing species to all identified phases, and the results obtained will also be used as a check against previous findings on Pt_2Ge formation.

The main focus of this study is on the behaviour of the Pt-Ge system in the lateral diffusion geometry. The sizes of microelectronic devises are shrinking, with lateral dimensions decreasing more rapidly than vertical dimensions [27]. Clear understanding and knowledge of processes associated with the edges of microelectronic devices therefore become increasingly important. The geometry of lateral diffusion couples paves the way to such understanding. The Pt-Ge system had not been investigated in the lateral diffusion regime before. An attempt is made in this study to use the lateral diffusion geometry to investigate various parameters mentioned earlier. A comparison will be made of the behaviour of Pt-Ge system in both lateral diffusion and conventional thin film regimes.

Techniques and procedures used in acquisition and analysis of data are explained in Chap-

ter 2. Experimental results of the study are all detailed, discussed and elaborated upon in Chapters 3 and 4. An overall summary and various conclusions are given in Chapter 5. On the same Chapter 5 we also hint on some few aspects regarding possible future work on this project.

Grimaldi et al [40]			Hsieh and Chen [1]			Marshal et al [2]	
Temp (°C)	Annealing time(h)	Phases Formed	Temp (°C)	Annealing time(h)	Phases Formed	Temp (°C)	Phases Formed
150-230	2	No interdiffusion	160	3	Pt_2Ge	250	Pt_2Ge
250	0.5	Pt_3Ge_2 + PtGe	250	1	PtGe	260-300	PtGe
300	0.5	PtGe	350	1	Pt_2Ge_3	400	Pt_2Ge_3
350	0.5	Pt_2Ge_3	400	1	$PtGe_2$	500-600	$PtGe_2$
400	0.5	$PtGe_2$	500	1	$PtGe_2$		

Table 1.2: *Summary of results for phase formation in Pt/Ge system obtained by Hsie and Chen [1], Marshal et al [2] and Grimaldi et al [40].*

Chapter 2

Experimental Techniques and Procedure

The analysis of material interactions in thin films require sensitive, and sometimes sophisticated, experimental techniques. Throughout this investigation, samples were prepared by vacuum deposition of Pt and Ge thin films on oxidised silicon substrates. The main analytical tool employed for characterization and analysis of samples was Rutherford Backscattering Spectrometry(RBS). Presented below is a brief review of theoretical concepts that underpin RBS, a brief explanation of marker technique, followed by details of sample preparation and experimental procedures.

2.1 Rutherford Backscattering

Rutherford backscattering spectrometry has proved both vital and sensitive an analytical tool in obtaining detailed microscopic information in the study of thin films. The concepts underlying backscattering technique have found application as early as 1967 in the first analysis of the composition of lunar soil. The origin of these concepts can be traced back to the famous Geiger and Marsden experiment of 1913. Both in concept and elementary execution, the simplicity of RBS remain unsurpassed. A more thorough and comprehensive

account of RBS can be found in refs [21, 41]. In brief, the RBS technique requires an ion source which generates charged particles whose energy is raised to a few MeV(typically 2-3 MeV) by a particle accelerator. The result is a monoenergetic beam of charged particles which is directed to the evacuated backscattering chamber chamber where it impinges on the sample to be analysed. Depending on the thicknesses involved, most particles are either transmitted through or absorbed by the target sample, while some are backscattered. The energy magnitude of the incident beam of particles is generally kept low enough to rule out possibilities of nuclear reaction during the collision process. Backscattered particles are detected with a solid state detector.

Throughout this study, the detector was positioned to detect particles with scattering angle of 165° and the sample normal was tilted 10° relative to the ion beam, see Figure 2.1. Backscatterd particles deposit energy into the detector, generating an electrical signal which

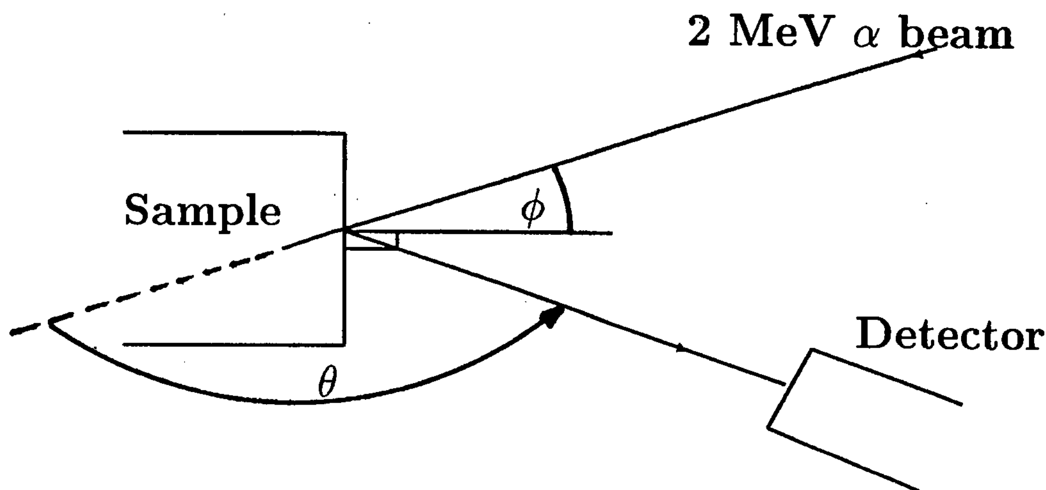

Figure 2.1: *Schematic diagram illustrating the experimental setup of Rutherford Backscattering. A 2 MeV alpha beam is incident on a sample. The sample normal is tilted by ϕ=10° from the incident beam and θ=165° is the scattering angle. The incident beam and the detector are on the same plane with the sample normal. All quantities refer to a laboratory frame of reference.*

is amplified and processed with fast analog and digital electronics. The final stage of the

data is a digitized spectrum. For purposes of correct interpretation of the spectrum, various factors are elaborated below, viz kinematic factor(K), energy loss(dE/dx) and differential scattering cross section($d\sigma/d\Omega$).

2.1.1 Kinematic Factor(k)

When a beam of monoenergitic α particles impinges on the target sample, energy is transfered from incident alpha particles to target atoms, and therefore energy deposited to the detector by backscattered particles is only a fraction of the incident energy. The interaction process between α paticles and target atoms is assumed to be a simple elastic collision. For this assumption to hold, two crucial conditions have to be satisfied: energy (E_0) of the projectile must be much larger than binding energy of the atoms in the target and there should be no resonance and nuclear reactions. This imposes an upper limit to the projectile energy, which limit depends on the specific choice of projectile and target atoms.

The simple elastic collision of alpha particles is best solved by applying the basic principles of conservation of energy and momentum. Figure 2.2 illustrates collision between an incident particle of mass m_1 and a stationary atom off mass M_2. After collision the projectile and

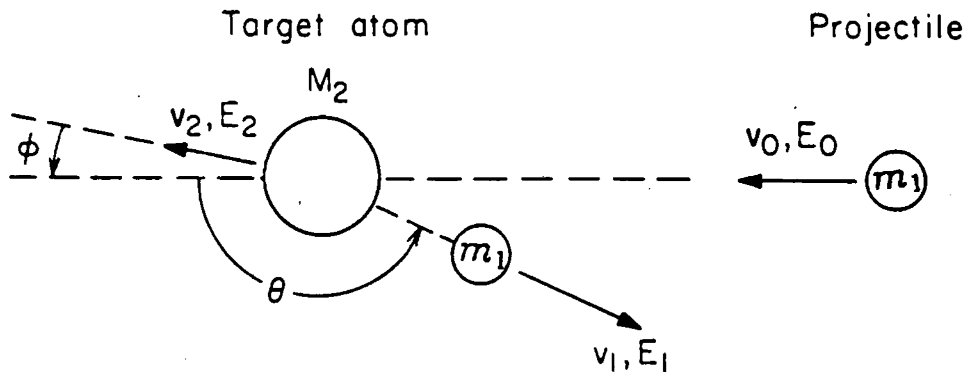

Figure 2.2: *Schematic representation of elastic collision between a projectile of mass* m_1*, velocity* v_0 *and a target of mass* M_2 *initially at rest.*

the target atom have velocities and energies v_1, E_1 and v_2, E_2 respectively. Angles θ and ϕ are positive, and all quantities refer to the laboratory frame of reference.

The magnitude of quantities v_i and E_i(i=1,2) explicitly depend on scattering angle θ and recoil angle ϕ. By considering basic principles of conservation of energy and momentum parallel and perpendicular to the direction of incidence, the following equations can be generated.

$$\frac{1}{2}m_1 v_0^2 = \frac{1}{2}m_1^2 v_1^2 + \frac{1}{2}M_2 v_2^2 \tag{2.1}$$

$$m v_0 = m_1 v_1 cos\theta + M_2 v_2 cos\phi \tag{2.2}$$

$$0 = m_1 v_1 sin\theta - M_2 v_2 sin\phi \tag{2.3}$$

By eliminating ϕ and v_2, one obtains the ratio

$$\frac{v_1}{v_2} = \frac{[(M_2^2 - m_1^2 sin^2\theta)^{\frac{1}{2}} + m_1 cos\theta]}{(m_1 + M_2)} \tag{2.4}$$

The kinematic factor is defined as the ratio of the projectile energy after the elastic collision to that before collision.

$$k \equiv \frac{E_1}{E_0} = \frac{v_1^2}{v_0^2} \tag{2.5}$$

From equation 2.5 the kinematic factor can be expressed as

$$\frac{E_1}{E_0} = k = \left[\frac{(M_2^2 - m_1^2 sin^2\theta)^{\frac{1}{2}} + m_1 cos\theta}{m_1 + M_2}\right]^2 \tag{2.6}$$

It is clear from the above equation that the energy of the projectile after scattering is dependent on scattering angle θ and the masses of projectile and target atoms. Energy E_1 of projectile has its maximum value if the scattering angle $\theta = 180^0$. It is also evident from the equation that energy of particles scattered by heavy elements is higher than that of those scattered by light ones.

2.1.2 Energy Loss (dE/dx)

When an incident particle enters a solid medium, its kinetic energy decreases as it traverses through the medium and collides with atoms in its inward path. The total energy loss depends on the thickness or total distance travelled by the incident particle, on the density and composition of the target, and on the velocity of the incident particle. If dE/dx is

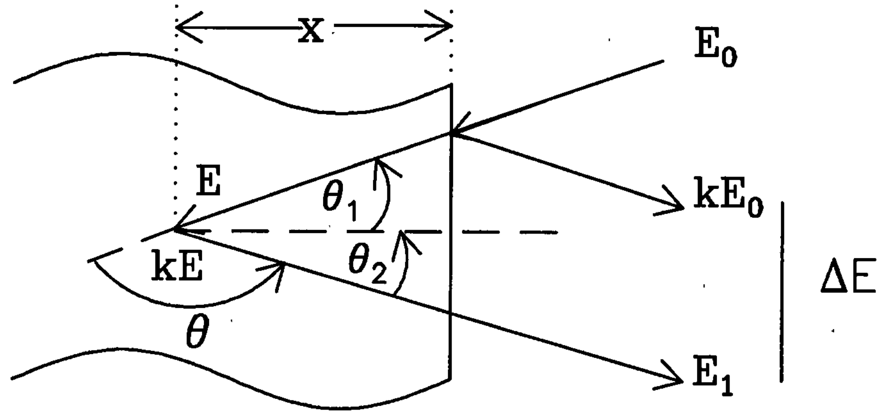

Figure 2.3: *Diagram illustrating scattering of incident particles on the surface and at depth x below the surface.*

known, energy E of a projectile can be calculated at any depth x below the surface of a thick sample into which the particle penetrates. For a projectile whose initial energy is E_0, see Figure 2.3, energy E at any depth x is given by the following equation.

$$E(x) = E_0 - (dE/dx)_{in} \frac{x}{cos\theta_1} \tag{2.7}$$

Where the subscript *in* denotes the inward path.

When a particle is scattered into the detector from the surface of the sample, the difference between its initial and final energy is only due to kinematic factor (K), and therefore the magnitude of its final velocity is KE_0. A particle scattered at depth x below the surface suffers a series of energy loses. It looses energy along its inward trip to the scattering point due to specific energy loss, at the scattering point due to kinematic factor, and finally along its outward trip. The magnitude of its final energy is therefore given by:

$$E_1 = kE(x) - (dE/dx)_{out} \frac{x}{cos\theta_2} \tag{2.8}$$

Where the subscript *out* denotes the outward path.

The difference in energy of particles scattered on the surface and those scattered at depth x is given by:

$$\Delta E = kE_0 - E_1 \tag{2.9}$$

By assuming constant energy loss per unit length, the above equation can be written as

$$\Delta E = \left[\frac{k}{cos\theta_1}\left(\frac{dE}{dx}\right)_{in} + \frac{1}{cos\theta_2}\left(\frac{dE}{dx}\right)_{out}\right] x \tag{2.10}$$

The short notation for the above equation is:

$$\Delta E = [S]x \tag{2.11}$$

Where

$$[S] = \left[\frac{k}{cos\theta_1}\left(\frac{dE}{dx}\right)_{in} + \frac{1}{cos\theta_2}\left(\frac{dE}{dx}\right)_{out}\right] x \tag{2.12}$$

$[S]$ is usually referd to as energy loss factor. By applying equation 2.11, the thickness x of a sample can be determined if ΔE and $[S]$ are known. This is one of the cornerstones of Rutherford backscattering spectrometry: quantitative analysis of thin film thicknesses.

2.1.3 Differential Scattering cross section ($\frac{d\sigma}{d\Omega}$)

The concept of differential scattering cross section defines the probabilty in which the scattering event will be recorded by a detector. It relates the number of detected particles to the total number of incident particles and the number of target atoms per unit area of irradiated sample. Rutherford derived the differential scattering cross section formula based on the assumption that during the collision, the distance of closest approach is small in atomic dimensions, but large in nuclear dimensions. The differential scattering cross section, in the laboratory frame of reference, is given by:

$$\left[\frac{d\sigma}{d\Omega}\right] = \left[\frac{zZe^2}{4E}\right]^2 \frac{4}{sin^4\theta} \frac{([1-((\frac{m_1}{M_2})sin\theta)^2]^{1/2} + cos\theta)^2}{[1-((\frac{m_1}{M_2})sin\theta)^2]^{1/2}} \tag{2.13}$$

where z and Z are the respective atomic numbers of projectile mass m and target mass M, and E the energy of projectile immmediately before scattering. For $m \ll M$, the power series expansion of equation 2.13 gives

$$\left[\frac{d\sigma}{d\Omega}\right] \simeq \left(\frac{zZe^2}{4E}\right)^2 \left[sin^{-4}\frac{\theta}{2} - 2\left(\frac{m_1}{M_2}\right)^2 + ...\right] \tag{2.14}$$

Our point of interest in the last expression is the dependence of differntial cross section on Z^2, the consequence of which is that elements with high atomic numbers give signals larger than those given by light elements, which further elevates the importance of RBS technique in that it allows for qualitative analysis of different compositions in thin films.

2.1.4 Interpretation of the spectrum.

The three aspects discussed above underpin the rules of analysis of a backscattering spectrum. Information about mass of the target atom is extracted from the kinematic factor. The heavier the element, the higher the energy of backscattered particles.
Thus, heavier elements have their energy peaks at channel numbers higher than those of light ones. Information about the amount of the element is provided by the differential scattering cross section. By comparing the heights of two peaks at a particular depth, the composition ratio of two different elements can be approximated from the following equation.

$$\frac{n_a}{n_b} = \frac{H_A/\sigma_A}{H_B/\sigma_B} \tag{2.15}$$

Where σ_i is the average differential scattering cross section of element i, $\frac{n_a}{n_b}$ the composition ratio, and H_i the signal height of particular element i.
The depth and thickness of thin films are obtained as a consequence of energy loss. Atoms buried deep in the sample will produce low energy signals, while the same atoms near the surface produce high energy signals. The difference in energies can be transformed into layer thickness.
To illustrate the above concepts, a typical backscattering spectrum for Pt-Ge system is displayed in Figure 2.4. The spectrum is a simulation of 2 Mev alpha particles, with scattering angle $\theta = 165°$, and sample angle $\phi = 10°$. Signals from Pt and Ge are clearly indicated. Large peak region at ~450 is due to scattering from Pt atoms in PtGe. Lower energy peak at about 330-400 is due to scattering from Ge atoms, and the step at channel ~370 is a result of less concentration of Ge atoms in PtGe. The germanide thickness is determined from ΔE_{Pt}. Composition ratio can be determined by equation 2.15 using peak heights H_{Ge}

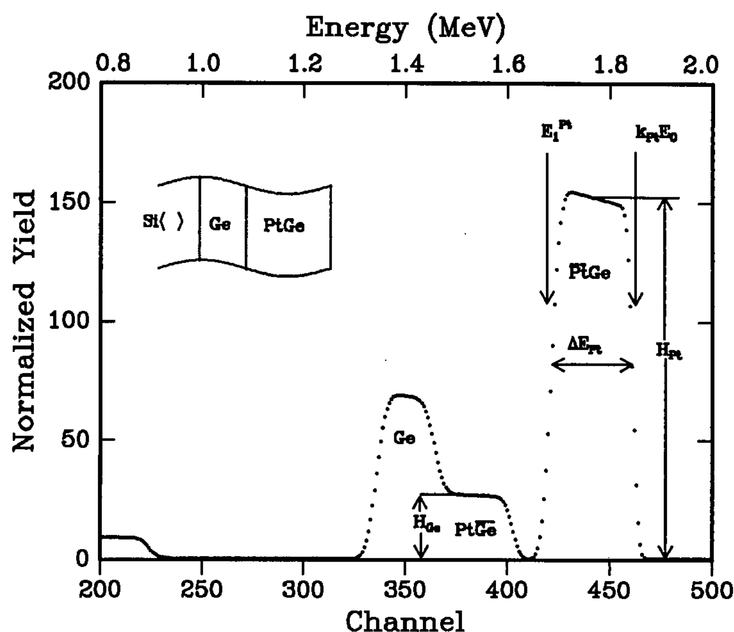

Figure 2.4: *A typical Backscattering spectrum simulated to show signal heights and compound thickness.*

and H_{Pt}.

2.2 Marker Technique

The marker technique had been used to advantage in the analysis of atomic mobility. During the process of germanides formation, either metal or germanium atoms (sometimes both), can be the diffusing species. In order to determine the moving species during solid state reactions, the marker technique is used. The term marker refers to a material deposited in the sample to serve as a reference point in monitoring the direction of flow of atoms during germanide formation.

Two types of markers exist, namely inert and isotope markers. A common example of an isotope marker is a radioactive silicon. An inert marker can be any element which satisfies certain requirements. The use of radioactive marker was not part of the scope of this study, only inert marker was used to determine the diffusing species. Early experiments on inert markers were carried out as early as 1942 by Kirkendal et al [42]. The technique has since re-

ceived wide applications in various interdiffusing systems, including the study of thin films. The inert marker technique involves the deposition of a relatively thin metallic layer between any two reacting elements under investigation. After thermal treatment, the RBS technique can be used to determine the relative shift in the position of the marker. To avoid complications in the interpretation of RBS results, the marker should ideally fulfill certain requirements.

- The inert marker should not partake in the diffusion and neither should it react with any of the components at temperatures at which thermal treatment takes place.
- The introduction of the marker should not influence the diffusion process by becoming a diffusion barrier to one or both interdiffusing components, it must introduce neither stress nor lattice defects.
- The marker should be immobile with respect to external reference frame.
- The marker should be readily identifiable both before and after annealing.

Like any other experimental analytical tool, the inert marker technique has its own shortcomings. It fails to provide any information about the diffusion mechanism gorverning the atomic mobility. It is difficult to tell if the marker took part in the diffusion process or influenced the solid phase formation. The possibility that the marker atoms were dragged along by the growth interface can never be ruled out with certainty. Despite its limitations, the inert marker technique remains one of the most useful techniques in the study of atomic mobility.
Titanium was employed as an inert marker in this study. The succesfull use of titanium as an inert marker was reported by Comrie et al [43] in determination of dominant diffusing species through an epitaxial Pd_2Si layer during silicide formation. In this study, titanium element was preferred because of its signal is well-seperated from both platinum and germanium RBS signals, so that the mobility of atoms can be systematically observed.

Figure 2.5 is a schematic representation of the marker movement. After the sample has been thermally treated to effect atomic diffusion, a relative shift in the position of the marker is observed. The direction in which the marker position shifts is in opposite to that of the dominant moving species. This state of affairs is clearly shown in Figure 2.5. If the metal is

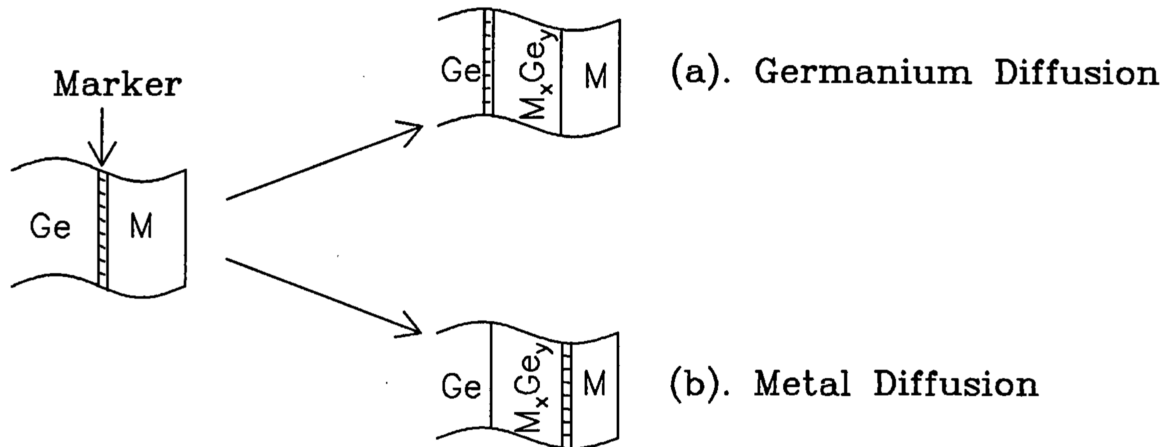

Figure 2.5: *Schematic representation of relative shift in the position of the marker.(a) Germanium diffusion. (b) Metal diffusion.*

the dominant diffusing species, it will diffuse through the marker to react with the underlying germanium substrate atoms, thereby resulting in the marker position relatively shifting to the surface, as shown in Figure 2.5(b). If on the other hand silicon is the diffusing species, the marker will be buried deep in the sample, as shown in Figure 2.5(a). The RBS technique is used to analyse the relative shift in the position of the marker.

2.3 Procedure

2.3.1 Sample Preparation

Silicon wafers of approximately 0.5 mm thickness, with an SiO_2 buffer layer of about 4000 Å, were cleaved into 1 cm^2 squares. Before deposition, wafers were ultrasonically cleaned with organic solvents to rid their surfaces of impurities. The cleaning process involved 5

minutes washing in acetone, 5 minutes in methanol, followed by a rinse in deionised water. Immediately before loading into the chamber for deposition, the wafers were etched into 40% hydrofluoric acid (HF) solution for 30 seconds to remove some of the native oxide, rinsed once more in deionised water and blown dry with nitrogen gas. After cleaning, wafers were immediately mounted on aluminium holders and then loaded into the vacuum evaporation system.

2.3.2 Vacuum Evaporation

The electron beam evaporation was carried out under pressure of the order of 10^{-7} torr. The vacuum system is shown in Figure 2.6. The pumping system is divided into upper and lower sections by a baffle valve. The high vacuum was achieved through several stages of vacuum pumping. In the upper section, the turbomolecular pump was backed by rotary pump to bring the pressure down to the order of 10^{-6} torr. This stage of the pumping system was usually left running overnight.

In the lower section of the pumping sytem a combination of Ti-sublimation with liquid nitrogen cooled cryopanel achieved a finer vacuum in the order of 10^{-8} torr. Prior to evaporation, the baffle valve was opened, reducing the total pressure to about 10^{-7} torr in the whole chamber. Evaporation was accomplished by electron beam heating process. Materials to be evaporated were placed in three copper crucibles. The system allowed for the movement of crucibles to appropriate beam position without breaking the vacuum. During the evaporation process, deposition rates were monitored by crystal monitor.

2.3.3 Annealing

Samples, with thin layers of platinum and germanium, were loaded into the Lindenburg quartz tube furnace for vacuum annealing and some were reserved for non-isothermal "*dynamic RBS*". The pressure in the furnace was always kept better than 5×10^{-7} torr.

The system had a total of 7 boats in which samples could be loaded into the furnace without breaking the vacuum. One after another, each boat was gently pushed down the quartz

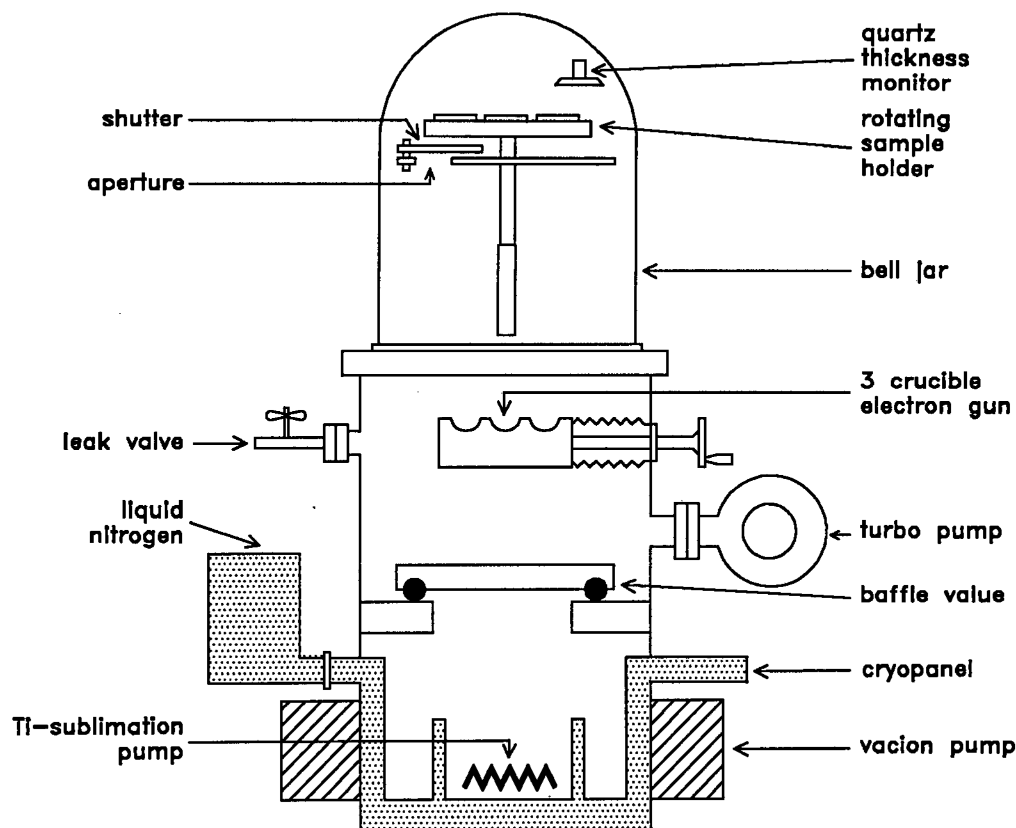

Figure 2.6: *Schematic illustration of high vacuum system used for the electron beam evaporation of thin films. Upper section contains sample holder, thickness monitor and electron gun. The baffle valve is closed to ensure that the lower section of the system is maintained under vacuum when the system is not in use or during sample changing.*

tube for isothermal treatment at elevated temperatures capable of initiating and promoting platinum germanides formation. The temperature settings were chosen in accordance with specific experimental requirements, but were generally in the range 200-350°C.

2.3.4 X-Ray Diffraction

X-Ray diffraction was used in sample analysis for identification of various growing phases. A diffractormeter with Cu tube was used with K_α radiation of wavelength $\lambda = 0.154$ nm. During X-Ray data collection, the diffractometer operated in the (θ-2θ) geometry. CCMILLER computer program was used to identify peaks of prominent intensities.

2.3.5 *Dynamic* RBS

The use of conventional furnace annealing to analyse reaction kinetics had always posed a problem of time and sample to sample variations during data collection.

To avoid this problem, a more convenient method of thermal treatment was also used, the *dynamic* RBS method. With *dynamic* RBS method, sample characterisation is achieved by doing continuous RBS *in situ* during thermal annealing. A rough sketch of *in situ* annealing stage is displayed in Figure 2.7. The backscattering chamber is the same one used for

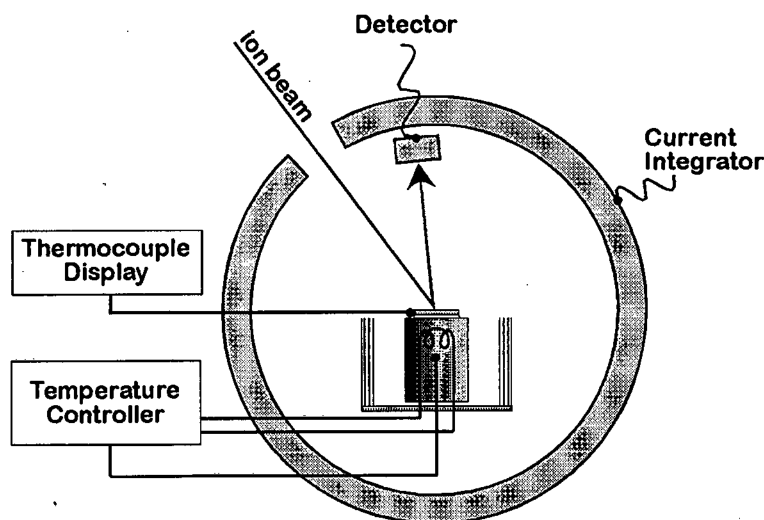

Figure 2.7: *Schematic diagram showing the scattering chamber containing the cylinder used as a heating stage during insitu RBS measurements of solid state reactions.*

backscattering of the conventionally annealed samples. The sample is mounted on the front surface of the cylindrical copper block which serves as the heating stage. To ensure good contact and conductivity, a thin layer of conducting silver paste is used to adhere the sample to the copper surface.

Behind the mounted sample, inside the copper cylinder, the actual heating element is in the form of a winding spring. The heating element can be programmed to a temperature of interest using a Eurotherm 818 temperature controller, see Figure 2.7. The K-type thermocouple behind the heating element records the temperature inside the copper cylinder. An

estimate of sample temperature is obtained from another thermocouple on the front surface of the copper cylinder.

During an experimental run, an RBS spectrum is collected and recorded every 10 seconds. Thus during *in situ* annealing, RBS becomes something akin to a 10 second glance into sample reaction, and so the reaction is continuously monitored as it takes place.

Chapter 3

Thin film study of Pt-Ge system

3.1 Phase Formation

3.1.1 Experimental conditions

Following sample cleaning described in section 2.3.1, amorphous germanium thin film of about 3000 Å was vacuum deposited on oxidised silicon at a rate of about 6-8 $Å.s^{-1}$ and pressure of $4 \sim 5 \times 10^{-7}$ torr. Thin film of platinum (~500Å) was then subsequently deposited at a rate of 5 $Å.s^{-1}$ and pressure of about 1×10^{-6} torr. Samples, with configuration Si<>/SiO_2/Ge(3000Å)/Pt(500Å), were then annealed at temperatures ranging from 200 to 400°C for annealing times of 10 and 20 minutes. Germanide compound formation and composition were monitored by RBS using 2 MeV (α particles) beam. The analysis was carried out using RUMP computer program, with an estimated thickness uncertainty of 10%.

3.1.2 Results

Figure 3.1 displays RBS spectra obtained from samples before and after annealing at 250 and 300°C for annealing periods of 10 and 20 minutes. Heights indicated alongside correspond to expected position of platinum "shoulder" for various phases.

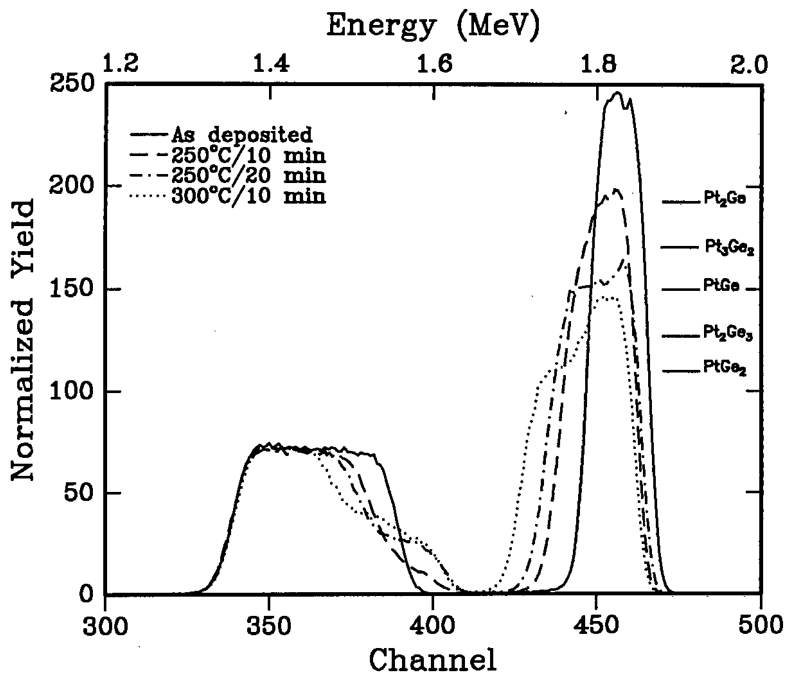

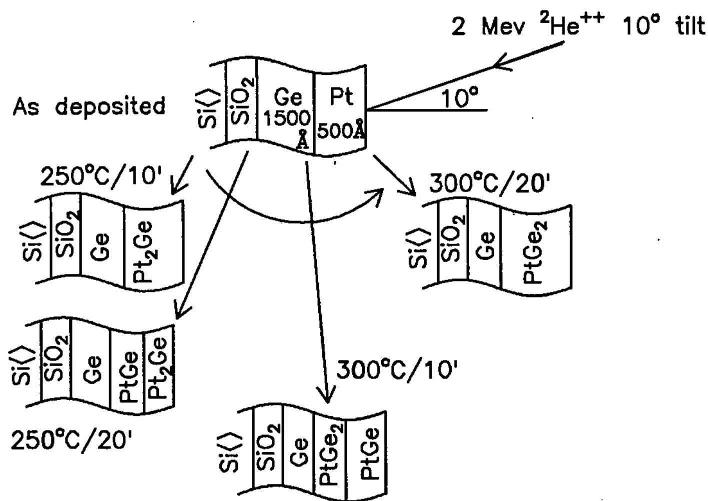

Figure 3.1: *RBS spectra(top) obtained from samples before and after annealing at 250 and 300°C for annealing periods of 10 and 20 minutes. RBS results are summarised in a schematic diagram below.*

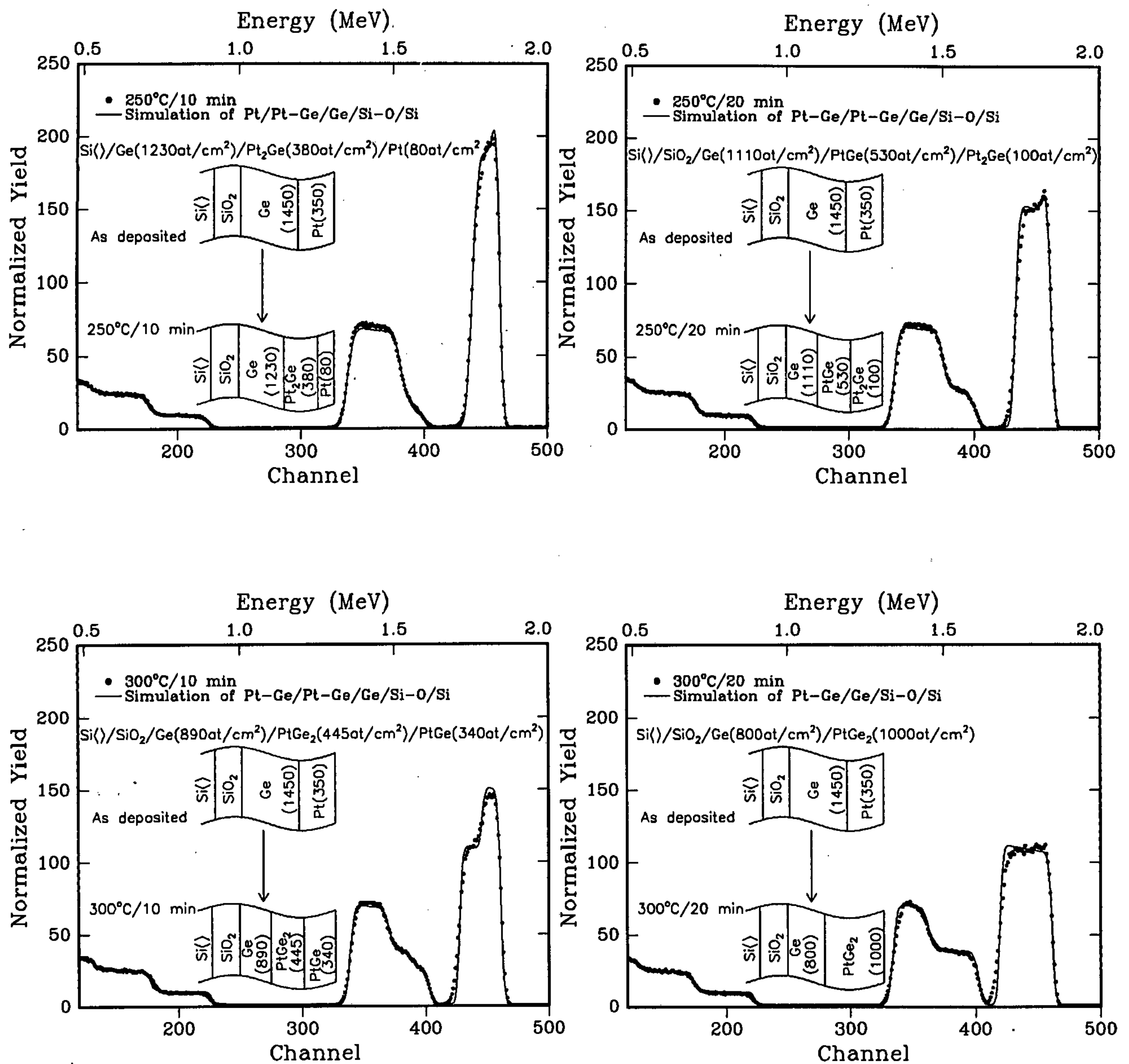

Figure 3.2: *RBS spectra obtained after annealing at 250 and 300°C for 10 and 20 minutes at each temperature. On each spectra, the solid line is a simulation obtained from RUMP showing good agreement with actual data.*

It is clear from the spectrum (Figure 3.1) that at 250°C/10 min, surface platinum is almost completely transformed into Pt_2Ge. PtGe formation is almost complete at 250°C/20 min. $PtGe_2$ shoulder (on platinum peak) is quite visible at 300°C/10 minutes, and its formation reaction is over at 300°C/20 minutes.

Composition and thicknesses of phases are corroborated by RUMP simulations, see Figure 3.2. It is important to note good agreement in phase composition between actual data and RUMP simulations without non-congruent phases Pt_3Ge_2 and Pt_2Ge_3.

X-ray diffraction was also used as a complementary tool in the samples analysis. A set of samples were first prepared with thicknesses chosen to "force" the system to form non-congruent phases. XRD results obtained from these samples are displayed with their corresponding RBS spectra in Figures 3.3 and 3.4. Several lines of high intensities corresponding to different phases were identified and labelled by their Miller indices.

Having prepared and analysed these samples, they were then used as standards in the XRD analysis of samples whose RBS results are displayed in Figure 3.1. [Note that standard samples were prepared on Si(100), and the rest on Si(111)]. RBS spectra from Figure 3.1 are re-displayed side by side with corresponding XRD spectra in Figure 3.5.

At 250°C/10min, a peak corresponding to Pt_2Ge was identified, see XRD spectra in Figure 3.5(a). The intensity of this peak decreased at 250°C/20min. A not so intense PtGe peak can be seen at 250°/20min, and its intensity increases at 250°C/20min. This is in agreement with the corresponding RBS results and simulations. At 300°C/10min, XRD spectra show a combination of PtGe and $PtGe_2$ rather than Pt_2Ge_3, see XRD spectra in Figure 3.5(b).

At 300°C/20min, see Figure 3.5(b), a number of intense $PtGe_2$ peaks were identified and also labelled by their Miller indices. With further increase in temperature and time, the intensities and positions of these peaks were observed to remain constant, confirming that $PtGe_2$ is the last stable phase of the Pt-Ge system. The overall XRD results agree with the observation from RBS. There appears no evidence of the presence of non-congruent phases.

A slightly different set of experiment was done with the same platinum and germanium

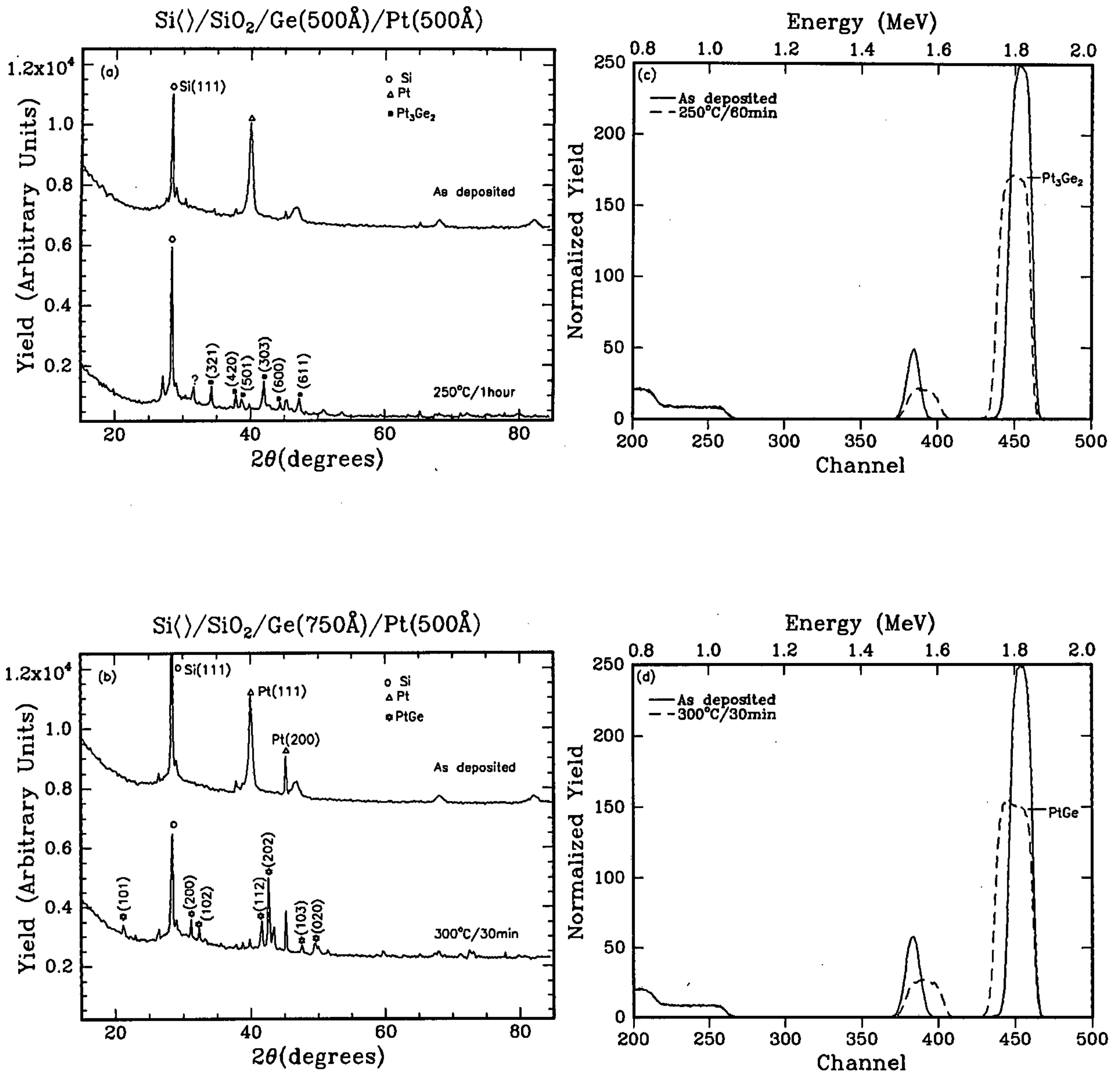

Figure 3.3: *X-ray diffraction spectra displayed side by side with their corresponding backscattering spectra. The spectra were obtained from samples annealed at 250°C/1hour to form Pt_3Ge_2 (a) and 300°C/30min to form PtGe(b). The lines of highest intensities on XRD spectra are indicated by their Miller indices.*

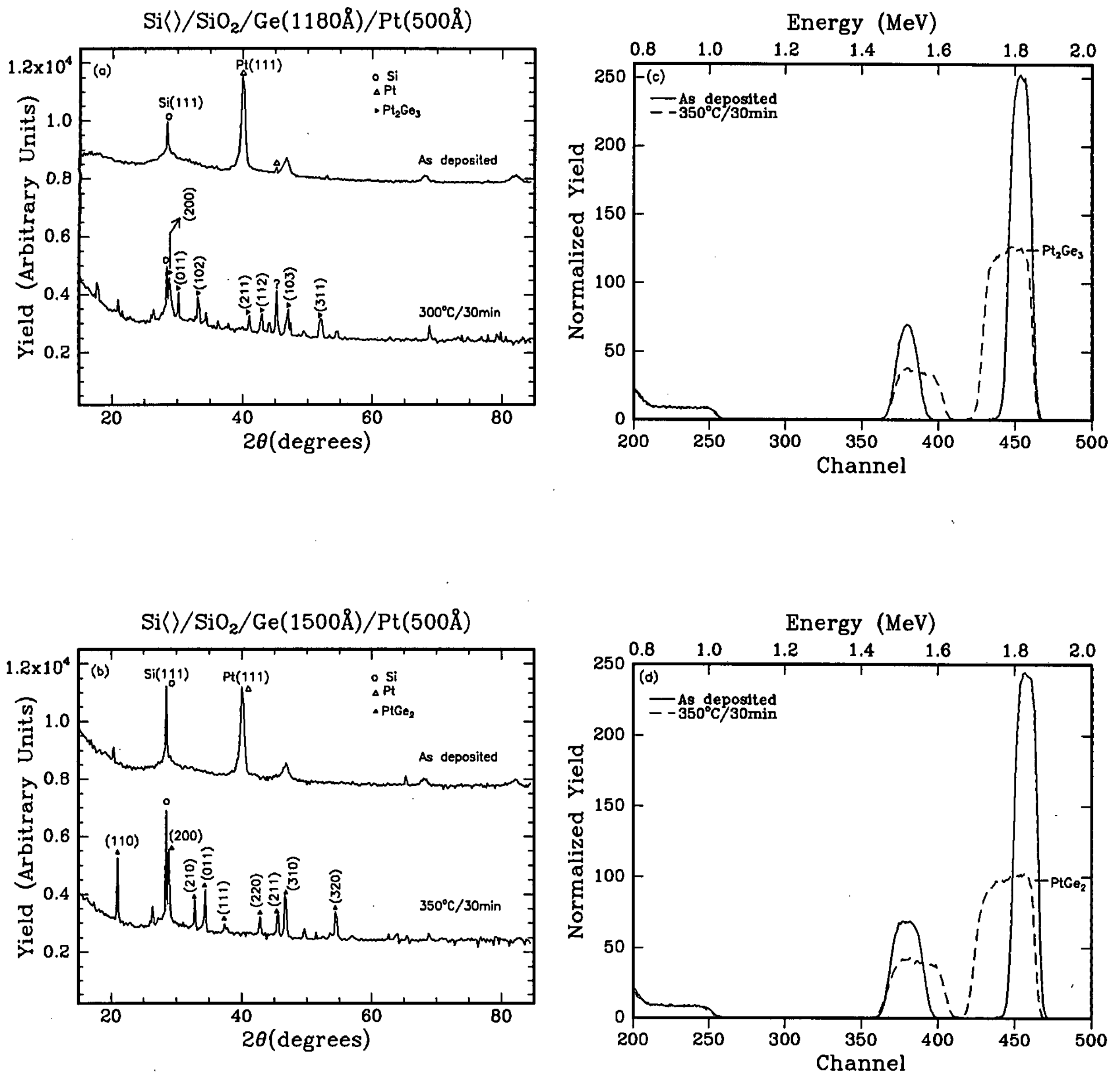

Figure 3.4: *X-ray diffraction spectra displayed side by side with their corresponding backscattering spectra. The spectra were obtained from two samples(with different thicknesses) annealed at the same temperature 350°C/30min to form Pt_2Ge_3(a) and $PtGe_2$(b). The lines of highest intensities on XRD spectra are indicated by their Miller indices.*

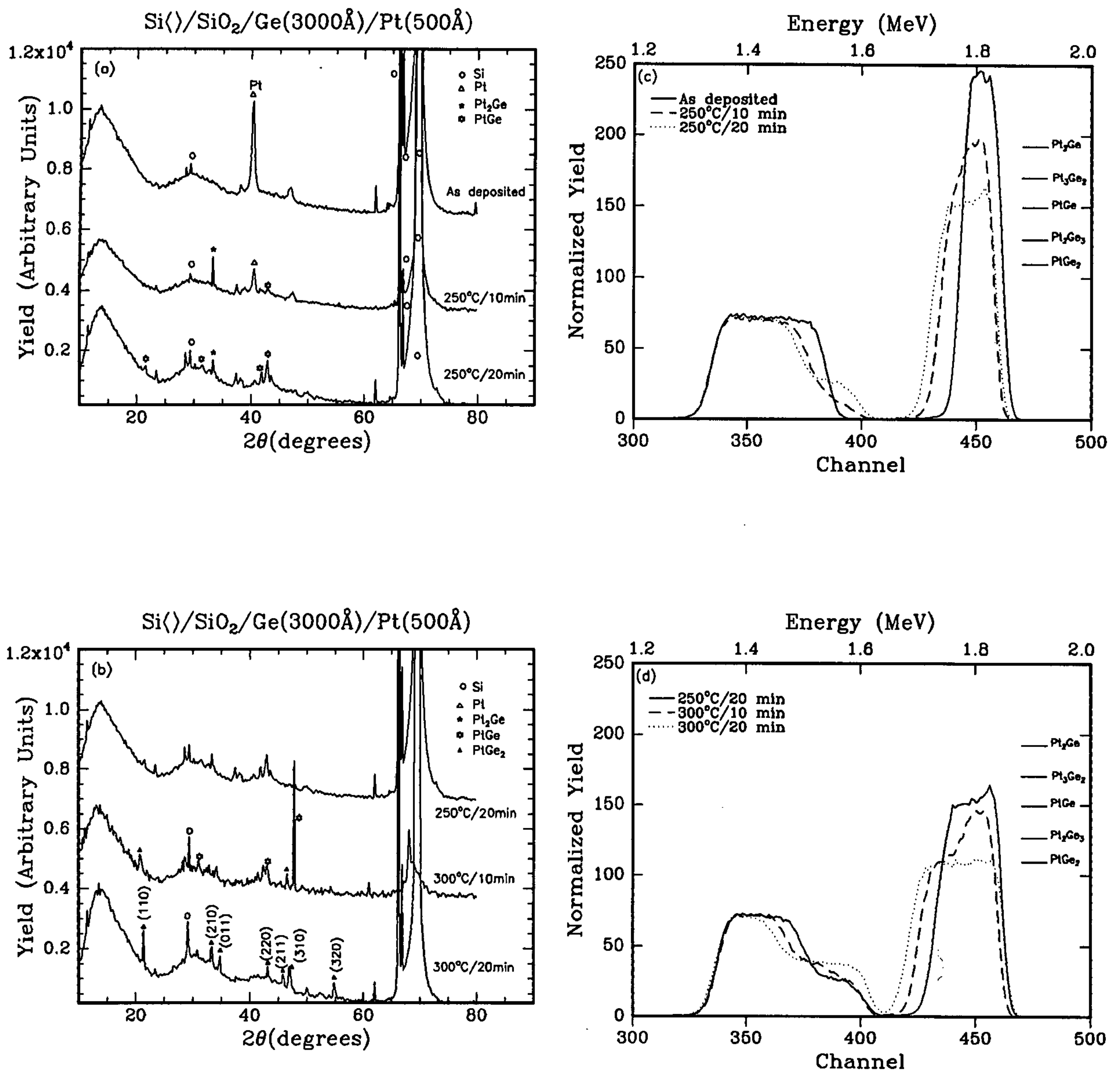

Figure 3.5: *X-ray diffraction spectra displayed side by side with their corresponding backscattering spectra. The spectra were obtained from samples annealed at 250 and 300°C for 10 and 20 minutes at each temperature. The lines of highest intensities on XRD spectra are indicated by their Miller indices. There is no convincing evidence of either Pt_3Ge_2 or Pt_2Ge_3 from both XRD and RBS data.*

thicknesses (500 Å and 400 Å respectively) in the temperature range 200-275°C for higher annealing times of 80 minutes. Figure 3.6 displays backscattering spectra obtained from an as deposited sample and samples annealed at temperatures 200, 220, 250 and 275°C, all for annealing periods of 80 minutes. It is evident that the obtained results are somewhat

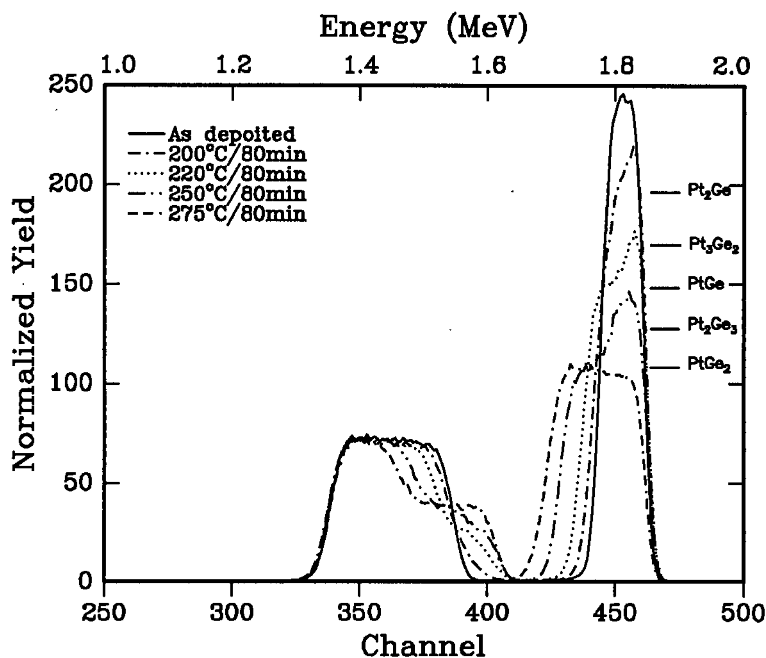

Figure 3.6: *RBS spectra obtained from an as deposited sample and from samples annealed at 200, 220, 250 and 275° C for higher annealing periods of 80 minutes.*

similar to the ones reported earlier. Pt_2Ge is detected at 200°/80 min, while the PtGe shoulder is evidently prominent at 220°C/80 min. At 250°C/80 min, the presence of $PtGe_2$ is clearly visible. The $PtGe_2$ formation process is over at 275°C/80 min. No other compounds were detected after $PtGe_2$. X-ray diffraction analysis was not carried out on these samples. However, a detailed simulation of the spectra with RUMP, see Appendix A, showed good agreement between data and simulation without Pt_2Ge_3 and Pt_3Ge_2 phases.

3.1.3 Discussion

The interaction between germanium and platinum thin films can be observed at temperatures as low as 200°C (for annealing periods of 80 minutes). However, when annealing times are lowered to 10~20 minutes, the Pt-Ge interaction is only evident from 250°C. The first phase to form is Pt_2Ge. It appears from the RBS spectra in both Figure 3.6 and Figure 3.1 that Pt_2Ge lacks a sharp interface, suggesting that it (Pt_2Ge) does not grow uniformly in a layer-by-layer mode of formation. [Subsequently it was found that the second phase, PtGe, starts growing even before surface platinum is completely consumed, resulting in some short period of coexistence of Pt_2Ge and PtGe with unreacted Pt.] PtGe formation then proceeds as a result of interaction between Pt_2Ge and unreacted germanium atoms.

The last phase observed is $PtGe_2$ which forms from interaction of PtGe with unreacted germanium. Both PtGe and $PtGe_2$ appear to grow uniformly following a layer-by-layer mode of formation. No other compounds were observed after $PtGe_2$. This agrees with the Pt-Ge phase diagram where $PtGe_2$ is predicted as the last phase to form in the Pt-Ge system, see Figure 1.3. Phase sequence of the results is also in agreement with prediction by EHF model. From both X-ray diffraction spectra and RBS simulations, there appears no convincing evidence of the presence of non-congruent phases, Pt_3Ge_2 and Pt_2Ge_3.

From these results, it can be inferred that the system under consideration has a tendency to skip its non-congruent phases. Apart from the absence of Pt_3Ge_2 and Pt_2Ge_3, the observed order of compound formation is consistent with results obtained in previous experiments [1, 2, 40], although variation exists in temperatures of formation, see Table 1.4.2. Marshall et al [2] reported detecting Pt-Ge interdiffusion at 250°C, with Pt_2Ge as the first phase to form. On the other hand, Hsieh and Chen [1] found the same phase (Pt_2Ge) as the first to form, but at a lower temperature, 160°C. Grimaldi et al [40] reported in their results that there was no evidence of Pt-Ge interdiffusion at temperatures below 250°C, see Table 1.4.2. The plausible explanation regarding inconsistency in the formation temperatures might be the presence of impurities, from both native oxide and that incorparated during deposition. The cleaning stage of sample preparation becomes more crucial when the expected inter-

action is between the substrate and deposited thin films, as was the case in these previous investigations [1, 2, 40]. Impurities such as O, N and C are reportedly known to impede reactions during compound formation, shifting the phase formation temperatures and sometimes forcing the system to skip other phases in the phase diagrams [44, 45]. Impurities may also explain the presence of non-congruent phases in the previous studies. The absence of non-congruent phases in the results of this study can therefore be interpreted as an indication of the cleanliness of samples. The Pt/Ge interface in this study was relatively clean in that germanium used was amorphous and not single crystalline as in the previous experiments. The results obtained in this study are more in agreement with those of Hsie and Chen [1] and Marshal et al [2]. A pronounced difference exists between the results of Grimaldi et al and those obtained in this study in that the former do not report Pt_2Ge as the first phase to form.

3.2 Growth Kinetics

3.2.1 Experimental conditions

To follow Pt-Ge reaction kinetics, thin film diffusion couples were prepared following similar procedure described in Section 3.1. Sample characterisation and analysis were accomplished by "*dynamic RBS*" technique where sample annealing and Rutherford Backscattering are performed simultaneously. As mentioned earlier, the advantage of using "*dynamic RBS*" technique is that all growing phases can be analysed and activation energies calculated from one sample, this eliminates the problem of sample to sample variation commonly encountered in conventional annealing. Another advantage is that RBS spectra are obtained at all stages of compound growth.

Pt_2Ge does not follow a well defined layer-by-layer mode of formation, and therefore kinetic analysis could not be done for this compound. The fact that PtGe compound starts to grow before Pt is completely consumed made it difficult to get good data for its kinetic analysis. Good data was obtained for $PtGe_2$ and a detailed kinetic analysis was only done for this

compound.

To follow PtGe reaction kinetics, a constant temperature *in situ* anneal was done at 260°C, and for $PtGe_2$ kinetics, *in situ* isothermal anneals were done at four different temperatures in the range 310-335 °C. At all temperatures, the *in situ* annealing process was left to proceed until complete formation of the desired phase.

Prior to activation energy analysis, it is necessary to determine the specific process governing compound growth. RBS data obtained from isothermal anneals can be manipulated to determine if the compound growth is diffusion or reaction limited. The constant temperature anneals were therefore a prelude to activation energy (E_a) analysis. From the same set of samples, an alternative method of kinetic analysis was used. The ramping method, as described in section 1.4, involves ramping over a specific temperature range where the compound of interest is known to form. For this set of experiment, the temperature was ramped from 240 to 350°C at a rate of 1°C/min, during which time both PtGe and $PtGe_2$ growth were observed.

Collected RBS spectra were fitted using RUMP program to obtain an estimate of compound thickness. The uncertainty in RUMP simulations was estimated to about 10%. Presented below are the growth kinetics results of PtGe and $PtGe_2$ obtained from constant temperature *in situ* anneals and from temperature ramping.

3.2.2 Results

Figure 3.7 displays three dimensional (3D) plots of RBS spectra captured during *in situ* annealing of one sample at two different constant temperatures. The sample was first annealed (*in situ*) at 260°C to grow PtGe phase, see Figure 3.7 (top). After PtGe formation was complete, sample temperature was increased to 320°C to grow $PtGe_2$ phase, see Figure 3.7 (bottom). Thus, RBS spectrum at 140 minutes on the top figure is essentially the same as the 0 minute spectrum at the bottom figure, see Figure 3.7. The spectra were all captured in two minutes interval. A curve can be clearly traced on both plots on the Pt signal, though it is more evidently clear during $PtGe_2$ growth.

To determine the kinetics of PtGe formation, the square of compound thickness (in units of atomic concentration) was plotted as a function of annealing time at constant temperature 260°C, see Figure 3.8 (left). On the same figure (right), the thickness of the compound is also plotted against annealing time, with error bars estimated from uncertaity in thickness simulations. It is clear from the two plots that the best fit is obtained with the parabolic relationship, indicative of a diffusion limited reaction.

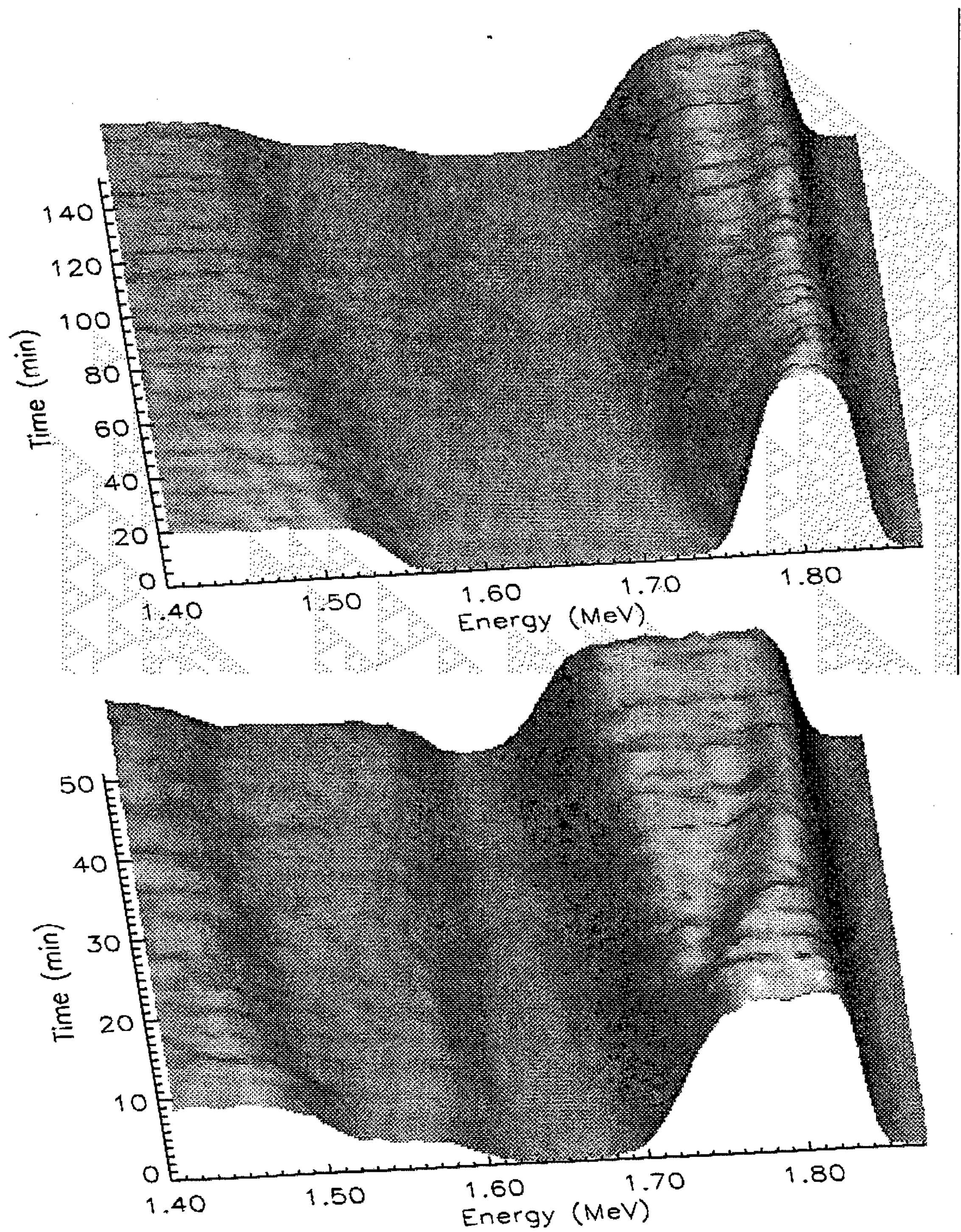

Figure 3.7: *RBS spectra collected from one sample annealed in situ at two different constant temperatures, 260 and 320°C. PtGe was first grown at 260°C (top). After complete formation of PtGe, the sample temperature was increased to 320°C to grow $PtGe_2$ (bottom). Thus the spectrum at 140 min from the top figure is essentially the same as the one at 0 min from the bottom. The $t^{\frac{1}{2}}$ nature of the growth is more evidently clear during $PtGe_2$ growth.*

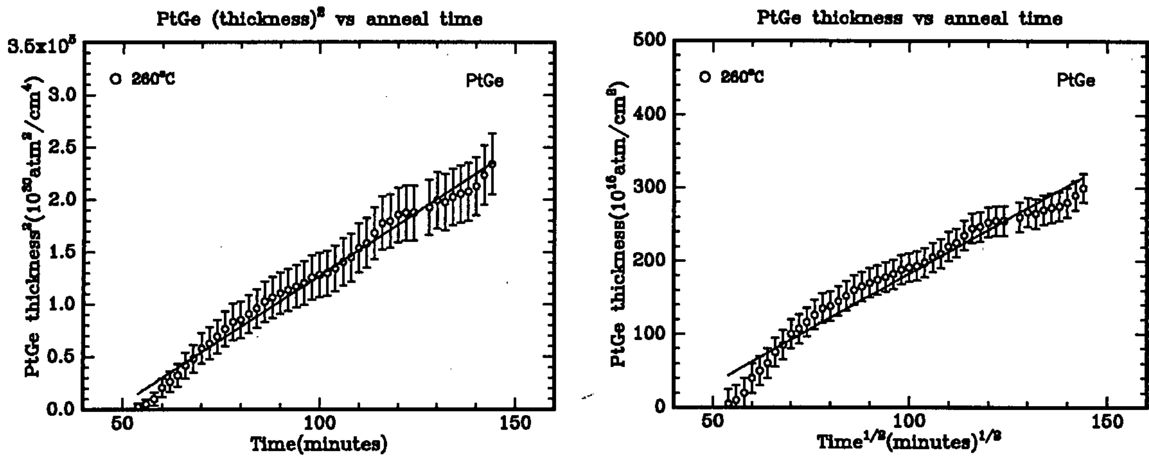

Figure 3.8: *The kinetics of formation of PtGe at 260° C. The thickness is expressed in total atoms(Pt+Ge) per unit area. The two plots display the same data. The best fit is more in agreement with the x^2 vs t data, suggesting that PtGe formation process is diffusion limited.*

In Figure 3.9, the squares of $PtGe_2$ thicknesses are plotted against annealing time at each constant temperature in the range 310-335°C. It is clear from the plots, that the $PtGe_2$ formation process also follows a square root of time law, indicative of a diffusion limited growth process. The plots do not go through the origin because of time delay when the system is still passing through initial phases before it starts growing $PtGe_2$. Following Equation 1.5, growth rates from different plots in Figure 3.9 are plotted against 1/T in the Arrhenius plot in Figure 3.10. The activation energy is found to be about 1.9 ± 0.1 eV.

Figure 3.11 displays results for the same phases PtGe (a) and $PtGe_2$(b), obtained by temperature ramping from 240 to 350°C at a rate of 1°C/min. Using equation 1.8, $ln(x^2/T^2)$ is plotted against $1/T$ on a so called Kissinger plot, and an estimate of activation energy is obtained from the slope. The activation energies determined from Kissinger plots are 1.52 ± 0.02 and 2.5 ± 0.2 eV for PtGe and $PtGe_2$ respectively, see Figure 3.11. Uncertainties in activation energies were all calculated using an estimation of 10% uncertainty in simulated thicknesses.

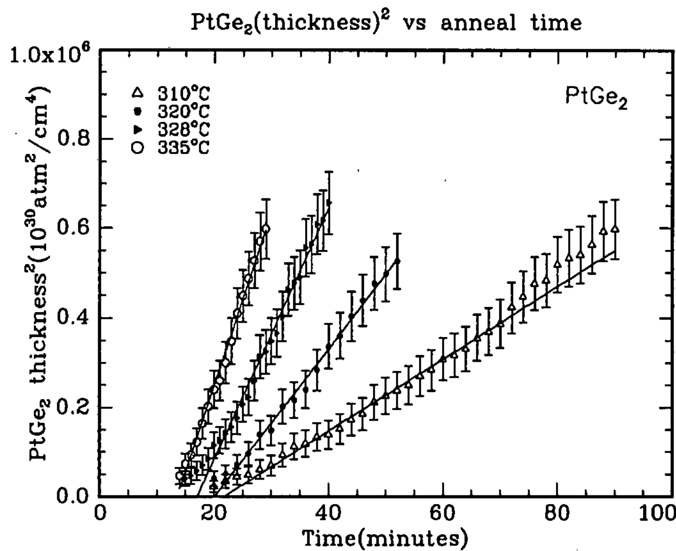

Figure 3.9: *Plots of x^2 vs t showing parabolic growth of $PtGe_2$ at 310, 320, 327 and 335° C. The thickness is expressed in total atoms(Pt+Ge) per unit area. The straight lines are indicative of a diffusion limited process.*

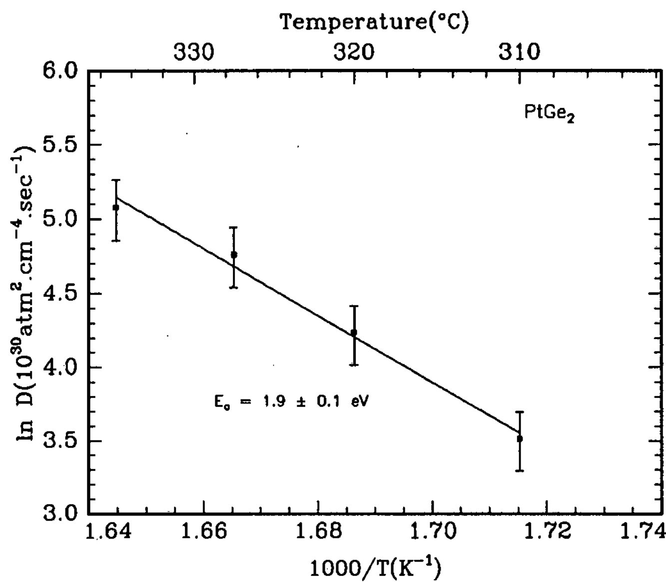

Figure 3.10: *Arrhenius plot, $ln(x^2/t)$ vs 1000/T, showing temperature dependence of $PtGe_2$ diffusion rate, yielding an average activation energy of 1.9 ± 0.1 eV. The interdiffusion coefficients are slopes obtained from plots in Figure 3.8*

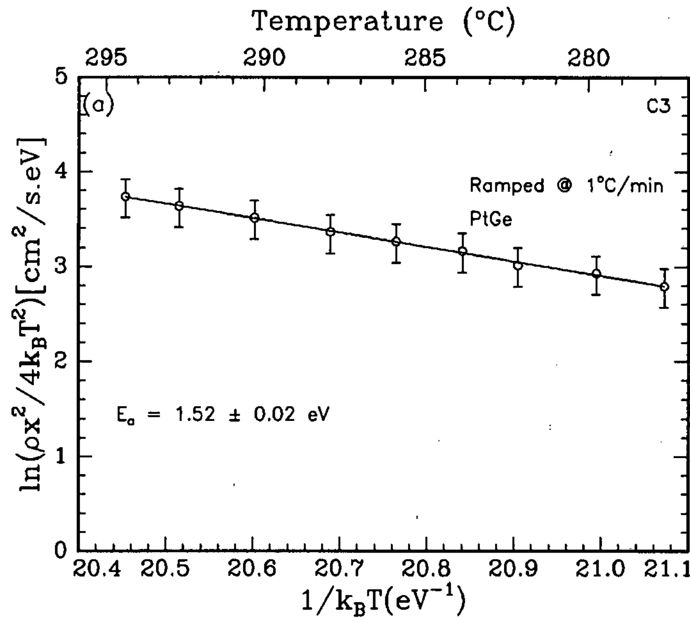

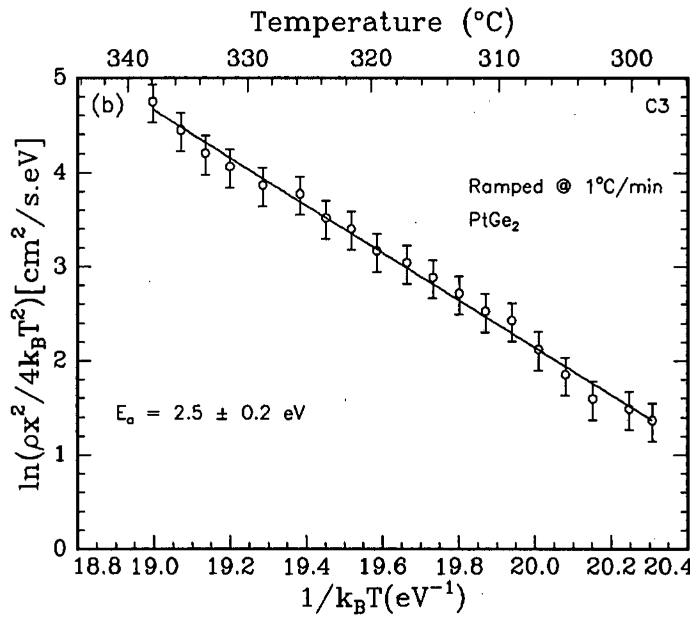

Figure 3.11: *Kissinger plot for PtGe(a) and $PtGe_2$(b) formation obtained from temperature ramping in the range 240-350°C at a ramp rate ρ = 1°C/min. The activation energies for PtGe and $PtGe_2$ are 1.52 $\pm$ 0.02 eV and 2.5 $\pm$ 0.2 eV respectively.*

3.2.3 Discussion

It has been observed from dynamic isothermal anneal measurements that the growth kinetics of PtGe and $PtGe_2$ compounds follow a diffusion limited process, where diffusion across growing film is the rate limiting step. The first phase, Pt_2Ge, was found not to obey a layer-by-layer growth process. This, and the fact that PtGe started growing before Pt_2Ge formation was over, made it difficult to investigate Pt_2Ge growth kinetics.

From isothermal anneal measurements, $PtGe_2$ activation energy (E_a) was calculated and found to be 1.9 ± 0.1 eV. Similar calculations could not be done for PtGe since only one isothermal anneal was done for this compound. Using the method of temperature ramping in the range 240-350°C at a rate 1°C/min, activation energies of of both PtGe and $PtGe_2$ were calculated and found to be 1.52 ± 0.02 and 2.5 ± 0.2 eV respectively. Only for $PtGe_2$ compound were activation energy measurements and calculations repeated several times. The results summarised in Table 3.1 show how ($PtGe_2$) activation energy values varied from sample to sample. The samples yield an average ($PtGe_2$) activation energy of 2.3 ± 0.1 eV. A considerable difference exists between two activation energies (for $PtGe_2$) obtained using two different methods. No plausible explanation was found to account for this difference.

ACTIVATION ENERGIES($PtGe_2$)		
Sample	**Ramp rate °C/min**	**E_a(eV)**
C1	1.0	2.5 (± 0.1)
C3	1.0	2.5 (± 0.2)
C4	1.0	2.1 (± 0.1)
B10	1.7	2.2(± 0.1)

Table 3.1: *Table showing sample to sample variation in $PtGe_2$ activation energy.*

3.3 Dominant Moving Species

3.3.1 Introduction

This experiment investigates the dominant moving species (DMS) during the formation of Pt_2Ge, PtGe and $PtGe_2$. An inert marker technique is used to monitor the atomic mobility during compound formation. In the previous Pt/Ge investigation, Marshal et al [2] used molybdenum (Mo) as an inert marker to determine the moving species during the formation of Pt_2Ge. A thin layer of Ti($12\AA$) is used as an inert marker in this experiment. Sandwiched between Pt and Ge layers, Ti produces a signal quite distinctive from platinum and germanium signals on RBS spectrum. The system gets complicated when platinum is on the surface in that platinum atoms shift germanium signal to lower energy channels, and Ti signal is subsequently over-shadowed in germanium signal. In order to separate the marker from Ge signal, Ge thin film was deposited on top of Pt thin film with Ti sandwiched in the middle.

To test the inertness of the marker, a preliminary investigation was done, with a thin film of Ti($\sim 1000\AA$) deposited on oxidised silicon substrate, followed by $\sim 1000\AA$ layer of germanium. Prepared samples were then annealed in vacuum furnace at temperatures in the range 250-700°C for various periods. RBS results obtained from this experiment are displayed in Figure 3.12. It is clear from the displayed spectra that there was no evident interaction between Ti and Ge in the temperature range 250-400°C. These findings are in agreement with those of Thomas et al [46, 47] who reported the first phase, Ti_6Ge, at temperatures in the vicinity of 500°C.

The last stable phase of Pt-Ge system, $PtGe_2$, was found in this study to form at temperatures around 300°C, which is far below 500°C, where Ti starts interacting with Ge. One of the critical requirements of an inert marker (at temperature of interest) was therefore satisfied.

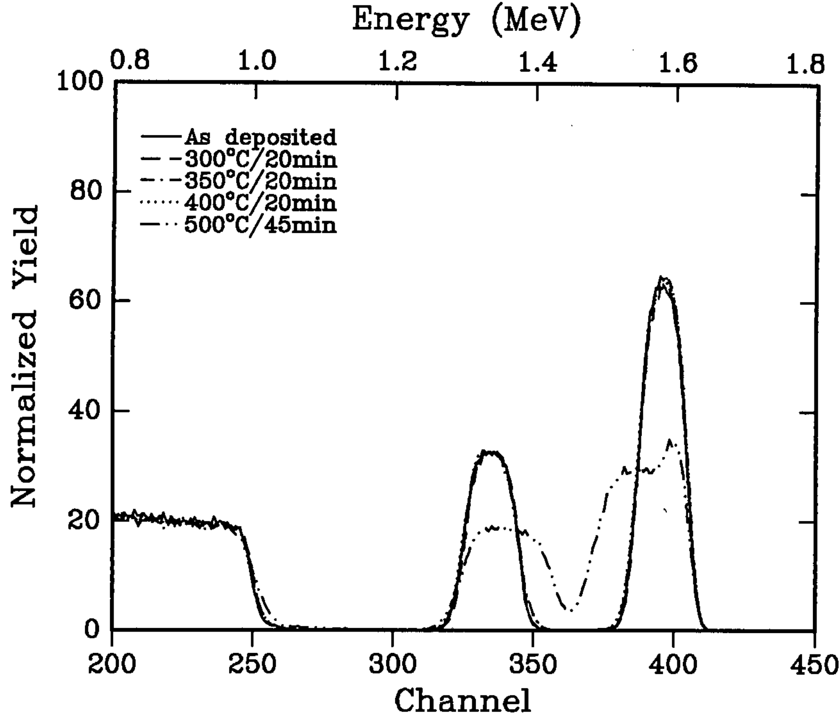

Figure 3.12: *Backscattering spectra from Ti-Ge samples annealed in the temperature range 300-500°C. The results clearly show no interaction between Ti and Ge at temperatures as high as 400°C. It is also evident that Ti-Ge interaction only starts at temperatures around 500°C.*

3.3.2 Dominant Moving Species during Pt_2Ge Formation

To determine the DMS during Pt_2Ge formation, samples of configuration Si<>/SiO_2 /Pt(320at/cm^2)/Ti(12Å)/ Ge(665at/cm^2) were prepared in high vacuum electron gun evaporator, following procedures outlined in Section 2.3.1, and annealed at 250°C for various periods.

Figure 3.13 displays backscattering spectrum from an as deposited sample together with that of a sample annealed at 250°C/10 min in order to show the relative shift of Ti signal. It is clear from the spectrum that the Ti signal had shifted to lower energy, from channel 337 to 331, suggesting that platinum is the dominant diffusing species during Pt_2Ge growth. To determine the amount of material that has diffused past the marker, the an-

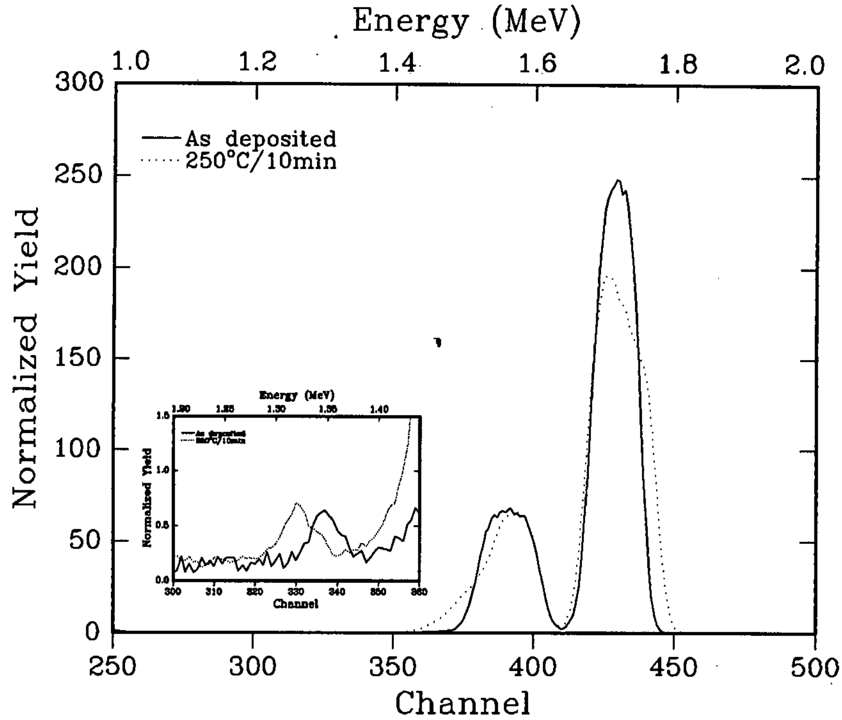

Figure 3.13: *RBS spectrum from an as deposited sample(~1500Å Ge on ~500Å with a thin layer of Ti(~12Å) between Ge and Pt) and from a sample annealed at 250°C/10 min showing atomic mobility during Pt_2Ge formation. The relative shift of the Ti marker signal to the lower energy is clearly visible.*

nealed spectrum was simulated with RUMP. The agreement between measured and RUMP simulated spectrum is shown in Figure 3.14. It is clear from the simulated thicknesses, see Figure 3.14, that platinum atoms had migrated from below the marker to interact with germanium atoms above the marker, forming Pt_2Ge phase in the process. The simulation also shows a measurable presence of PtGe(215at/cm^2) above the marker, between Pt_2Ge and unreacted germanium, refer to a much neater sketch in Figure 3.15 summarising the results. The presence of PtGe(215at/cm^2) between Pt_2Ge and unreacted germanium could only be a result of interaction between Pt_2Ge (above the marker) and surface germanium atoms. The formation of PtGe from Pt_2Ge can come about as a result of one of the two possible mechanisms. Pt_2Ge may dissociate into PtGe through the mechanism $Pt_2Ge \rightarrow$

$PtGe + Pt$, or Pt_2Ge can interact with unreacted germanium atoms through the mechanism $Pt_2Ge + Ge \rightarrow 2PtGe$. If the PtGe in our results was to have formed from Pt_2Ge below the marker, either of the above mechanisms would still have left PtGe below the marker. From

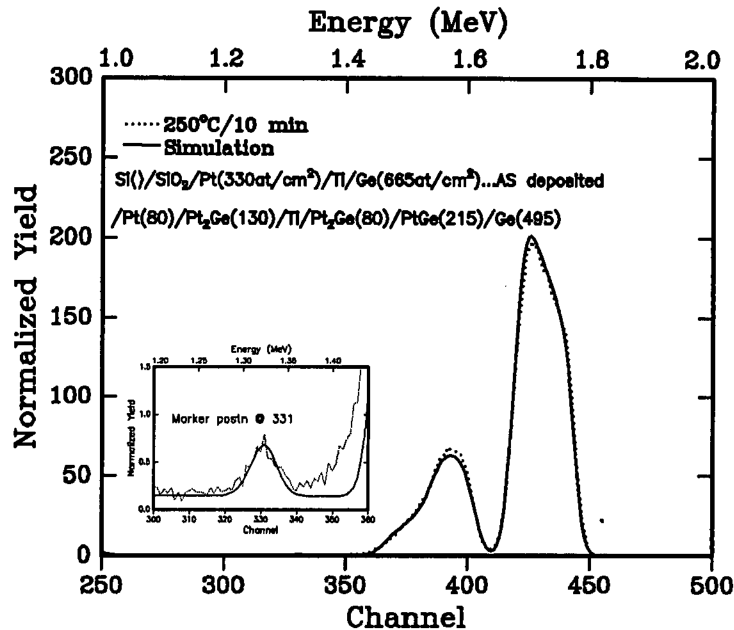

Figure 3.14: *RBS spectrum from a sample annealed at 250°/10 min. Simulation suggests platinum as the dominant diffusing species during Pt_2Ge formation. Thicknesses are given in units of 10^{15} at/cm^2. The region with Ti signal has been blown up on to show the agreement on marker position between actual data and RUMP simulation.*

the results obtained, see Figure 3.14, there is no evident presence of PtGe below the marker, and therefore the PtGe above the marker could only be a result of interaction between Pt_2Ge above the marker and surface germanium atoms, through one of the two possible mechanisms. This, of course, says nothing about the moving species during PtGe formation, but it does, however, suggests that platinum atoms in PtGe do not come from Pt_2Ge below the marker. It is therefore safe to infer that all platinum atoms above the marker, in both Pt_2Ge and PtGe, diffused past the Ti marker only during Pt_2Ge formation, and therefore the observed marker movement is not a consequence of PtGe but Pt_2Ge formation. The presence of Pt_2Ge below the marker suggests that some germanium atoms also diffused from

above the marker during Pt_2Ge formation. The atomic diffusion ratio was calculated and found to be 4:1, Pt:Ge. See Appendix B for a brief but detailed calculation.

It is concluded from the results of this experiment, that platinum atoms are the dominant diffusing species during Pt_2Ge formation. The results are in good agreement with the ones obtained by Marshal et al [2] who used molybdenum to determine the moving species during Pt_2Ge formation. The fact that platinum was found to be the dominant diffusing species using two different markers lends credibility to the results. Figure 3.15 summarises the overall results of this experiment.

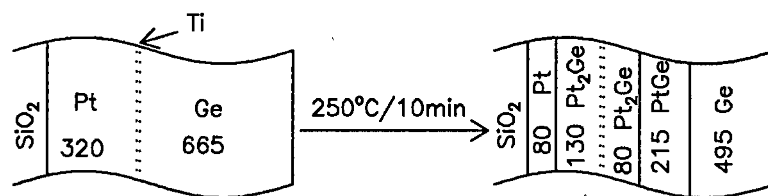

Figure 3.15: *Schematic representation illustrating relative marker movement during Pt_2Ge formation. Dominant diffusing species is determined from amounts of Pt_2Ge and PtGe above and below the marker. Pt is found to be the dominant diffusing species during Pt_2Ge formation. Thicknesses are in units of $10^{15}atm/cm^2$.*

3.3.3 Dominant Moving Species during PtGe Formation.

Due to the marker results obtained during the formation of the first phase, Pt_2Ge, Ti marker was subsequently rendered "useless" in monitoring the direction of atomic mobility during 2nd and 3rd phase formations. The marker had been shifted back during first phase formation process, and therefore the 2nd and 3rd phase formation processes took place in front of the marker. At this stage the Ti marker was no longer a marker. Sample configuration therefore had to be altered.

To determine the diffusing species during PtGe formation, samples of configuration Si<>/SiO_2 /Pt(240at/cm^2)/Ge(120at/cm^2)/Ti(12Å)/Ge(370at/cm^2) (the given thicknesses are nominal at this stage) were prepared so that the system could be forced to form the first phase below

the marker without atoms diffusing past the marker, see the ideal sketch in Figure 3.16. Upon further annealing, the marker would then start to monitor the direction of atomic mobility when PtGe forms from interaction of Pt_2Ge and surface germanium atoms.

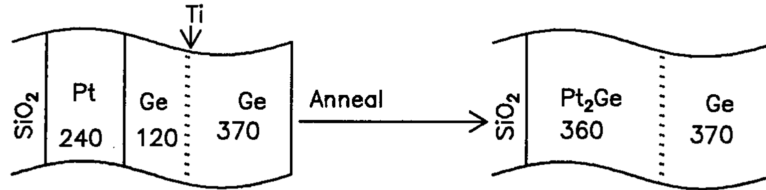

Figure 3.16: *Schematic representation of a sample prepared and annealed to form Pt_2Ge without atoms diffusing past the Ti marker. Upon further annealing, Ti marker will start to monitor the direction of atomic mobility during the formation of PtGe. The nominal thicknesses are given in units of 10^{15} atm/cm^2.*

The RBS spectrum obtained from an as deposited sample showed that germanium below the marker turned out to be slightly more than required to completely consume 240×10^{15}at/cm^2 of platinum during Pt_2Ge formation. The simulation measured 135×10^{15}at/cm^2 of Ge, and the ideal should have been 120×10^{15}at/cm^2. Figure 3.17 displays with simulation a backscattering spectrum obtained from a sample annealed at 250°C/80 min.
A surprising feature from the simulation is the distinctive presence of Pt_3Ge_2, a phase which has not been detected in the earlier investigation of this study when samples were prepared without Ti marker interposed at the platinum/germanium interface. Pt_3Ge_2 phase is a non-congruent phase situated between Pt_2Ge and PtGe on the Pt-Ge phase diagram, see Figure 1.3. It would then appear that after the formation of Pt_2Ge, the Ti marker prohibited the formation of PtGe from Pt_2Ge, and in the process stimulated the system to form Pt_3Ge_2.

However, it is clear from the RBS simulation, see Figure 3.17, that small amounts of PtGe are already present, both above and below the marker. It is also interesting to note that the total number of germanium atoms above the marker is still the same as that from an as deposited sample, suggesting that germanium atoms had not migrated from above the marker to below, and neither have they diffused from below to above the marker.

The only plausible explanation is that platinum atoms diffused from below the marker to interact with germanium atoms above the marker, and in the process, they (Pt atoms) leave PtGe below, and form PtGe above the marker. If platinum is the sole diffusing species during the formation of PtGe phase, and the simulation in Figure 3.17 suggests it is, then one would expect the total number of germanium atoms above the marker to remain conserved as PtGe grows above and below the marker.

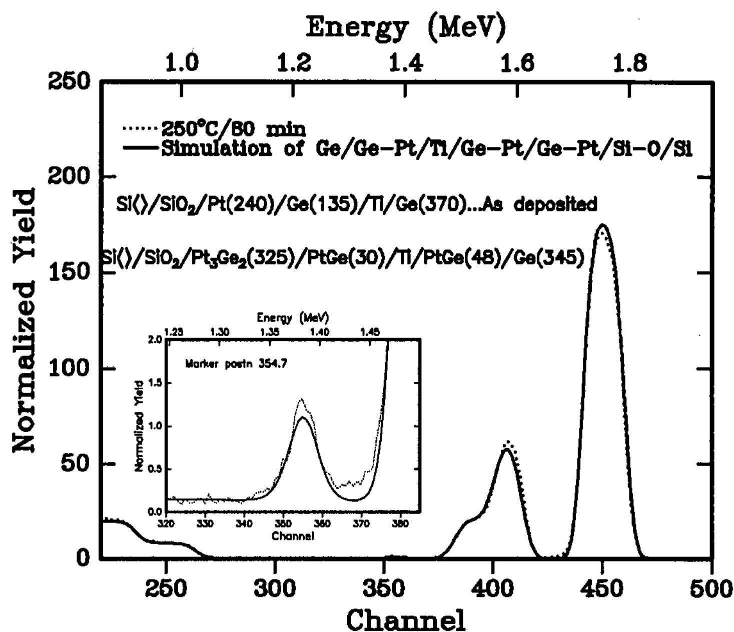

Figure 3.17: *RBS spectra from a sample annealed at 250°C/80 min. The total number of germanium atoms(~370) above the marker suggest that platinum is the sole diffusing species during PtGe formation. Thicknesses are given in units of 10^{15}at/cm^2. The region with Ti signal has been blown up to show the agreement on marker position between actual data and RUMP simulation.*

The spectra displayed in Figure 3.18 reflects this state of affairs. An attempt to anneal for times longer 80 minutes at 250°C proved futile in that the system started growing $PtGe_2$. The spectra in Figure 3.18 was obtained from a sample annealed at 280°C/40min. It is clear from the simulation that the total number of germanium atoms above the marker is still the same as that from an as deposited sample, and that PtGe had grown thicker both above and

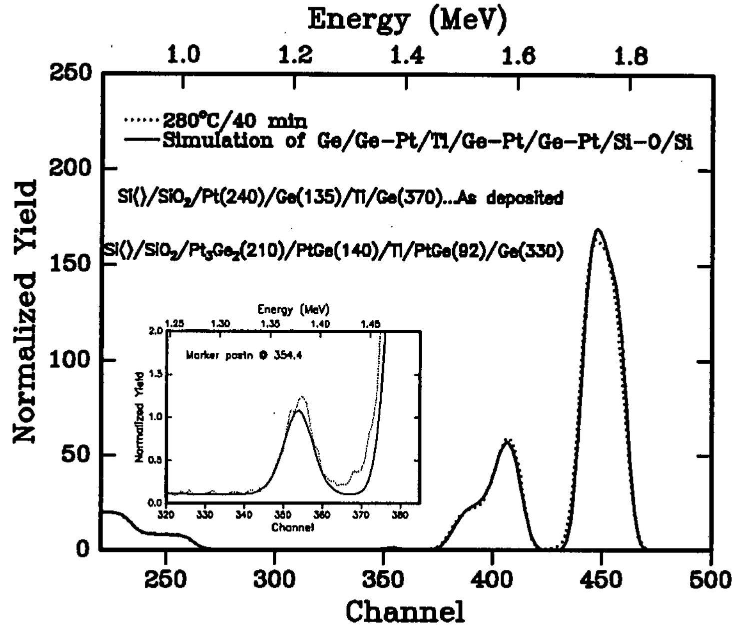

Figure 3.18: *RBS spectra from a sample annealed at 280°C/40 min. The total number of germanium atoms(~370) above the marker suggest that platinum is the sole diffusing species during PtGe formation. Thicknesses are given in units of 10^{15}at/cm^2. The region with Ti signal has been blown up on the bottom spectrum to show the agreement on marker position between actual data and RUMP simulation.*

below the marker. It therefore appears from these results that platinum is the sole diffusing species during the formation of PtGe phase. It must also be pointed out that the PtGe growth below the marker in this case came as a result of Pt_3Ge_2 decomposition and not from Pt_2Ge as is generally the case in the absence of the marker. If there is any limitation to the validity of the PtGe marker results, it is that the results are based on relatively small amount of PtGe growth, resulting in slight shift in marker position. The PtGe marker results are therefore not as authentic as those of Pt_2Ge phase.

3.3.4 Dominant Moving Species during $PtGe_2$ Formation.

To determine the diffusing species during $PtGe_2$ formation, techniques similar to the ones described in the preceding experiments were applied to prepare samples of the following

configuration:

Si<>/SiO_2/Pt(185at/cm^2)/ Ge(185at/cm^2)/Ti(12Å)/Ge(185at/cm^2). The nominal thicknesses are such that Ti marker will only start monitoring the direction of atomic flux during $PtGe_2$ formation. PtGe is expected to form below the marker without displacing the marker position, see ideal sketch in Figure 3.19.

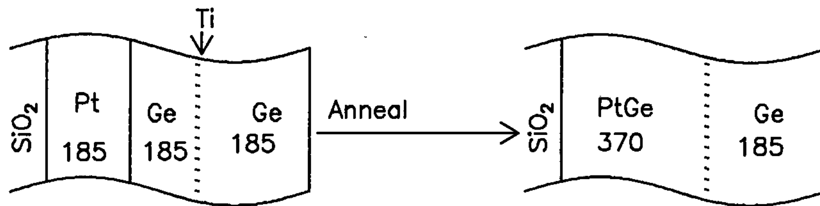

Figure 3.19: *Schematic representation of a sample prepared and annealed to form PtGe without atoms diffusing past the Ti marker. Upon further annealing, Ti marker will monitor the direction of atomic mobility during the formation of $PtGe_2$. The nominal thicknesses are given in units of 10^{15}at/cm^2.*

RBS spectrum from an as deposited sample is displayed with its simulation in Figure 3.20. It must be noted from the simulation that surface germanium turned out less thick than was expected to drive the system to $PtGe_2$ phase completely, it is about 145×10^{15}at/cm^2 when it should have been 185×10^{15}at/cm^2. However, valuable information could still be extracted. Figure 3.21 displays a spectrum from a sample annealed at 260°C/40 min. The simulation clearly shows that the system behaved as expected, PtGe phase had formed below the marker, the total thickness of which is 370×10^{15}at/cm^2. It is also interesting to note that the marker position remained the same as that of an as deposited sample(channel ~364.5), and so is germanium thickness on the surface.

Figure 3.22 shows an RBS spectrum from a sample annealed at 300°C/50 min. It can be seen from the simulation that $PtGe_2$ phase had grown above and below the marker. Only 110×10^{15}at/cm^2 $PtGe_2$ is above the marker, i.e 73×10^{15}at/cm^2 germanium atoms/cm^2 had remained above the marker, the rest (~70×10^{15}) have diffused past the marker to form $PtGe_2$ and Pt_2Ge_3 below the marker. [Note that the non-congruent phase, Pt_2Ge_3 was also

not observed in the earlier experiment without the marker]. On the other hand, there are now about 37 platinum (one third of 110) atoms/cm^2 above the marker. As was the case in the second phase (PtGe), the observed $PtGe_2$ growth seems very limited, resulting with only a slight shift of the marker position. The overall $PtGe_2$ results suggest that germanium is the dominant diffusing species during the formation of $PtGe_2$ phase, with the ratio of about 2:1, i.e 73(Ge):37(Pt).

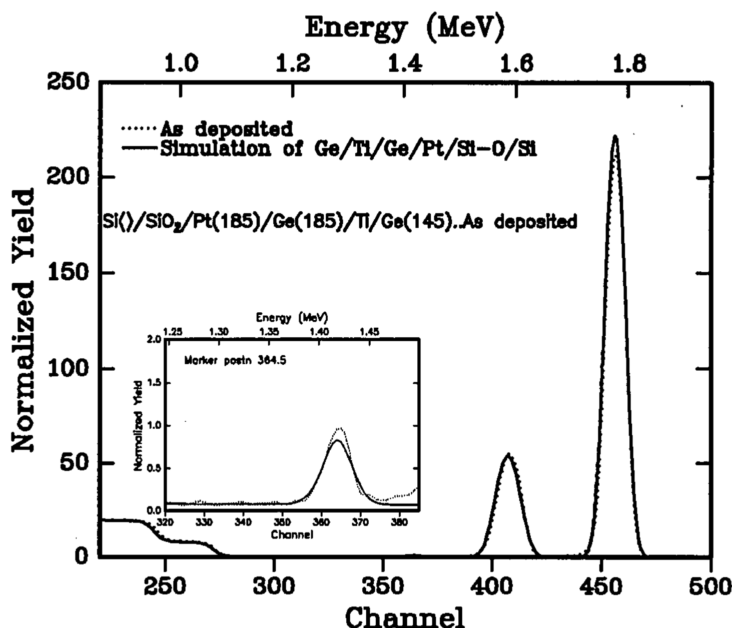

Figure 3.20: *RBS spectrum from an as deposited sample. A thin layer of Ti(12Å) between two germanium layers serves as an inert marker to monitor atomic mobility during $PtGe_2$ formation. The region with Ti signal has been blown up to show the agreement on marker position between actual data and RUMP simulation.*

3.3.5 Discussion

By observing the movement of Ti marker, the direction of atomic mobility was monitored during the formation of three germanide phases of platinum. During Pt_2Ge formation, platinum atoms were found to be the dominant diffusing species with an estimated ratio of 4:1. The formation of PtGe phase was found to occur solely by platinum diffusion. The

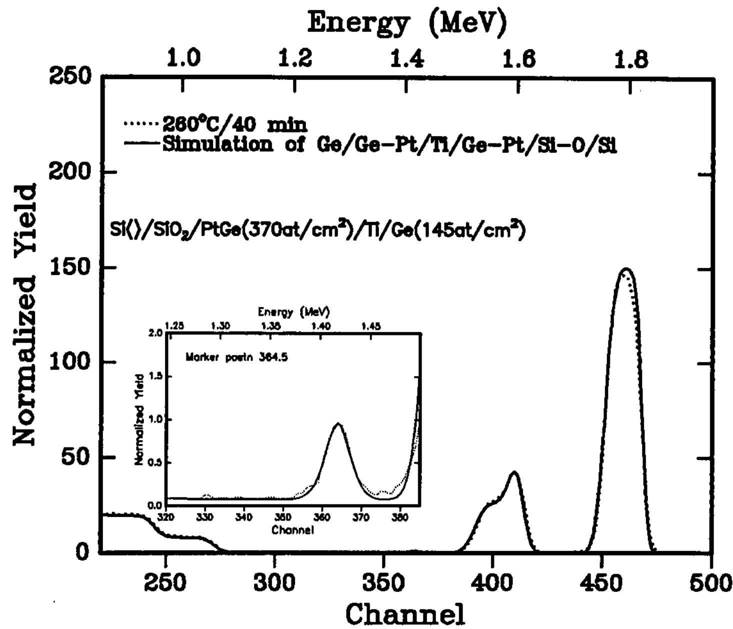

Figure 3.21: *RBS spectra from a sample annealed at 260°C/40 min. The simulation shows that PtGe phase had formed completely behind the marker. The marker position is still the same as that of the an as deposited sample, and so is surface germanium thickness. The marker would then start to monitor atomic mobility during $PtGe_a$ formation.*

last germanide of platinum, $PtGe_2$, was found to form through the mechanism in which germanium is the dominant diffusing species, with an estimated ratio of 2:1.

The observation of platinum as the dominant diffusing species during Pt_2Ge formation is consistent with previous findings in which Marshal et al Marshal:1 used a different marker (molybdenum) and arrived at similar conclusion. In their experiment, Marshal et al also noted that the behaviour of several germanide systems exhibited a one-to-one correspondence with Metal/Silicon systems. The dominant diffusing species during the formation of Pt_2Si were investigated by Tu [48] and Poate et al [49] who both observed Pt as the dominant species. It is interesting to note that the similarity in behaviour of germanides and silicides, as observed by Marshal et al Marshal:1, also exists in dominant diffusing species during first phase formation of germanide and silicide of platinum, Pt_2Ge and Pt_2Si respectively.

Tu and Mayer [50] also observed that for Metal/Silicon systems, metal atoms tend to be

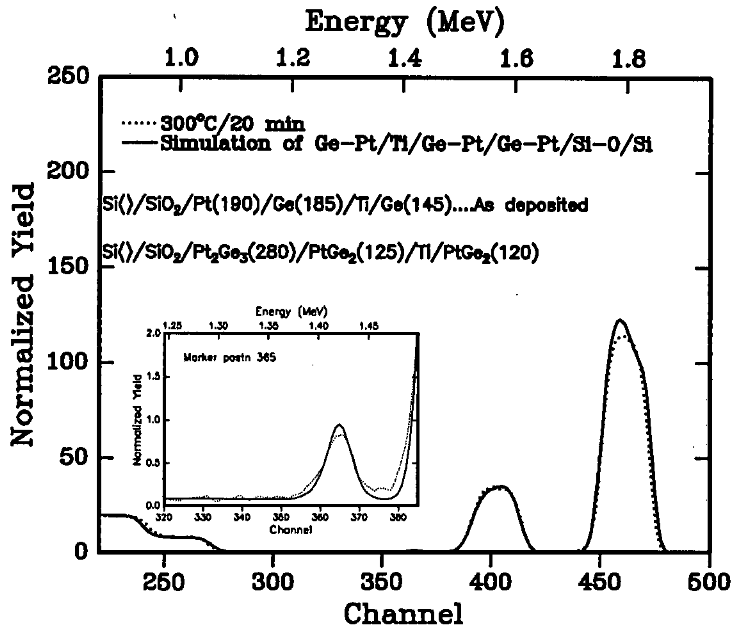

Figure 3.22: *RBS spectra from a sample annealed at 300° C/50 min. The simulation shows that* $PtGe_2$ *phase had formed below and above the marker. Thicknesses are given in units of* $10^{15} at/cm^2$. *The total number of germanium atoms above the marker suggest that germanium is the dominant diffusing species.*

the dominant diffusants during the formation of metal rich silicides (M_2Si) while silicon atoms become the dominant diffusing species during the formation of disilicides (MSi_2). The overall results obtained in this study are consistent with this picture, which further affirms the germanide-silicide similarity suggested by Marshal et al [2].

In the two experiments designed to investigate the DMS during PtGe and $PtGe_2$ formation, the presence of Ti marker stimulated the formation of non-congruent phases, Pt_3Ge_2 and Pt_2Ge_3 (respectively). This can be taken as basis to speculate that Ti acted as a barrier after the formation of precursor phases. Compared to Pt_2Ge, both PtGe and $PtGe_2$ were limited in their growth. The results of the two phases (PtGe and $PtGe_2$) are therefore not as conclusive as those of Pt_2Ge. Further confirmation is clearly required on the dominant diffusing species during PtGe and $PtGe_2$ formation.

Chapter 4

Lateral Diffusion in Pt-Ge system

4.1 Introduction

Lateral diffusion couples of both Pt and Ge islands on Ge and Pt thin films were prepared respectively using conventional electron gun evaporation. For one set of samples, Pt($\sim$330$\mathring{A}$) thin film was deposited on SiO_2 buffered silicon substrate. Si mask was then brought into close contact with the substrate without breaking the vacuum, and Ge($\sim$1350$\mathring{A}$) was then evaporated through $780\mu m \times 390\mu m$ rectangular windows in the Si mask, so that Ge islands were formed on top of Pt thin film, see Figure 4.1(a).

A similar procedure was followed to prepare Pt($\sim$1500$\mathring{A}$) islands on Ge($\sim$400$\mathring{A}$)thin film, see Figure 4.1(b). The layer thickness for Ge island samples was specifically designed to result in atomic ratio of Ge to Pt larger than the most Ge rich phase in Pt-Ge system, viz $PtGe_2$, so as to allow for sufficient number of unreacted germanium atoms to diffuse laterally out into the surrounding thin film. By the same token, the atomic ratio of Pt to Ge, for Pt island samples, was designed to be larger than the most Pt rich phase of Pt-Ge system, viz Pt_3Ge.

Both evaporations were sequentially carried out in the evaporation chamber without breaking the vacuum. After evaporation, samples were annealed in a vacuum furnace at 500°C for 30 - 180 minutes. Sample analysis was carried out in two stages, first with SEM and then

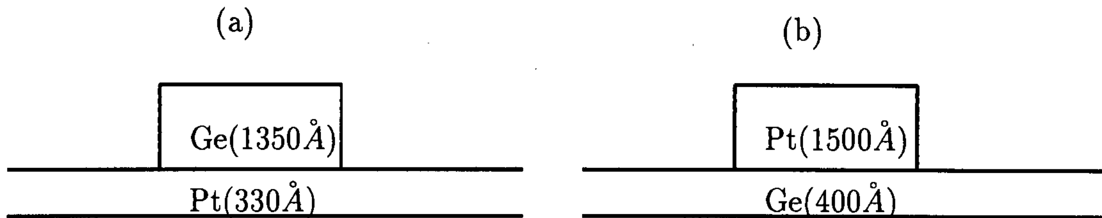

Figure 4.1: *Schematic diagram showing the side view of the specimens prepared and examined in this study. (a) Germanium island on platinum thin film, (b) Platinum Island on germanium thin film.*

RBS using Microprobe scanning of selected reacted zones with a 2 MeV α beam focussed down to ~1 μm. Results obtained are presented below.

4.2 SEM Results

The observed lateral diffusion was very limited on samples of Pt island on Ge thin film configuration. For this set of samples, only a few SEM micrographs shall be presented to show the initial processes that took place. It was on samples of Ge islands on Pt thin films that lateral diffusion was observed on a large scale.

4.2.1 Pt islands on Ge thin Film

SEM results obtained from Pt islands samples are shown in Figure 4.2 and Figure 4.3. The micrograph in Figure 4.2 was obtained from an "as deposited" sample. The surrounding Ge thin film appears dark, and the Pt island appears bright. The edges of Pt islands are relatively sharp, showing no signs of Pt-Ge mixture, see Figure 4.2.

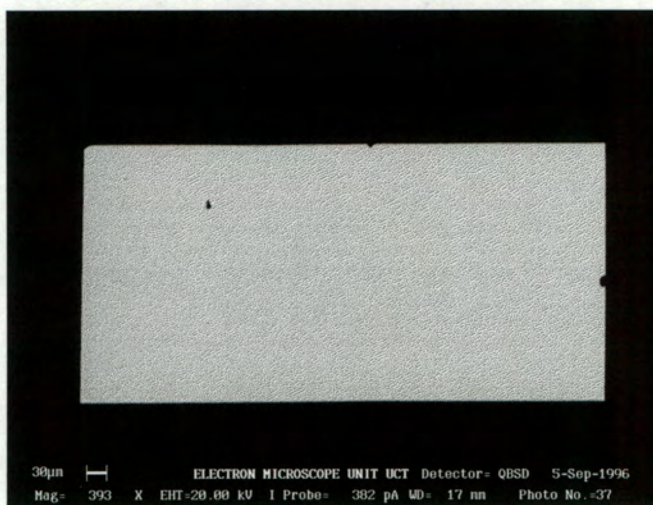

Figure 4.2: *Scanning Electron Micrograph from an as deposited sample with Pt island(1500Å) on Ge(400Å) thin film. The image was recorded using backscattered electrons*

The micrographs in Figure 4.3 were obtained from samples annealed at 500°C/30min(top) and 500°C/180min(bottom). On both micrographs in Figure 4.3, a "white line" appears at the island edge, followed by a "greyish" area inside the island.

A comparison of top and bottom micrographs reveals that the lateral extent of the greyish region inside the island proceeds only to a certain point and stops. The lateral distance of the greyish region is about 4.5 μm on both top and bottom micrograph despite the fact that the two specimen were respectively annealed at 500°C for 30 and 180min.

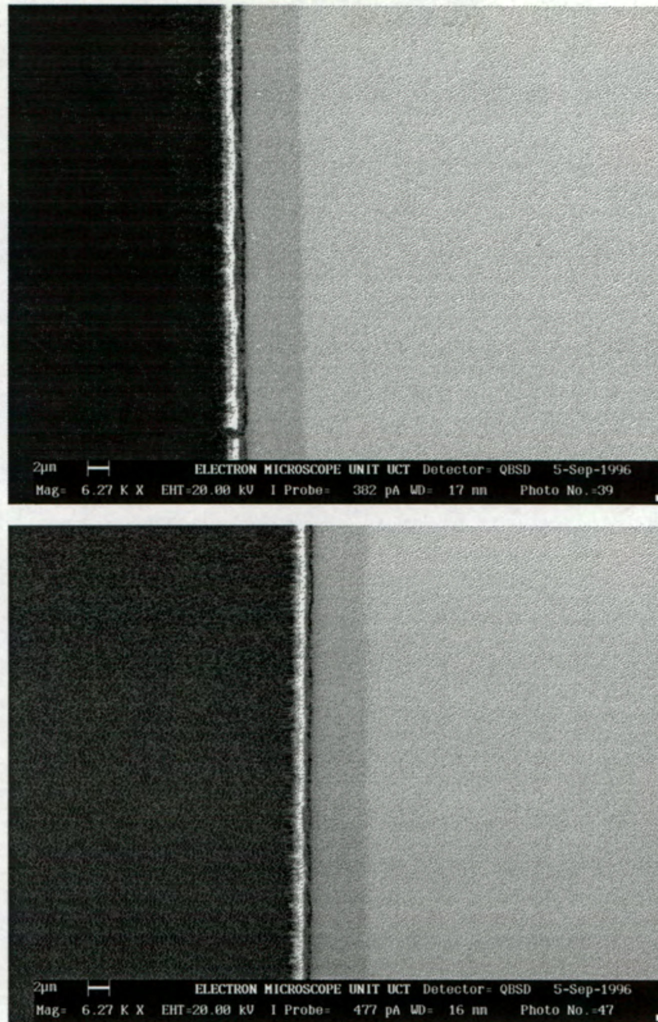

Figure 4.3: *Scanning Electron Micrographs obtained from samples of Pt island(1500Å) on Ge(400Å) thin film annealed at 500°C/30min(top) and 500°C/180min(bottom). Both images were recorded using backscattered electrons.*

It can therefore be inferred that the reaction resulting in the greyish region was stopped at a certain point. An observation like this is usually a result of high inward mobility of atoms from thin film into the "source" region which consequently forms a thin diffusion region and ultimately a crack between thin film and island region [51]. It therefore appears that after the underlying germanium atoms were consumed in the source region, there was a lateral flux of Ge atoms into the source region which resulted in a crack between the island boundary and the thin film, hence the reaction could not proceed. The "bridge" between surrounding

thin film and the island had been "broken". Micro-probe RBS was not performed on these samples.

4.2.2 Ge islands on Pt thin film

SEM micrograph, from backscattered electrons, displaying an as prepared state of Ge island /Pt thin film lateral diffusion couple is shown in Figure 4.4. The dark region represents bare Pt(~330Å) thin film, and the bright region represents Ge island(~1350Å). The edges of Ge islands appear relatively sharp, with no indication of phase formation.

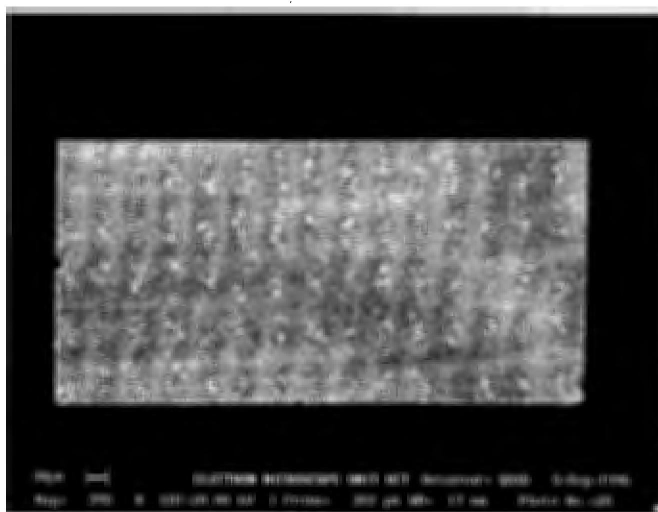

Figure 4.4: *Scanning Electron Micrograph obtained from an as prepared sample with Ge island(1350Å) on Pt(330Å) thin film. The bright region represents the Ge island and the dark the Pt thin film. The image was recorded using backscattered electrons.*

When samples were annealed at 500°C for 30, 90 and 180 minutes, SEM results revealed a series of distinct regions both inside and outside the source region. Depletion of Ge atoms from the source region was strikingly clear. The samples were all analysed using the same procedure. A detailed description of reacted samples is therefore only given for a sample annealed at 500°C/90min. The results from two other samples are displayed without further interpretation.

The lateral extent of diffusion zones for a sample annealed at 500°C/90min is displayed in

the scanning electron micrograph(backscattered electrons) in Figure 4.5.

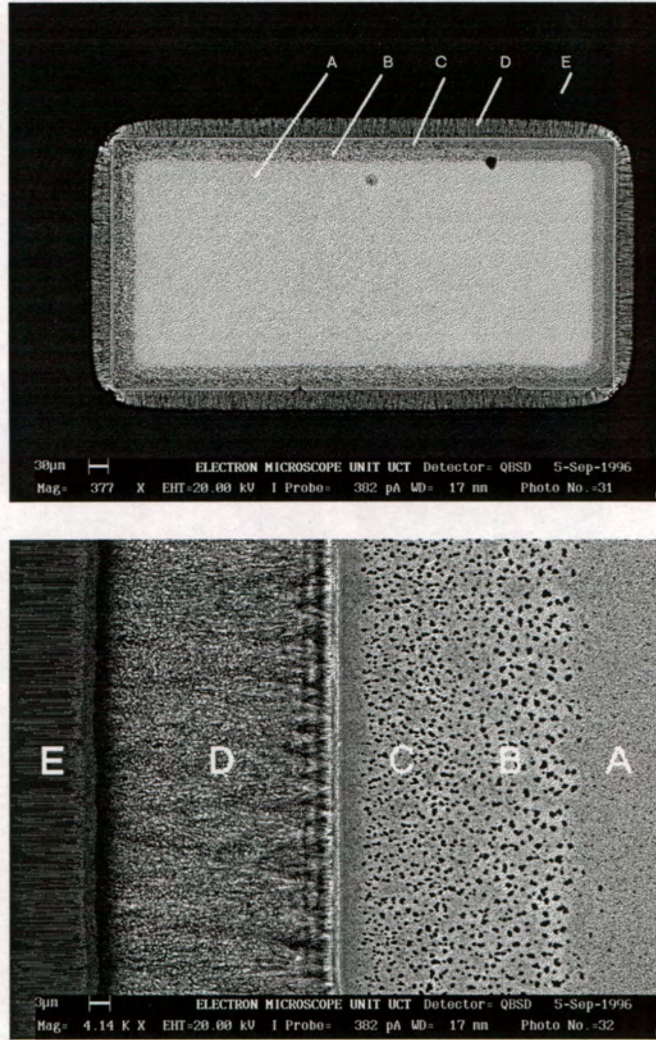

Figure 4.5: *Scanning Electron Micrographs obtained from a sample of Ge island(~1350Å) on Pt(330Å) thin film annealed at 500°C/90min. The bottom image is the enlarged end of the top one. Region E is the Pt thin film and A is the Ge source. Regions B, C and D are mixtures of Pt and Ge. Both images were recorded from backscattered electrons.*

The bottom image is the enlarged end of the top one. A total of 5 regions numbered from A to E appear distinct on the electron micrographs. On the top micrograph, the original source region is clearly indicated by a visible white line separating regions C and D. With the exception of thin film and source regions, i.e. E and A, there are 3 distinct regions, 2

inside (B and C) and one (D) outside the original island. Furthermore, the outside region (D) appears relatively different from regions inside the island, in both brightness and texture, see Figure 4.5(bottom). The appearance of dark patches is a common feature between regions B and C. However, a closer look reveals that the dark patches are more evenly spaced in B and more congested in C. Such dark patches are absent in region D, instead region D is textured in a dendroid form, suggesting a formation mechanism quite different from the ones at play in regions B and C. The texture in region D is further confirmation that Ge atoms are being depleted from the source and are diffusing into the surrounding film. An interesting feature can be seen on the periphery of the island corners, region D is limited in growth at these areas. This might be an indication that as germanium atoms migrate from the source, they diffuse in all directions, tracing a kind of "cone shape on the horizontal plane". The area supported by the corner of the island is therefore relatively large, and continues to be enlarged as the source shrinks in, resulting in limited growth on the island corners. This hypothesis is further supported by the V-shaped dendroids in region D.
The bottom micrograph further shows a thin dark region at the interface between the surrounding Pt thin film (E) and Pt germanide film (D). Also note that the boundary line (between C and D) appears brighter than all regions. Using backscattered electrons, the intensity of the region will be a consequence of either thickness, or density of the compound or element in that region. The two possibilities cannot be clearly resolved with SEM.
The micrographs corresponding to two other samples (500°C/30 and 180min) both bear similar features as the ones observed in Figure 4.5, differing only in the extent of their growth. SEM results from these two other samples are therefore displayed without further interpretation in Figure 4.6 and Figure 4.7.

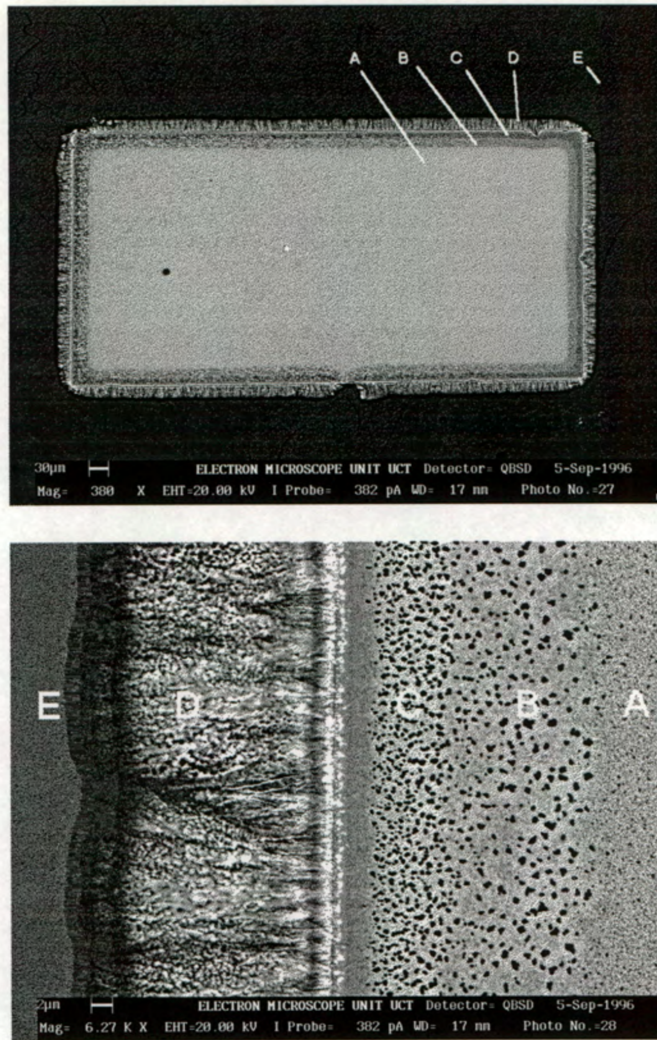

Figure 4.6: *Scanning Electron Micrographs obtained from a sample of Ge island(∼1350Å) on Pt(330Å) thin film annealed at 500°C/30min. Region E is the Pt thin film and A is the Ge source. The bottom image is the magnified end of the top one. Both images were recorded from backscattered electrons.*

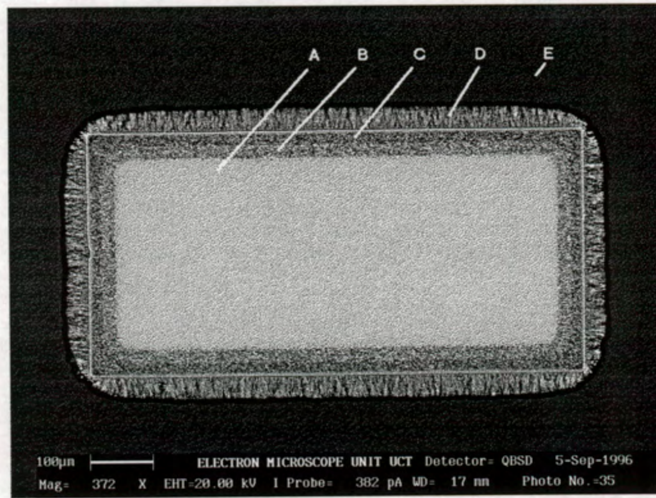

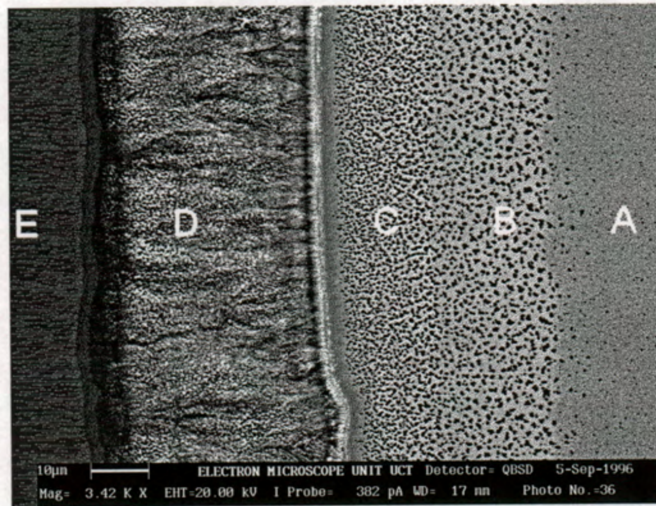

Figure 4.7: *Scanning Electron Micrographs obtained from a sample of Ge island(~1350Å) on Pt(330Å) thin film annealed at 500°C/180min. Region E is the Pt thin film and A is the Ge source. The bottom image is the magnified end of the top one. Both images were recorded from backscattered electrons.*

4.3 Microprobe Results

A technique which has been termed μRBS was recently introduced at the National Accelerator Center (NAC) in the nuclear microprobe facility [52]. In this technique, a beam of α particles is focussed down to ~1 μm and scanned across a well defined selected area on a specimen. A typical area of $128\mu m \times 128\mu m$ is covered on a specimen and scanned in one experimental run. Backscattered particles are detected using an annular detector at a scattering angle of 176°. The energy of each detected particle is recorded, along with the position of the beam at that moment. At a subsequent time, this list of data is analysed, enabling the determination of an RBS spectrum emanating from any specific point. To optimally exploit beam position without losing out on RBS statistics, points along a vertical or horizontal line can be grouped together, giving an RBS spectrum at any specific distance from the original island edge. In this way, sets of spectra can be obtained which reflect both thickness and composition data as a function of lateral diffusion distance.

In the analysis of lateral diffusion samples, μRBS technique evidently suggests itself as a preferable analytical tool.

In this study, μRBS was done on samples of Ge islands on Pt thin film.

4.3.1 Ge islands on Pt thin film

To perform μRBS on the samples, a window of area $128\mu m \times 128\mu m$ was set to include all types of regions observed on SEM micrographs, i.e Pt thin film and part of Ge island on an as prepared sample, and Pt thin film + all reacted zones (A-E) on annealed samples.

A micro-beam($\sim 1\mu m$) of α particles was scanned across this area, generating RBS spectra as a function of beam position. Each RBS spectrum was averaged from a "slice" of area $1\mu m \times 128\mu m$ in order to improve RBS statistics.

Two RBS spectra selected from an as deposited sample are displayed in Figure 4.8(top). The displayed spectra correspond to two different regions of the specimen, on the Ge island, see Figure 4.8(a), and on Pt thin film, see Figure 4.8(b). From RBS spectra, both Pt and

Ge peaks were then separately integrated to get their respective yields at different beam positions. On the bottom part of the same figure (Figure 4.8), a total number of both Pt and Ge counts obtained from RBS spectra is plotted as a function of beam position. Note that around $60\mu m$, germanium counts drop rapidly, confirming the relatively sharp Ge edge observed on SEM micrograph, refer to Figure 4.4 for the corresponding SEM micrograph. The interesting feature in Pt data is a slight drop in Pt counts in the region outside the island, i.e. where platinum is not covered with Ge island. The drop in platinum counts in this region is not a result of variation in Pt concentration, but a consequence of the inverse proportionality between differential scattering cross section and energy of backscattered particles, i.e $\frac{d\sigma}{d\Omega} \propto \frac{1}{E^2}$ [21]. Particles backscattered from underneath the island already had lower incoming energy as a result of energy loss along their inward path. The differential scattering cross section for Pt atom is therefore high in the Ge source region than it is in the Pt thin film region.

RBS results obtained from a sample annealed at 500°C/90min are displayed in Figure 4.9 (a) and (b). The RBS spectra were collected from different regions observed with SEM in Figure 4.5. Using RUMP program, both platinum and germanium peaks were integrated and their yield plotted as a function of beam position in Figure 4.9(c). The platinum data in Figure 4.9(c) reveals some interesting features. The vertical line, drawn at $\sim 76\mu m$ corresponds to the original interface between Ge island and the surrounding Pt thin film. For simplification, this line will be referred to as the interface line. Platinum yield remains relatively constant in the region left of the interface line, while germanium yield drops thrice across the same region, at 39, 59 and $\sim 75\mu m$.

The fact that germanium yield drops thrice in the same region where platinum yield is constant suggests a variation in compound composition. A sharp peak on the interface line is also notable on platinum data. Around $111\mu m$, a well pronounced platinum dip suggests that platinum was "sucked" during the formation of the compound in the region labelled D, see Figure 4.9(c). It can therefore be inferred that as the compound in region D grows laterally out, it "feeds" on the lateral movement of both germanium (from the source region)

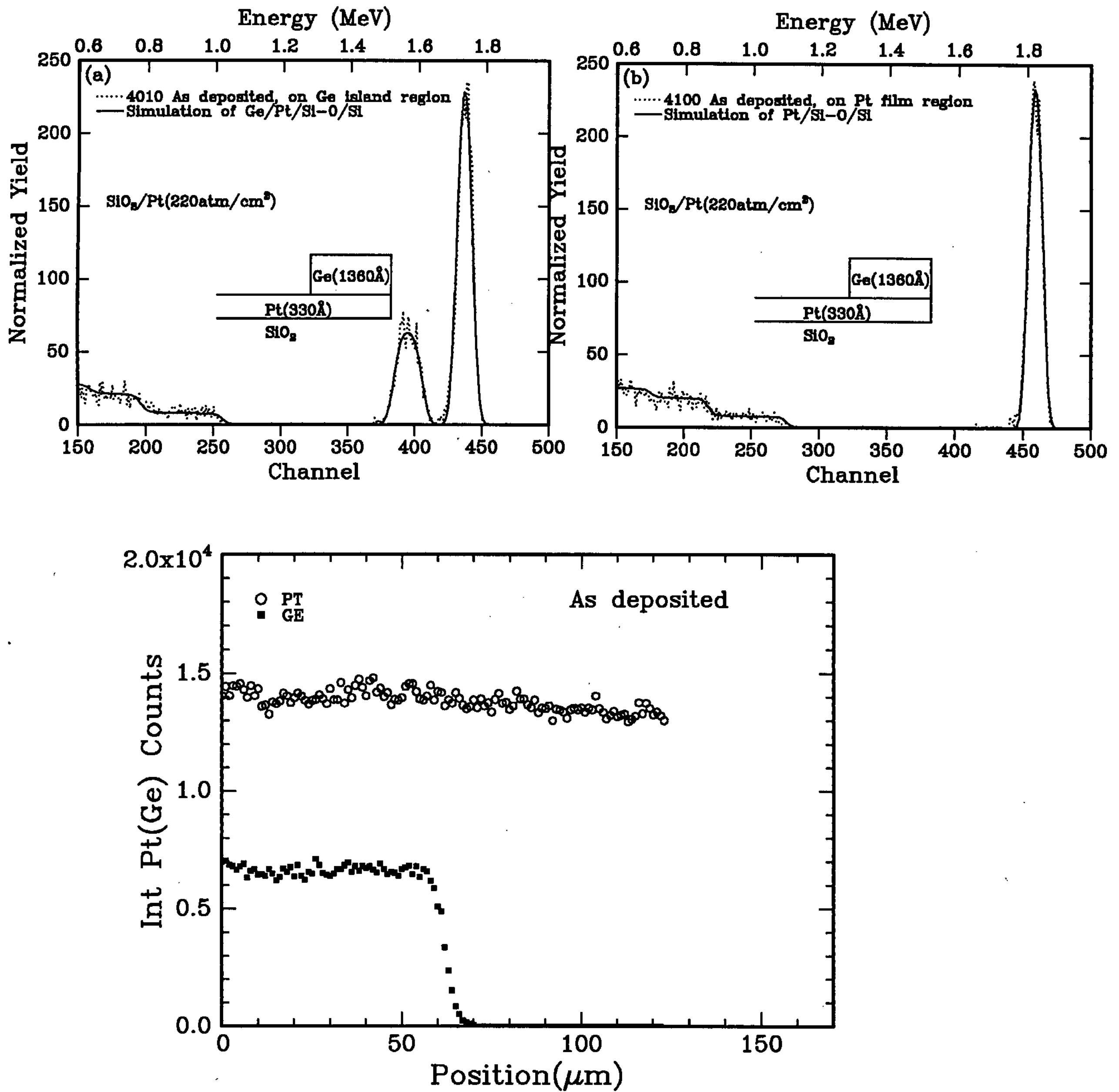

Figure 4.8: *Two RBS spectra(top), (a) and (b), obtained from an as prepared lateral diffusion couple of Ge island(~1360Å) on Pt thin film(~330Å). The spectra are displayed with their RUMP simulation to show good agreement with collected data. At the bottom is a plot of Pt and Ge integrated counts from RBS peaks across Ge island and Pt thin film regions.*

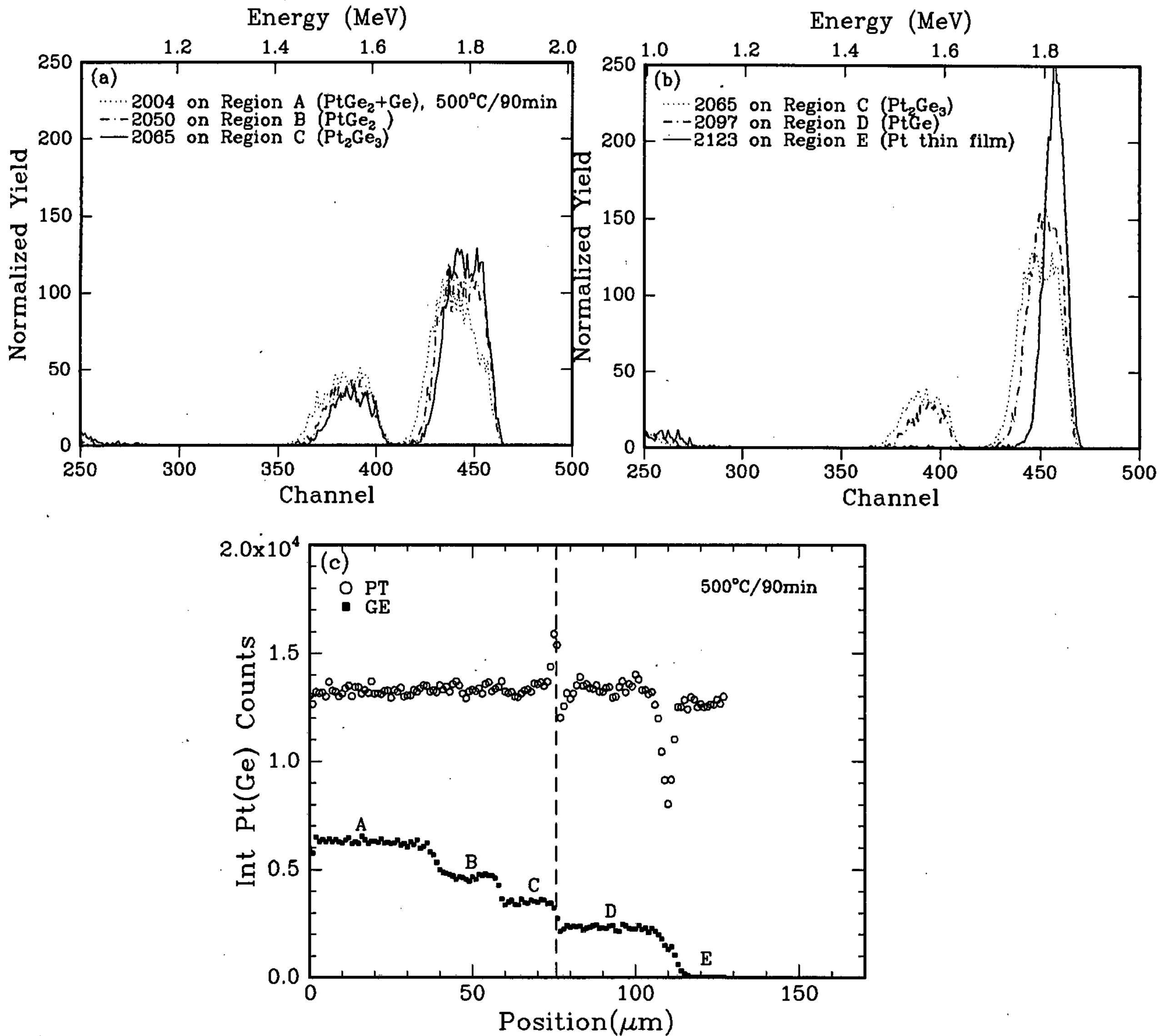

Figure 4.9: *RBS spectra, (a) and (b), obtained from lateral diffusion couple of Ge island(~1360Å) on Pt thin film(~330Å) annealed at 500°C/90min. The spectra are displayed in the sequence ranging from the innermost region(A) to the outermost one(E). The numbering of regions corresponds to that used in the SEM micrographs. Both Pt and Ge peaks were integrated and their counts plotted against beam position in (c). Four different regions are clearly in their decreasing order of germanium content. The vertical line corresponds to the original interface between Ge island and the surrounding Pt thin film.*

and platinum atoms from the surrounding thin film.

Using platinum and germanium number of counts in Figure 4.9(c), compound composition was calculated at different reacted zones. Figure 4.10(a) is a composition profile, normalised for platinum ($PtGe_x$) across the reacted regions. The plot shows different compositions at different regions. The composition in regions B, C and D were found to correspond to $PtGe_2$, Pt_3Ge_2 and PtGe respectively. While region E remained unreacted platinum, it was found that region A composed of both $PtGe_2$ and unreacted Ge.

A plot of thickness versus position displayed in Figure 4.10(b) shows that thickness is fairly uniform on Ge+$PtGe_2$ region(A), the $PtGe_2$ region(B) is also fairly uniform, while Pt_2Ge_3 and PtGe regions (C and D) are not as uniform. PtGe region is more thicker around 95-105μm, but drops rapidly around 110μm, a position corresponding to the platinum dip observed in Figure 4.9(c).

Around the original interface line(~75μm), PtGe also appears thicker, this thickness is more prominent on plots corresponding to samples annealed at 500°C/30 and 180minutes which are displayed later. A quick glance back at the SEM micrograph in Figure 4.5 will therefore suggest that the white line on the micrograph was not a result of a different compound, but thickness of PtGe compound. PtGe region therefore starts thicker at the original interface line and spreads out all the way to its interface with the surrounding Pt thin film. The region where PtGe interfaces with the surrounding thin film (~110-111μm) is thinner, but still of composition PtGe, see Figure 4.10(b). The position of this narrow region corresponds to that of a "dark" wedge separating region C and D on SEM micrograph in Figure 4.7.

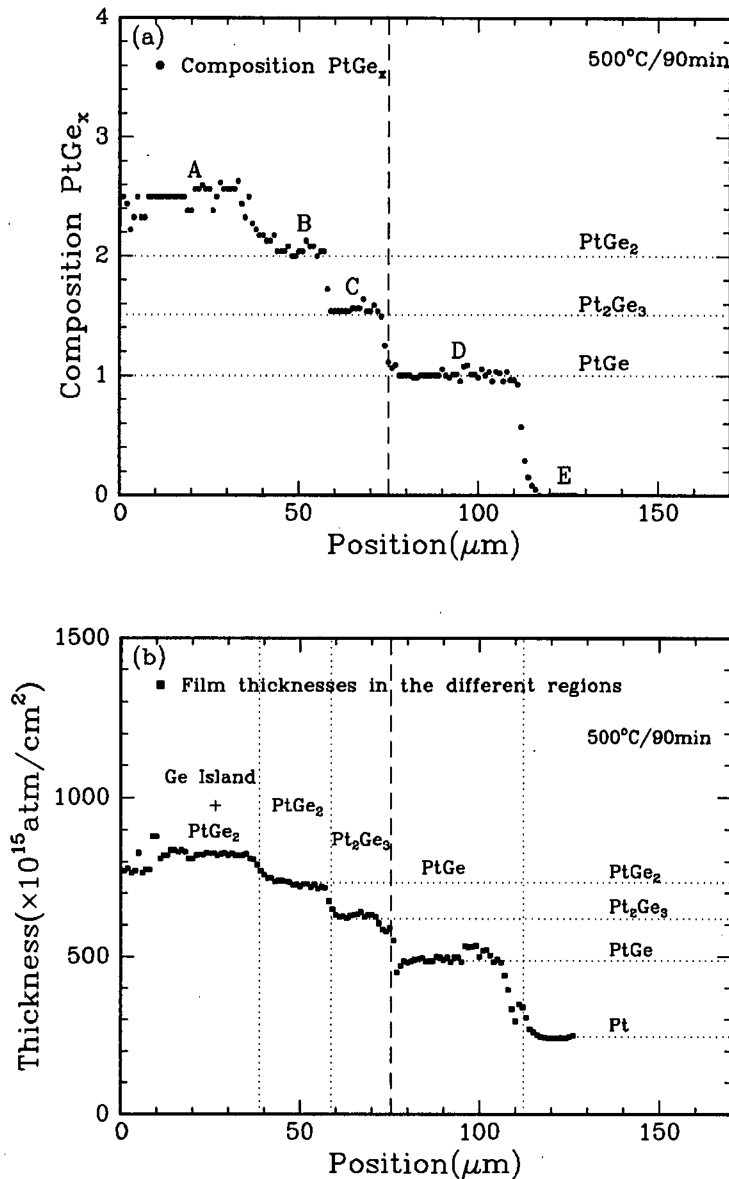

Figure 4.10: *(a) A plot of compound composition ($PtGe_x$) versus beam position for a lateral diffusion couple of Ge island (~1350Å) on Pt (~330Å) thin film annealed at 500°C/90min. The vertical line at ~76μm indicates the initial position of island/thin film boundary (or interface line). (b) A plot of compound thickness versus beam position across the reacted zones. Thicknesses were obtained from RUMP simulations. Vertical dotted lines were drawn to partition different Pt-Ge compounds identified in (a). The horizontal dotted lines indicate the expected total thickness for a particular germanide, assuming that the deposited platinum film was uniform and that only germanium atoms were the moving species.*

Similar results were obtained from two other samples annealed at 500°C/30min and 500°C/180min, with relative differences in the width of reacted zones. The results corresponding to these samples are displayed in Figure 4.11 → Figure 4.14.

The major difference between the sample discussed (500°C/90min) and the other two samples (500°C/30, 180min) is the size of platinum dip. The dip is expectedly wider on a sample annealed at 500°C/180min, and notably extends deeper than on the two other samples, see Figure 4.13. It is however disturbing to note that the platinum dip from a sample annealed at 500°C/30min (see Figure 4.11) appears wider and deeper than that from a sample annealed at 500°C/90min (see Figure 4.9). A further significant difference is that the "spur" on the interface line appears more pronounced on samples annealed at 500°C/30min and 500°C/180min than it is on a sample annealed at 500°C/90min.

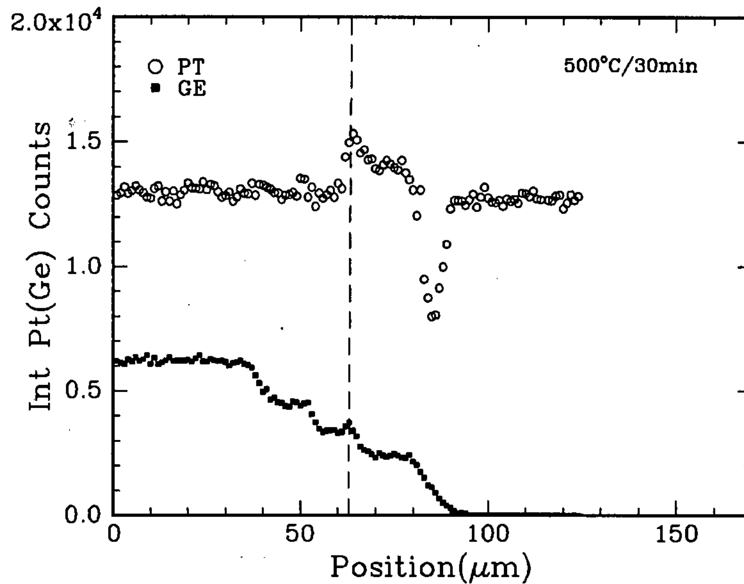

Figure 4.11: *A plot of Pt and Ge counts versus beam position for a diffusion couple of Ge island(~1360Å) on Pt thin film(~330Å) annealed at 500°C/30min. The number of counts were obtained from RUMP using integration command. The vertical line corresponds to the position of the initial interface between Ge island and the surrounding Pt thin film. A well pronounced platinum dip at ~85μm is clear indication that platinum atoms have migrated to the left of the dip and are congregating in the region between the interface line and the dip. On both platinum and germanium data, a "spur" is notable on the interface line.*

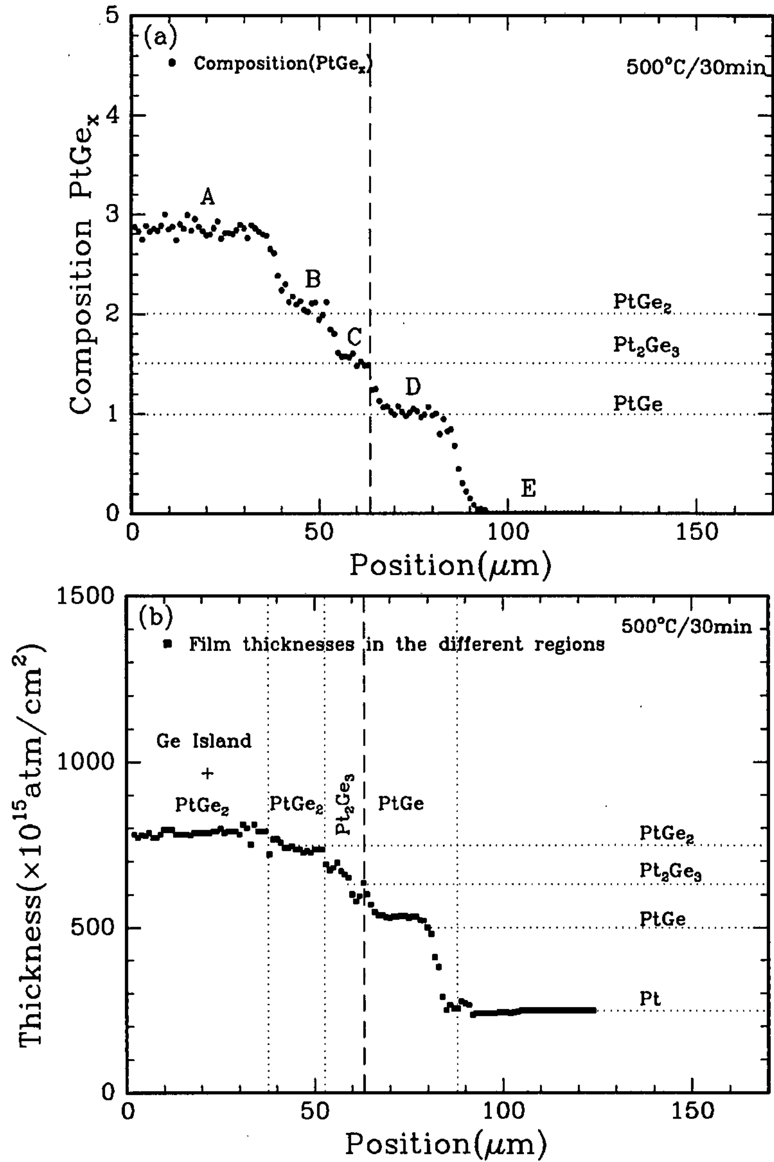

Figure 4.12: *(a) A plot of compound composition(PtGe$_x$) versus position for a lateral diffusion couple(Ge island(~1350Å)) on Pt (~330Å) thin film annealed at 500°C/30min. The vertical line at ~62μm indicates the initial interface between island and surrounding thin film. (b) A plot of compound thickness versus beam position across the reacted zones. Thicknesses were obtained from RUMP simulations. Vertical dotted lines were drawn to partition different Pt-Ge compounds identified in (a). The horizontal dotted lines indicate the expected total thickness for a particular germanide, assuming that the deposited platinum film was uniform and that only germanium atoms were the moving species.*

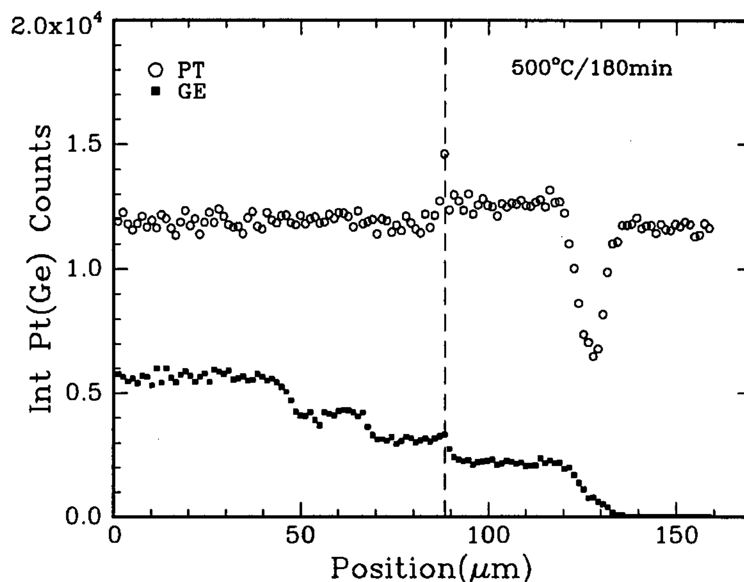

Figure 4.13: *A plot of Pt and Ge counts versus beam position for a diffusion couple of Ge island(~1360Å) on Pt thin film(~330Å) annealed at 500°C/180min. The number of counts were obtained from RUMP using integration command. The vertical line corresponds to the position of the initial interface between Ge island and the surrounding Pt thin film. A more prominent platinum dip at ~129μm is clear indication that platinum atoms have migrated to the left of the dip and are congregating in the region between the interface line and the dip. On both platinum and germanium data, a "spur" is notable on the interface line.*

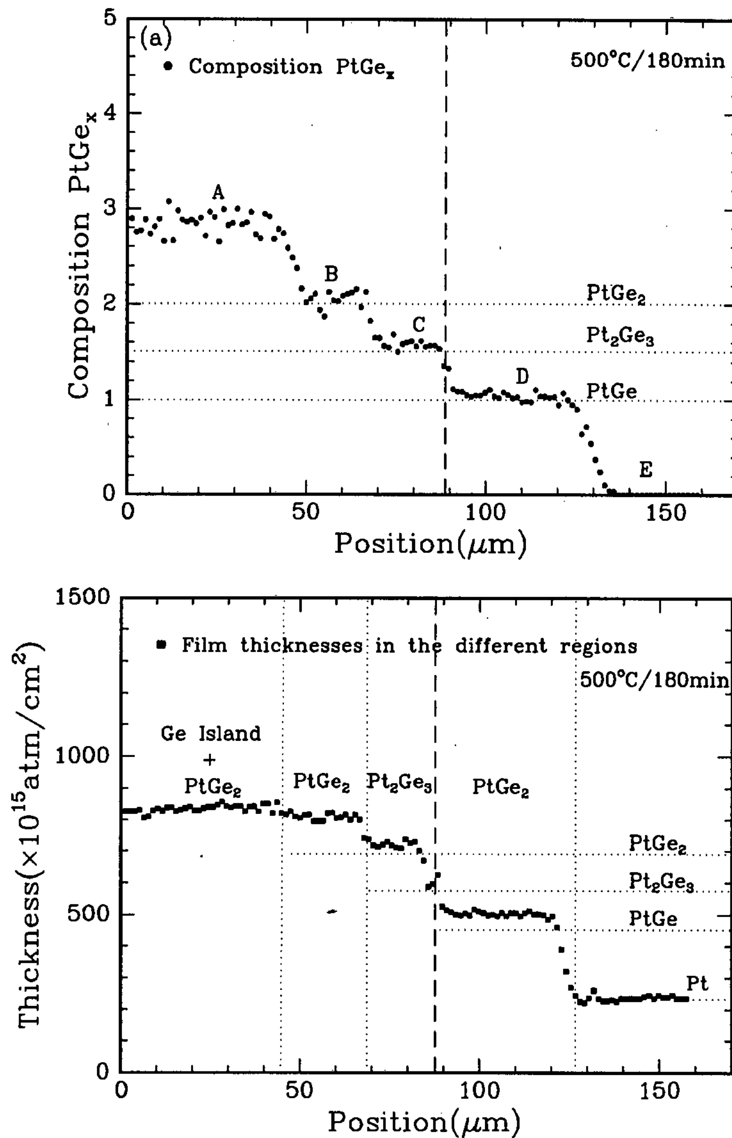

Figure 4.14: *(a) A plot of compound composition($PtGe_x$) versus position for a lateral diffusion couple(Ge island(~1350Å)) on Pt (~330Å) thin film annealed at 500°C/180min. The vertical line at ~89μm indicates the initial interface between island and surrounding thin film. (b) A plot of compound thickness versus beam position across the reacted zones. Thicknesses were obtained from RUMP simulations. Vertical dotted lines were drawn to partition different Pt-Ge compounds identified in (a). The horizontal dotted lines indicate the expected total thickness for a particular germanide, assuming that the deposited platinum film was uniform and that only germanium atoms were the moving species.*

To determine the kinetics of reactions, lateral measurements of reacted zones were done on both SEM micrographs and microprobe data. The measurements were taken from composition plots on microprobe data and from the widths of regions labelled B, C and D on SEM micrographs. Table 4.1 is a summary of lateral thicknesses from both SEM and microprobe data, given for all compounds observed at 500°C/30, 90, 180min. In Figure 4.15(a), plots of annealing time *vs* film length(L_D) of individual germanide phases are displayed to show phase formation sequence and parabolic dependence of compound growth on annealing time. The plots in Figure 4.15(b) were obtained using the same data and are only displayed to show a more conventional form of those in Figure 4.15(b). It is evident from the plots that all three phases, $PtGe_2$, Pt_2Ge_3 and PtGe, follow a diffusion limited process during their formation reactions. Activation energy calculations could not be done as the three samples analysed were all annealed at 500°C.

LATERAL MEASUREMENTS, $L_D(\mu m)$			
S E M			
Temp(°C/min)	PtGe(**D**)	Pt_2Ge_3(**C**)	$PtGe_2$(**B**)
500°C/30'	21	10	12
500°C/90'	31	15	17
500°C/180'	37	20	21
micro-PROBE TRACING			
Temp(°C/min)	PtGe	Pt_2Ge_3	$PtGe_2$
500°C/30'	20	10	11
500°C/90'	35	18	18
500°C/180'	37	19	19

Table 4.1: *Table summarising lateral dimensions(widths) of growing platinum germanide compounds observed using SEM and micro-Probe measurements. Alphabetical letters* **B**, **C** *and* **D** *indicate different regions as labelled on SEM micrographs.*

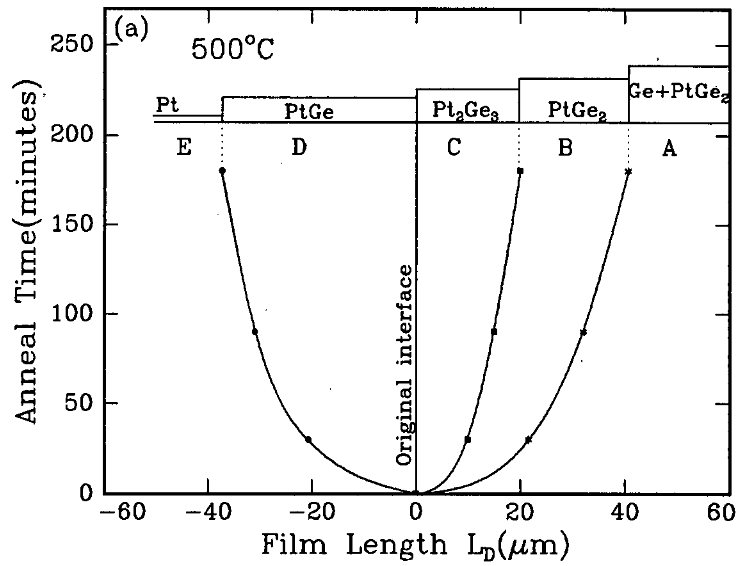

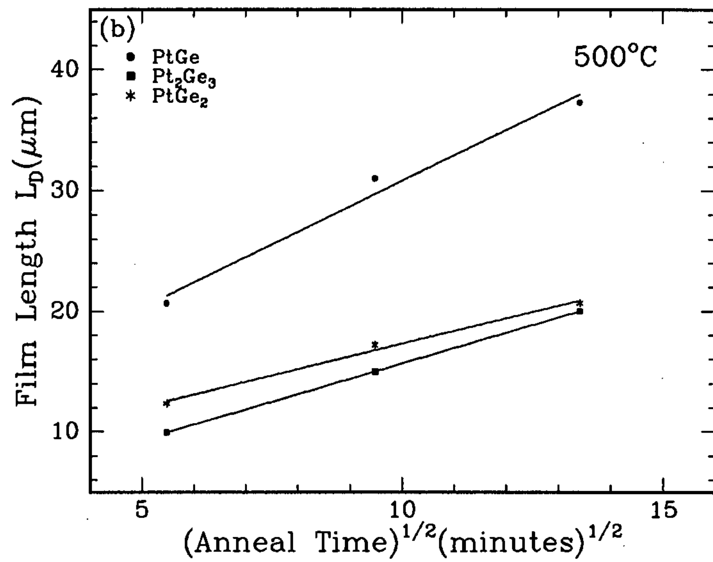

Figure 4.15: *(a) Annealing time vs length(L_D) of individual germanide phases at 500°C showing phase formation sequence and parabolic dependence of compound growth on annealing time in Pt-Ge lateral diffusion couples. Lateral measurements used are those from SEM micrographs. Alphabetical letters indicate different regions as labelled on SEM micrographs. The plots in (b) are only displayed to reflect a more conventional version of the ones in (a).*

4.4 Discussion

4.4.1 Dominant Moving Species and Phase Formation Sequence

Lateral diffusion couples provide a qualitative pointer to the dominant diffusing species without the need to interpose markers between coupling layers. Results obtained from Pt-rich samples in this study, see Figure 4.3, seem to suggest high inward mobility of atoms from the surrounding Ge thin film. When the inward diffusing species has a much higher mobility than the outward diffusing one, the diffusion zone gets thinner and eventually breaks the linkage between island and thin film regions, which in turn halts the reaction process. Similar behaviour was observed by Zingu [51] in his investigation of Si-Pd interaction using lateral diffusion couples with Si island on Pd thin film. Zingu ascribed the cracks he observed on his samples to high mobility of Pd atoms into the Si-source region.

From results obtained using Ge-rich samples (annealed at 500°C/30, 90 and 180minutes), it was very clear that Ge atoms have diffused out from the island into the surrounding thin film, forming PtGe compound. By observing all SEM micrographs and their corresponding μRBS data, the overall lateral diffusion results are best summed up in the following picture. Upon annealing, interaction took place in the source region between Ge and Pt atoms (from the source and the underlying thin film). The Pt-Ge interaction continued until underlying Pt atoms were consumed. At this stage, Ge atoms were still in excess, and they continued to transform the system through to its last phase, $PtGe_2$, in the source region. Thus, ideally, one envisions a stage where the source region consisted of $PtGe_2$ covered with unreacted Ge. Annealing process continued and Ge atoms started diffusing out of the island to form PtGe in the surrounding thin film region, leaving $PtGe_2$ exposed in the source region. As the reaction proceeded, Ge flux decreased, and its supply to the reaction interface was no longer sufficient to maintain PtGe formation. Exposed $PtGe_2$ then started to decompose through the mechanism $2PtGe_2 \rightarrow Pt_2Ge_3 + Ge$.

The decomposition process did two things. It left Pt_2Ge_3 compound in the source region, and it aided the Ge supply at the reaction interface in the surrounding thin film to continue the

PtGe formation process. This analogy suggests the third thing the decomposition process should have done, decreasing the width of exposed $PtGe_2$ (as annealing times increased). However, the plots displayed in Figure 4.15(a) show that this was not the case. Instead of shrinking at higher annealing times, exposed $PtGe_2$ continued to expand. The only plausible explanation for this observation is that depletion of unreacted Ge atoms from the source region continued in parallel with $PtGe_2$ decomposition [the rate of supply of unreacted Ge had only decreased at the PtGe reaction zone in the surrounding thin film, but the depletion process continued].

On the one hand, the two competing processes, viz $PtGe_2$ exposure and $PtGe_2$ decomposition, complemented each other in supplying Ge to form PtGe outside the source region, on the other hand they competed against each other in the resulting width of exposed $PtGe_2$. While the depletion process increased the total width of exposed $PtGe_2$, the decomposition process decreased it. The fact that exposed $PtGe_2$ was observed to continue growing, see Figure 4.15(a), is evidence that the rate at which $PtGe_2$ was exposed was faster than that at which it was decomposed.

Atomic calculations were done using lateral measurements from SEM micrographs to obtain the number of germanium atoms present inside and outside the source region. By comparing these values, it could be established if the total number of Ge atoms was conserved. The calculations are well detailed in Appendix C. Although based on a somewhat un-substantiated assumption of a uniform platinum thin film across the sample, the agreement in the conservation of total number of Ge atoms is striking. The agreement is 100%, 99% and 97% for samples annealed at 500°C/30min, 90min and 180min respectively, see Appendix C.

It can be speculated from the overall results and the above analogy, that upon further annealing, the formation sequence of Pt-Ge phases would have continued in its "reverse order" forming phases poor in germanium away from the source region, i.e. Pt_3Ge_2 phase would have followed after PtGe, and then Pt_2Ge and finally Pt_3Ge. However, it is possible that in the samples analysed, Pt_2Ge phase might be present in the region between PtGe

and Pt thin film, with lateral dimensions of sub-microns, in which case the observation of its presence would have been suppressed by the resolution of the beam. The failure to observe the remaining platinum rich phases can be ascribed to either limited annealing time or low temperature (maybe both).

4.4.2 Growth Kinetics

Three of the compound phases predicted by the phase diagram have been found to grow simultaneously, viz $PtGe_2$, Pt_2Ge_3 and $PtGe_2$. Growth kinetics of these phases are all indicative of diffusion limited behaviour where the square of the width of growing compound exhibits parabolic dependence on annealing time, see Figure 4.15. Diffusion across the growing film is therefore the rate limiting step. The kinetics results are in agreement with the ones reported by Marshal et al [2] and the ones obtained using thin film samples in this study (see Chapter 3).

Chapter 5

Summary, Conclusion and proposal for possible future work

Established techniques, viz *RBS, XRD, SEM and μRBS*, have been used to obtain a basic understanding of interaction between platinum and germanium. The investigation was carried out in two parts, one using conventional thin film couples and the other using lateral diffusion couples.

Using conventional thin film couples, three of the six phases predicted on the Pt-Ge phase diagram (see Figure 1.3) were observed, viz Pt_2Ge, PtGe and $PtGe_2$. The observed phases formed in the following sequence. Pt_2Ge was the first phase to form, followed by PtGe. $PtGe_2$ was observed as the third and last stable phase. This phase sequence is in agreement with prediction by the EHF model.

Reaction kinetics were only investigated for PtGe and $PtGe_2$ phases. The first phase, Pt_2Ge, was found to grow non-uniformly. This and the fact that PtGe phase was found to start growing before complete consumption of surface platinum, made it difficult to investigate Pt_2Ge growth kinetics. The growth kinetics of both PtGe and $PtGe_2$ were found to follow a square-root-of-time law, indicative of diffusion limited growth processes.

Only one isothermal anneal was done to study PtGe formation (at 260°C), and therefore an Arrhenius plot (to estimate activation energy) could not be done for this phase. Four

isothermal anneals were done for $PtGe_2$ phase, yielding an activation energy(E_a) of 1.9 $\pm$ 0.1 eV. Using Kissinger plots obtained from temperature ramp (in the range 240-350°C at a rate of 1°C/min), activation energies were calculated for both PtGe and $PtGe_2$, yielding 1.52 $\pm$ 0.02 eV and 2.5 $\pm$ 0.2 eV respectively. The two results of E_a values for $PtGe_2$ obtained using two different methods are not in agreement. No plausible explanation was found to account for this difference, and it may well be that the ramped kissinger approach is not appropriate for the system under consideration. The activation energy values can therefore not be regarded as conclusive.

By interposing a thin layer of Ti(12$\AA$) to act as an inert marker between two coupling layers of Pt and Ge, the direction of atomic mobility was successfully monitored during the formation of the first phase, Pt_2Ge. Platinum was found to be the dominant diffusing species during Pt_2Ge formation. These results are in agreement with those of Marshal et al [2] who used molybdenum as an inert marker to monitor dominant diffusing species during Pt_2Ge formation. Since germanium was on the surface and platinum underneath, the Pt_2Ge marker results obtained in this study meant that Ti could no longer continue to monitor the direction of atomic mobility during the formation of subsequent phases, which necessitated the alteration of sample configuration to Si<>/SiO_2/Pt/Ge/Ti/Ge. With this configuration, it was crucial that the thicknesses of intimated platinum and germanium layers be confined to just enough to form the first phase, Pt_2Ge. It proved difficult to obtain ideal thicknesses due to the erratic evaporation of germanium resulting from change in current during vacuum deposition process. Owing to this imbalance in Pt and Ge thicknesses, after the formation of Pt_2Ge, the presence of Ti stimulated the formation of Pt_3Ge_2, the non-congruent phase not observed in the thin film experiment done without Ti marker between coupling layers. After Pt_3Ge_2 formation, PtGe phase was observed growing above and below the Ti marker. A detailed atomic calculation showed that the total number of Ge atoms above the Ti marker remained conserved as PtGe grew on both sides of the marker. This led to the conclusion that Pt atoms were the sole diffusing species during PtGe formation, resulting from the mechanism $Pt_3Ge_2 \rightarrow 2PtGe + Pt$. However, relative to Pt_2Ge, the observed growth (of

PtGe) and the extent of the marker movement was very limited.

In the subsequent experiment similarly designed to monitor the diffusing species during $PtGe_2$ formation, the presence of Ti also stimulated the formation of the previously skipped non-congruent phase Pt_2Ge_3. After Pt_2Ge_3 formation, $PtGe_2$ subsequently formed, with germanium as the dominant diffusing species.

The fact that Ti marker was consistently observed to stimulate the formation of phases that were otherwise skipped in its absence might be indication that Ti acted as a diffusion barrier after the formation of precursor phases. This however, may not necessarily render the marker results inconclusive since the "barrier" was ultimately broken and atoms started diffusing across. Unlike in the case of Pt_2Ge where compound growth and marker movement proceeded to an appreciably large scale, the fact that PtGe and $PtGe_2$ results were derived from very limited film growth consequently made the PtGe and $PtGe_2$ marker results not as reliable as would have been wished. Furthermore, diffusing species during PtGe and $PtGe_2$ formation have not been investigated before, and therefore no comparison can be made. At the very best, the PtGe and $PtGe_2$ marker results (from thin films) cannot be strongly relied upon.

Our investigation of the behaviour of Pt-Ge system using the lateral diffusion couples presented some exciting aspects. It is generally believed that when preparing lateral diffusion samples, thick islands of dominant diffusing species should be evaporated on a thin film of interest. As a consequence of the first phase (Pt_2Ge) marker results obtained using conventional thin films, platinum islands were therefore prepared on Ge thin film. For this set of samples, the lateral extent of diffusion zone upon annealing was limited. The reaction seemed not to proceed beyond a certain point despite annealing for longer times. The possible explanation for this observation is that after Ge was consumed beneath the Pt island, Ge atoms from the surrounding thin film started diffusing into the source region much faster than platinum diffused out. It has been observed before that when the inward diffusing species has higher mobility than the outward diffusing species, the diffusion zone becomes

thin, and could eventually lead to a crack formation between the advancing interface and the surrounding thin film, consequently halting the lateral reaction [51].

Sample geometry was therefore reversed from Pt islands on Ge thin film to Ge island on Pt thin film. Upon annealing at 500°C/30, 90 and 180 minutes, lateral reaction was observed proceeding to a relatively large scale, with a total of three different phases growing simultaneously, viz $PtGe_2$, Pt_2Ge_3 and PtGe. The Pt_2Ge_3 and $PtGe_2$ regions were located inside the source region, with $PtGe_2$ as the innermost, while PtGe region was on the periphery of the source region, i.e. between the surrounding thin film and the initial island/thin film interface line.

The observation of PtGe and $PtGe_2$ phases was a common feature between thin film and lateral diffusion results. Pt_2Ge_3 was only observed in lateral diffusion samples but not in conventional thin film, except in (thin film) cases where evaporated thicknesses were confined to form particular phases. It must be pointed out that the presence of Pt_2Ge_3 in lateral diffusion samples was a result of $PtGe_2$ disintegration ($2PtGe_2 \rightarrow Pt_2Ge_3 + Ge$) and not interaction of PtGe with Ge ($2PtGe + Ge \rightarrow Pt_2Ge_3$).

While Pt_2Ge phase was observed to be the first phase to form in thin films, results from lateral diffusion showed no evidence of its presence. Due to the fact that germanide phases were seen spreading out from the source in their decreasing order of germanium content, one would have expected Pt_2Ge to form between PtGe layer and the surrounding thin film. It is speculated that the Pt_2Ge layer could have been present as a very thin layer (less than a micron), which is below the resolution power of the microprobe.

From both SEM and μRBS results, it was clear that germanium was diffusing from the source to the surrounding thin film to form PtGe. However, in the region where PtGe interfaced with the surrounding Pt thin film, a deep in platinum yield was consistently observed on all samples analysed, suggesting that platinum atoms also diffused in the opposite direction (towards the source region), giving rise to the observed platinum dip. What is not clear, though, is whether the platinum deep resulted during the formation of precursor phases or during PtGe formation. In any event, at the very least, the lateral diffusion results point to

Ge as the dominant diffusing species during PtGe formation. These results appear to be in conflict with those from thin film investigation, but, as alluded to earlier, the extent of thin film growth in the latter investigation was limited and therefore not entirely reliable.
Using lateral distances (L_D) and annealing time, the three observed compounds, $PtGe_2$, Pt_2Ge_3 and PtGe, were all found to obey the square-root-of-time law, indicative of a diffusion limited growth. This compares and agrees well with PtGe and $PtGe_2$ results obtained using thin film samples

A basic understanding has been achieved of interaction between platinum and germanium using both conventional thin films and lateral diffusion couples. The study did not go a long way in clearing out the apparent confusion existing in the Pt-Ge phase sequence formations reported in previous experiments (carried out using conventional thin films). However, except for the absence of non-congruent phases (Pt_2Ge_3 and Pt_3Ge_2), the phase sequence results from thin films are more in agreement with those of Hsieh and Chen [1] and Marshal et al [2]. The reaction kinetics and dominant diffusing species during Pt_2Ge also agree with those of Marshal et al [2].

A combination of SEM and μRBS has proven effective in analysing Pt-Ge interaction using lateral diffusion couples. This combination should be enhanced with XRD so that different phases in the reacted zones can be identified without ambiguity. Without XRD, RBS strictly limits identification of reacted zones to phase compositions. Since Scanning Electron Microscopy (SEM) is only restricted to surface topography, Transmission Electron Microscopy (TEM) would also make a strong supplement to SEM. It remains to be verified if lateral diffusion samples of thicker germanium islands (on Pt thin film) annealed at 500°C for times longer than 180 minutes would result in the formation of all Pt-Ge phases predicted in the phase diagram. Sample annealings also have to be done at different temperatures so that activation energies can be calculated from Arrhenius plots.
The project therefore still has some potential areas to exploit. Future work on the project

can finally extend it to other binary systems.

Appendix A

RBS simulations

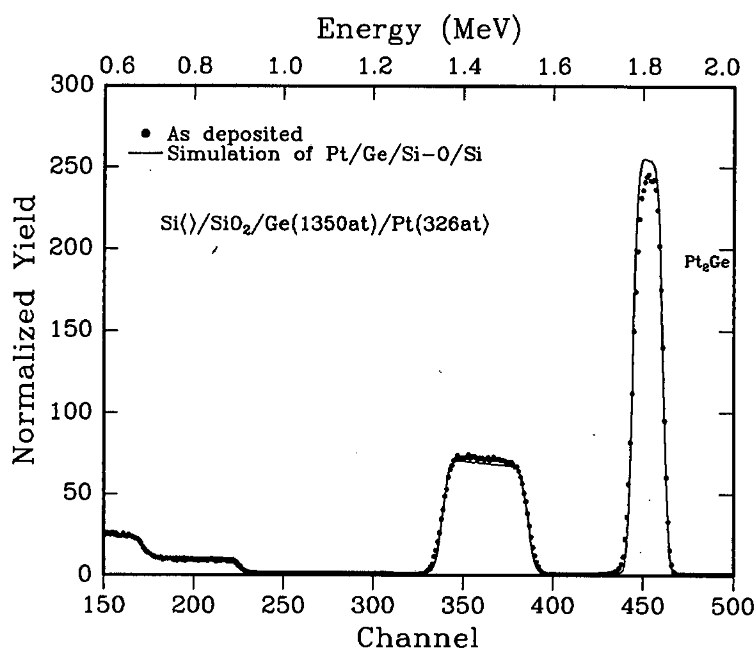

Figure A.1: *RBS spectra obtained from an as deposited sample displayed with RUMP simulation to confirm composition and thickness agreement with actual data.*

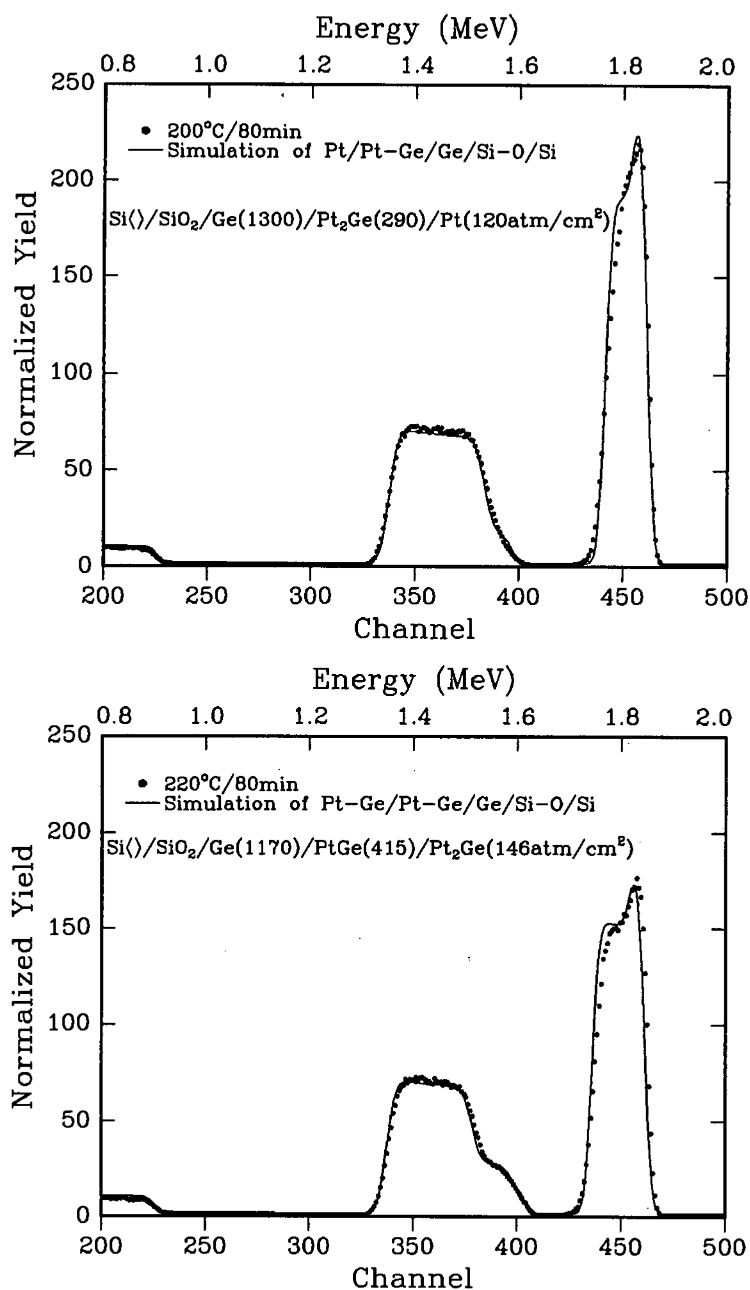

Figure A.2: *RBS spectra(top) obtained from samples annealed at 200(top) and 220° C(bot) for annealing periods of 80 minutes. Both spectra are displayed with their RUMP simulations to confirm agreement with actual data.*

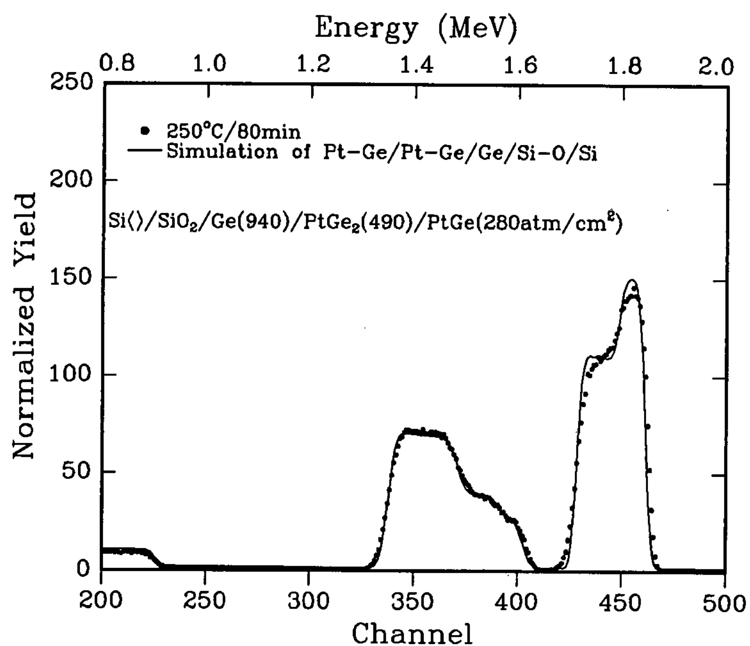

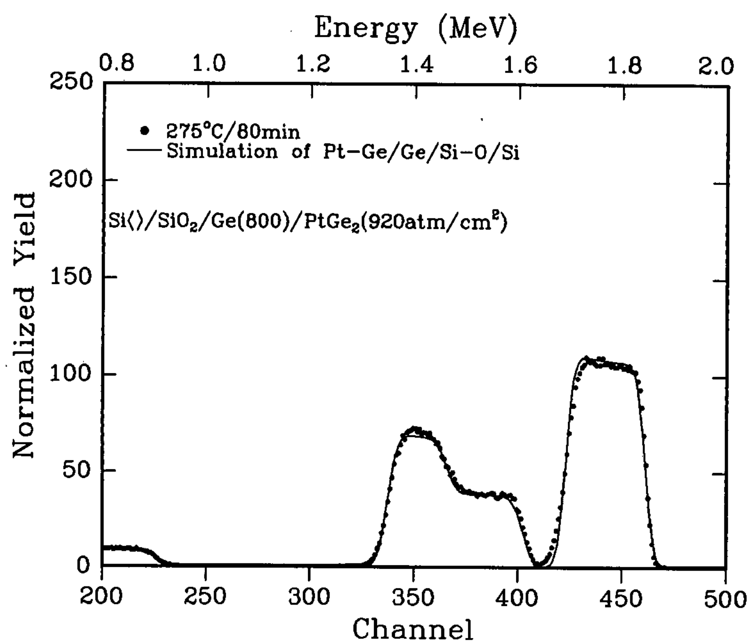

Figure A.3: *RBS spectra(top) obtained from samples annealed at 250(top) and 275° C(bot) for annealing periods of 80 minutes. Both spectra are displayed with their RUMP simulations to confirm agreement with actual data.*

Appendix B

Calculations of Diffusion ratios to estimate dominant diffusing species

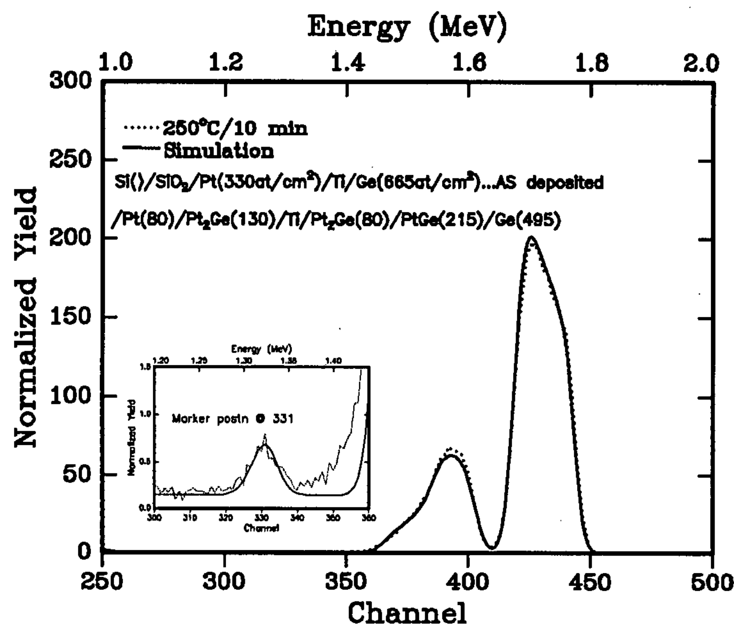

Figure B.1: *RBS spectrum from a sample annealed at 250°/10 min. Simulation suggests platinum as the dominant diffusing species during Pt_2Ge formation. Thicknesses are given in units of $10^{15} at/cm^2$.*

The following calculations, based on Figure B.1, estimate atomic diffusion ratio during PtGe formation.

Amount of platinum above the marker in units of $10^{15} at/cm^2$ is given by:

♯ Pt = $\frac{2}{3}(80)$(from Pt_2Ge) + $\frac{1}{2}(215)$(from PtGe) = 160×10^{15} Pt at/cm^2

Amount of germanium below the marker is given by:

♯ Ge = $\frac{1}{3}(130)$(from Pt_2Ge) = $\sim 45 \times 10^{15}$ Ge at/cm^2

The Pt:Ge ratio is about 4:1. Pt is therefore the DMS.

Appendix C

Calculations of the total number of Ge atoms present in reacted zones.

All answers have a multiplicative factor of 10^{15}.

500°C/30min

♯ Ge atoms in PtGe: $21 \times 10^{-4}cm \times 440\frac{atm}{cm^2} \times 1cm \times \frac{1}{2} = 0.462$

♯ Ge atoms in Pt_2Ge_3: $10 \times 10^{-4}cm \times 550\frac{atm}{cm^2} \times 1cm \times \frac{3}{5} = 0.330$

♯ Ge atoms in $PtGe_2$: $12 \times 10^{-4}cm \times 660\frac{atm}{cm^2} \times 1cm \times \frac{2}{3} = 0.528$

♯ Ge atoms in the source region before annealing: $22 \times 10^{-4}cm \times 1cm \times 600\frac{atm}{cm^2} = 1.320$

$$\frac{0.462+0.330+0.528}{1.320} \times 100\% = 100\%$$

500°C/90min

♯ Ge atoms in PtGe: $31 \times 10^{-4}cm \times 440\frac{atm}{cm^2} \times 1cm \times \frac{1}{2} = 0.682$

♯ Ge atoms in Pt_2Ge_3: $15 \times 10^{-4}cm \times 550\frac{atm}{cm^2} \times 1cm \times \frac{3}{5} = 0.495$

♯ Ge atoms in $PtGe_2$: $17 \times 10^{-4}cm \times 660\frac{atm}{cm^2} \times 1cm \times \frac{2}{3} = 0.748$

♯ Ge atoms in the source region before annealing: $32 \times 10^{-4}cm \times 1cm \times 600\frac{atm}{cm^2} = 1.920$

$$\frac{0.682+0.495+0.748}{1.920} \times 100\% = \sim 99.7\%$$

500°C/180min

♯ Ge atoms in PtGe: $37 \times 10^{-4}cm \times 440\frac{atm}{cm^2} \times 1cm \times \frac{1}{2} = 0.814$

♯ Ge atoms in Pt_2Ge_3: $20 \times 10^{-4}cm \times 550\frac{atm}{cm^2} \times 1cm \times \frac{3}{5} = 0.660$

♯ Ge atoms in $PtGe_2$: $21 \times 10^{-4}cm \times 660\frac{atm}{cm^2} \times 1cm \times \frac{2}{3} = 0.924$

♯ Ge atoms in the source region before annealing: $40.67 \times 10^{-4}cm \times 1cm \times 600\frac{atm}{cm^2} = 2.460$

$$\frac{0.814+0.660+0.924}{2.460} \times 100\% = 97\%$$

Bibliography

[1] Y.F. Hsieh and L.J Chen, *J. Appl. Phys.* **63**(4)1177, 15 February 1988

[2] E.D. Marshal, C.S. Wu, C.S. Pai, D.M. Scott and S.S Lau, *MRS Symp. Proc.* **47** 161 (1985)

[3] G.A . Smith et al, *J. Vac. Sci. Technol,* **A7**(3), May/June 1989

[4] Sorab K. Ghandi, *VLSI FABRICATION PRINCIPLES, Silicon and Gallium Arsenide*, (John Wiley and sons, New York, 1982)

[5] Otto F. Sankey, Roland E. Allen and John D. Dow, *J. Vac. Sci. Technol.* **B 2**(3)491 Jul/Sept 1984

[6] H.K. Liou, X. Wu and U. Gennser, *Appl. Phys. Lett.* **60**(5)577, 3 Feb 1992

[7] K. Ismail, M Arafa, K.L. Saenger, J.O. Chu and B.S. Meyerson, *Appl. Phys. Lett.* **66**(9)1077, 1995

[8] T. Koester, J. Gondermann, B. Hadam, B. Spangenberg, M. Schütze, H.G. Roskos, H. Kurz, J. Brunner and G. Abstreiter, *J. Vac. Sci. Technol.* **B 14**(2)698, 1996

[9] R. People, J.C. Bean, D.V. Lang, A.M. Sergent, H.L. Stormer, K.W. Wecht, R.T. Lynch, and K. Baldwin, *Appl. Phys. Lett.* **45**(11)1231 Dec 1984

[10] Capasso and Alfred Y. Cho, *Surface Science, the first thirty years*, edited by Charles Duke, North Holland (1994) p.879.

[11] E.D Marshal, B. Zhang, L.C. Wang, P.F. Jiao, W.X. Chen, T. Sawada and S. Laul, *J. Appl. Phys.* **62**(3)942, 1 August 1987

[12] M. Genut and M. Eizenburg, *Appl. Phys. Lett.* **53**(8)672, 22 August 1988

[13] J.C. Bean, *Proceedings of the First International Symposium on Si Molecular Beam Epitaxy*, edited by J.C. Bean, p.337, 1985

[14] Peixin Zhong and Youndou Zheng *Appl. Phys. Lett.* **62**(25)3258, 21 June 1993

[15] Q.Z. Hong, J.G. Zhu C.B. Carter and J.W. Mayer, *J. Appl. Phy. Lett.* **58**, 905 (1991)

[16] E. Philofsky, *Sol. State. Electr.* **13**, 1391 (1970)

[17] Joyce C. Liu, J.W. Mayer and J.C. Barbour, *J. Appl. Phy.* **64**(2)656 15 July 1988

[18] S.H. Chen, L.R. Zheng, C.B. Carter, and J.W. Mayer, *J. Appl. Phys.* **57**(2)258 15 Jan 1985

[19] King-Ning Tu, James W. Mayer and Leonard C. Feldman, *Electronic Thin Film Science for Electrical Engineers and Scientist* Macmillan, New York 1992

[20] U. Gosele and K.N. Tu, *J. Appl. Phys*, **66**(6)2619, 15 Sept 1989

[21] Wei-Kan Chu, James W Mayer, Marc-A. Nicolet, *Backscattering Spectrometry*, Academic Press, New York 1978

[22] J.B. Rubin and R.B. Schwarz, *Appl. Phys. Lett.* **55**, 36 (1989)

[23] L.R. Zheng, Ph.D. Thesis, Cornell University, 1985

[24] L.R. Zheng, L.S. Hung, and J.W. Mayer, *J. Vac. Sci. Technol.* bf A1(2)758 Apr.-June 1983

[25] W.K. Chu, H. Krautle, J.W. Mayer, H. Muller, M.A. Nicolet and K.N. Tu, *Appl. Phys. Lett.* **25**, 454 (1974)

[26] R.M Walser and R.W. Bene, *Appl. Phys. Lett.*, **28**624 (1976)

[27] P.J. Ding, R. Talevi, W.A. Lanford, S. Hymes and S.P. Murarka, *Nucl. Instr. and Meth. in Phys. Res.* **B***85 1994*

[28] M.Wittmer, M.A. Nicolet and J.W. Mayer, *Thin Solid Films.*, **42**(59)51 (1975)

[29] B.Y. Tsaur, S.S. Lau, J.W. Mayer and M.A. Nicolet, *Appl. Phys. Lett* **38**(11)922, 1 June 1981

[30] R. Pretorius, A.M. Fredenberg, F.W. Saris and R. de Reus, J. Appl. Phys. **70**(7) 1 October 1991

[31] R. Pretorius, *MRS Proc.*, 25 (1984) 15

[32] R. Pretorius, Vacuum, 41 (1990) 1038

[33] R.Pretorius, T.K. Marais and C.C. Theron, *Materials Science & Engineering*, 10, 1 July 1993

[34] F.M. d'Heurle, *J. Mater. Res.* **3**(1)167, 1988

[35] C.S. Petersson, *Thin Solid Films*, **128**, 283(1985)

[36] G. Ottaviani, *J. Vac. Sci. Technol*, **16**(5)1112 Sept/Oct 1979

[37] Alan J. Walton, *Three Phases of Matter*, 2nd Edition, Oxford Science Publications

[38] C.M. Comrie and J.M. Egan, *J. Appl. Phys* **64**(3)1173, August 1988

[39] S. Petersson, J. Baglin, W. Hammer, T.S. Kuan, I. Ohdomari, J. de Sousa Pires and P. Tove, *J. Appl. Phys.* **50**(5)3357 (May 1979)

[40] M.G. Grimaldi, L. Wielunski and M.A. Nicolet, *Thin Solid Films*, **81** 207 (1981)

[41] Leornard C. Feldman and James W. Mayer, *Fundamentals of Thin Film and Analysis*, North-Holland 1986

[42] E.O. Kirkendal, *Trans. AIME.*, **147**, 104(1942)

[43] C.M Comrie J.C Liu, L.S. Hung and J.W. Mayer, *J. Appl. Phy.* **63**(7)2402 (April 88)

[44] L. Zhang, D.G. Ivey, *J. Mater. Res.* **6**, 1518 (1991).

[45] L.J. Chen, H.C. Cheng and W.T. Lin, *MRS Proc.*, **54**, 245 (1986)

[46] O. Thomas, F.M. d'Heurle and S. Delange, *J. Mater. Res.*, **5**(7)1453 Jul 1990

[47] O. Thomas, S. Delange, F.M. d'Heurle and G. Scilla, *Appl. Phys. Lett.* **54**(3)228 Jan 1989

[48] K.N. Tu. *Appl. Phys. Lett.*, **27**221 (1975)

[49] J.M. Poate and T.C. Tisone, *Appl. Phys. Lett.*, **24**,391 1974

[50] K.N. Tu, J.M. Poate and J.M Mayer, *Thin Films Interdiffusion And Reactions, p380*, Princeton, New Jersey, John Wiley and Sons

[51] E.C. Zingu, *Atomic Mobility in Thin Solid* Pd_2Si *Films, PhD Thesis*, UCT January 1985.

[52] C.L. Churms *Fascilitating the Identification of Solid State Phases and Concentration in Micro Volume, Phd thesis*, Stellebosch August 1995